Health monitoring techniques for rotating machinery.

Sinha, Jyoti K

HEALTH MONITORING TECHNIQUES FOR ROTATING MACHINERY

JYOTI K. SINHA,
B.Sc. (Mech. Engg.), M. Tech. (Aerospace Engg.), Boyscast Fellow

Thesis submitted to the University of Wales Swansea
for the degree of Doctor of Philosophy

OCTOBER 2002

SCHOOL OF ENGINEERING
UNIVERSITY OF WALES SWANSEA SA2 8PP (UK)

DECLARATION

This work has not previously been accepted in substance for any degree and is not being concurrently submitted in candidature for any degree.

Signed (candidate): _____

Date: 28-10-2002

STATEMENT 1

This thesis is the result of my own investigations, except where otherwise stated. Other sources are acknowledged by the use of explicit references. A list of references is included.

Signed (candidate): _____

Date: 28-10-2002

STATEMENT 2

I hereby give consent for my thesis, if accepted, to be available for photocopying and for inter-library loan, and for the title and summary to be made available to outside organisations.

Signed (candidate): _____

Date: 28-10-2002

TO MY PARENTS

ACKNOWLEDEGEMENTS

I would like to express my gratitude to Prof. M. I. Friswell and Prof. A. W. Lees, for their able guidance, supervision and motivation throughout the duration of this programme, and for their careful checking and helpful comments on the thesis, to bring this work to a positive conclusion.

I wish to thank Mr. R. K. Sinha, Associate Director, Reactor Design and Development Group, Bhabha Atomic Research Centre, Mumbai (India) for his consistent encouragement, guidance and support throughout my study.

Special thanks are also due to Dr. Simon Edwards, Dr. C. Zang, and the staff of the workshop at Swansea for their valuable help in the experimental work and related discussions.

I would also like to thank my friends and relatives, both at India and in the UK, for consistently cheering me up throughout my study at Swansea.

Last but not the least, I am short of words to express my sincerest thanks to my wife Sarita and my loving son Aarambh for their perseverance when long working days would not leave me with enough time for them.

Summary of Thesis

The present research is concerned with health monitoring techniques for rotating machinery, for example Turbogenerator (TG) sets in the power industry. Vibration based condition monitoring is widely accepted for rotating machinery and hence the vibration response of a machine is again utilized in the present research study.

Experience shows that faults develop in rotating machines during normal operation and hence their quick identification and remedy are important from safety and plant productivity considerations. The vibration based fault identification procedures are well developed for rotating machinery. However the quantification part of the identified faults has still not matured, and is an ongoing research topic. Hence the remedial action is usually time consuming, even though the machine is known to have some known faults, due to lack of knowledge of their locations and the extent of the faults. In general such a quantification of the identified fault relies on the mathematical model of the complete system along with the measured vibration response of the system.

Rotating machinery consists of three major parts – a rotor, fluid journal bearings and a foundation which is often flexible. Often a good model of the rotor (usually a finite element model) and an adequate model of the fluid bearings may be constructed. However, a reliable model for the foundation is difficult to construct due to a number of practical difficulties. Hence the present study has concentrated on two objectives - reliable modelling for the foundation and the quantification of faults using the measured vibration response at the bearing pedestals and the mathematical model of the rotor and the fluid bearings.

For the foundation model, the theory which was developed to estimate the models for flexible foundation has been described in the thesis. The method uses measured vibration response at bearing pedestals during machine run-downs, a priori rotor and journal bearing models, and a knowledge of the rotor unbalance, to estimate the stiffness, damping and mass matrices of the foundation. The method was tested on both simulated and experimental examples. The prediction capability of the estimated foundation model was also demonstrated.

For the fault estimation a different approach has been used. It has been assumed that the foundation mathematical model is not known, and it is demonstrated that the two faults - the state of rotor unbalance and the misalignment in the rotor can be estimated reliably. The theory of the proposed methods is discussed in the thesis. The method uses measured vibration response at bearing pedestals during a single machine run-down, and a priori rotor and journal bearing models, to estimate the rotor unbalance and the misalignment along with the foundation parameters, so that the dynamics of the foundation is also accounted for during the estimation. The methods were tested on simulated and experimental examples and the estimation accuracy was found to be excellent and generally robust to errors in the rotor and bearing models.

CONTENTS

LIST OF TABLES

LIST OF FIGURES

ABBREVIATION

DoF	:	Degree of freedom.
FE	:	Finite element.
FRF	:	Frequency response function.
TG	:	Turbo-Generator

NOMENCLATURE

Subscripts *R, B, F* : Rotor, Bearing, Foundation.

$\mathbf{K}$, $\mathbf{C}$, $\mathbf{M}$	:	Stifness, Damping and Mass matrices.
$\mathbf{Z}$	:	Dynamic stiffness matrix, $-\omega^2\mathbf{M} + j\omega\mathbf{C} + \mathbf{K}$.
$\mathbf{e}$	:	Vectors of the rotor unbalance parameters.
$\mathbf{e}_m$	:	Vectors of the forces and moments at couplings in the multi-rotors.
$\mathbf{f}_u$	:	Rotor unbalance force.
$\mathbf{f}_m$	:	Rotor misalignment force.
j	:	Imaginary number, $\sqrt{-1}$.
$\mathbf{r}$	:	Responses of a machine.
$\mathbf{r}_{F,b}$	:	Responses at foundation connected to bearing DoFs i.e., bearing pedestals.
$\mathbf{r}_m$	:	Measured responses at bearing pedestals.
$\mathbf{S}$	:	Sensitivity matrix – first order derivative of the response with respect to the vectors of the foundation parameters.
$\mathbf{T}$, $\mathbf{T}^*$, $\mathbf{T}_m$	:	Transformation matrix.
$\mathbf{v}$, $\mathbf{v}^*$	:	Vectors of the foundation parameters.
x, y, z	:	Rotor axis, Horizontal and Vertical directions.
λ	:	Regularization parameter.
ω	:	Rotor running speed in rad/s.
Δy , Δz	:	Horizontal and vertical linear misalignment at a coupling in a multi-rotors (mm).
$\Delta\theta_y$, $\Delta\theta_z$	:	Angular misalignment at a coupling in a multi-rotors in the horizontal and vertical direction (degree).

CHAPTER 1

INTRODUCTION

1.0. INTRODUCTION

Turbogenerator (TG) sets in power stations consist of three major parts – a rotor, fluid journal bearings and a foundation which is often flexible. A typical schematic of the steam TG set is shown in Figure 1.1 and generally consists of a *High Pressure (HP) turbine, a Low Pressure (LP) turbine and an Electric Generator.* In some high capacity power plants the TG sets also have a few *Intermediate Pressure (IP) turbines* that are not shown in Figure 1.1. The shafts of the individual systems are joined together by means of couplings, and the complete shaft is known as the rotor of the TG set. The shafts of each turbine are designed to have a number of rows of turbine blades along the shaft length. Each rotor of an individual system is normally supported by its own fluid journal bearings, which are supported on foundation structures which are often flexible.

Experience shows that faults develop in rotating machines during normal operation, for example bends, cracks, or mass unbalance in the shaft (due to scale deposits and/or erosion in last stage blades of the LP turbine). If a fault develops and remains undetected for some time, then, at best, the problem will not be too serious and can be remedied quickly and cheaply. However, at worst, it may result in expensive damage and down-time, injury, or even loss of life. Such a situation warrants the use of a reliable condition monitoring technique to reduce the down time of plant.

Successful condition monitoring generally depends on two facets – detection of the presence of faults and their quantification - so that remedial action can be planned in time. The vibration based prediction of the presence of faults in rotating machines is now well known and well understood for many known problems of rotating machines. Past research studies (Orbit, 1981-2001) gave many guidelines to detect faults and these are used extensively in power plants. However the quantification part of fault diagnosis is still an ongoing research topic. In general the quantification of faults relies on the mathematical model of the complete system along with the measured vibration response of the system.

1.1. THE SYSTEM MATHEMATICAL MODEL

Often a good model of the rotor (usually a finite element (FE) model) and an adequate model of the fluid journal bearings may be constructed. The modelling aspects of the rotor and fluid bearings are discussed in Chapter 3. However, a reliable FE model for the foundation is difficult, if not impossible, to construct due to a number of practical difficulties (Lees and Simpson, 1983).

1.2. MEASURED VIBRATION DATA

It is well known that the direct measurement of vibration on the rotor during its normal operation is not easy. However it is convenient to perform vibration measurements at the easily accessible locations, such as bearing pedestals, that will reflect the dynamic response of the rotor, the bearings and the foundations. In addition the relative shaft vibration near the bearing pedestals may also be measured. In fact most of the diagnosis methods developed utilize these measured data which are briefly summarized in Chapter 2. However many of the older power plants are not equipped the proximity probes required to measure the relative rotor vibration and so this information may not always be available. Hence the present studies are confined to the use of the bearing pedestal vibration only.

1.3. THE PRESENT STUDY

The present research study has concentrated on the following two objectives utilizing the measured bearing pedestal vibration in both the vertical and horizontal directions during machine run-downs, and *a priori* models for the rotor and fluid bearings.

(a) Foundation model estimation so that a reliable mathematical model of the complete system can be developed.
(b) Reliable fault estimation (Rotor unbalance and misalignment) even if the foundation model is not known.

1.3.1. Estimation of the Foundation Models

The FE modelling methods (Cook *et al.*, 1989, Zienkiewicz and Taylor, 1994) are well known and mature techniques for modelling structurally and geometrically complex structures with a variety of analysis capabilities. Many commercial codes are available to perform this analysis. The DYNROT (Genta, 1997) code based on the MatLab platform (Mathwork, Inc., 1999) is written for rotating machine modelling and analysis. Even with these advances in modelling, it has been observed that often a good FE model of the rotor is possible, but a reliable FE model for the foundation is difficult to construct (Lees and Simpson, 1983). However a reasonably reliable model of fluid journal bearings may be constructed using short bearing theory (Hamrock, 1994).

Lees and Simpson (1983) argued that the modelling of the foundation, in principle, is possible by the FE method, but there are a number of practical difficulties. It is often found that similar units, built to the same drawing, display substantially different dynamic behaviour. The different behaviour is mainly due to small changes in a huge number of joints, which combine to give a substantial change in the stiffness of the structure. With these difficulties, it is unlikely that model updating methods (Friswell and Mottershead, 1995) could be used, as there are too many uncertain parameters in the joints. Thus the most promising avenue is to identify a model of the foundations directly from the measured vibration at the bearing pedestals during a run-down.

For the foundation model estimation, the machine dynamics are assumed to be linear. The responses of two runs (one with residual unbalance and the other with added unbalance at a number of balance disks) of a machine were subtracted to produce a response of the machine for a known unbalance in the rotor. These informations have then been used for the direct estimation of the foundation model from the system equation of motion. Initially Lees (1988) has suggested the least squares method for the foundation model estimation by utilizing these measured responses for a known unbalance along with *a priori* rotor and fluid bearings models. Since then several research studies used different estimation techniques on this topic have been carried out. Once again an attempt has been made to estimate the foundation model in a simple manner.

Broadly two types of foundation model identification have been proposed by different researchers. One is the identification of the system matrices (Lees, 1988, Zanetta, 1992, Feng and Hahn, 1995, Vania, 1996, Smart *et al.,* 2000) and other is the modal model identification (Provasi *et al.*, 2000) for the foundation. Zanetta (1992), Feng and Hahn (1995), and Provasi *et al.* (2000) used the relative shaft vibration along with the bearing pedestal vibration. However others have used only the bearing pedestal vibration. But most of these studies were restricted to simple simulated examples, and limited experimental data was used. The most important aspect is the prediction capacity of the estimated foundation model, and this was only considered by Smart *et al.* (2000).

Smart *et al.* (2000) used experimental data to test their estimation method. The size of the estimated foundation model was restricted to the measured DoF and the frequency was split into bands to accommodate more modes than measured DoF. The estimation method has modelled the transfer function using polynomial matrices for estimation of foundation mass, damping and stiffness matrices. The success of this method is critically dependent on the regularization of the resulting equations and requires considerable user judgement. The present estimation method is a simplified approach of the study by Smart *et al.* (2000) and has used the bearing pedestal vibration measured in the vertical and horizontal directions along with *a priori* models of the rotor and fluid bearings. In the proposed method (Sinha *et al.*, 2002a) the elements of the system mass, damping and stiffness matrices are directly modelled and estimated giving a significant reduction in the number of parameters estimated by Smart *et al.* (2000). Regularization based on physical constraints, for example symmetric system matrices, was also applied to further reduce the number of unknown foundation parameters to be estimated. Different regularizations were used and their usefulness has also been highlighted in the study by Sinha *et al.* (2002a). The prediction capability of the estimated foundation model was found to be excellent. These are discussed in detail in Chapters 5 and 6.

1.3.2. Rotor Unbalance Estimation

Several researchers have proposed many methods since the early 1930s for balancing a rotor to reduce the machine vibration. These are briefly summarized in Chapter 2. The best option is to use a mathematical model of the system that can estimate the

state of the rotor at multi-planes using the measured responses from a single run-down of the machine. However the reliable model of the machine may not be readily available for many machines installed at site. Modelling of the rotor and the fluid bearings may be quick and straightforward but the estimation of a reliable foundation model is difficult and time consuming. Hence this option is not practical in many cases. Many other conventional balancing methods are time consuming – several run-downs of the machine are needed and substantial experience in field balancing is required. Hence a quick and reliable method for the estimation of rotor unbalance is required that would be appreciated and welcomed in practice. Significant effort has been made to achieve this objective of the minimum possible machine down time with reasonably accurate unbalance estimation. These are briefly discussed in Chapter-2. Among them the technique suggested by Lees and Friswell (1997) has been found to be the most viable alternative. The suggested method seems to have the potential for fast and reliable rotor unbalance estimation just using measured pedestal vibration from a single run-down of a machine. In the present study the method has been further modified to suit plant conditions.

Lees and Friswell (1997) demonstrated the method on a simple simulated example. The method uses the rotor and the bearing model along with the measured pedestal vibration, and estimates the rotor unbalance along with the foundation parameters. The method has been further validated on a small simple experimental rig (Edwards *et al.*, 2000). In both the cases the number of modes of the system were less than the measured DoF in the run-down frequency range. Hence the experimental example only indicates that the method is robust to the measured responses that may be contain some structure and instrument noise. However for systems like TG sets the number of modes excited may be more than the measured DoF in the run-down frequency range. Thus the estimated unbalance may not account for all the critical speeds. Hence the method has been modified further to reliably estimate the rotor unbalance by splitting the whole frequency range into bands for the foundation so that the band dependent foundation models account for all critical speeds. The advantages of the suggested approach have been demonstrated on a more complex simulated example and an experimental rig (Sinha *et al.*, 2001, 2002b). The sensitivity of the method with respect to the error in the rotor and the bearing models are also highlighted (Lees, Sinha and Friswell, 2002). These are discussed in detail in Chapters 5, 7 and 8.

1.3.3. Estimation of both Rotor Unbalance and Misalignment

The general perception and observation is that the misalignment in the multi-coupled rotors generates a 2X (twice the rotating speed) component in the response of the machine (Ehrich, 1992b, Dewell and Mitchell, 1984). The affect on the 1X component is assumed to be small. Many simple analytical simulations have been carried out to understand this phenomena (Gibbsons, 1976, Sekhar and Prabhu, 1995). But none of the earlier studies have suggested any method for the direct quantification of misalignment. Hence in the present study the identification of rotor unbalance and misalignment has been carried out using the 1X response at the bearing pedestals of the machine from the single run-down, even though the influence on the 1X response due to misalignment may be small.

For this identification it has been assumed that the source of misalignment in the rotor is the coupling of the multi-rotor system. Such a misalignment will generate constant forces and moments at the couplings depending upon the extent of the off-set between the two rotors and irrespective of the machine rotating speed. Hence the unbalance estimation method discussed earlier in Section 1.3.2 has been further modified by including such constant forces and moments at the couplings along with the rotor unbalance and both of these sets of parameters along with the foundation parameters have been estimated. The estimation theory has been presented in Chapter 5 and its experimental qualification in Chapter 7.

1.4. LAYOUT OF THE THESIS

The present chapter serves as a general introduction and gives detailed objectives and the highlights of the advantages of the present studies. The organization of the thesis is as follows.

Chapter 2 gives a simplified overview on the condition monitoring of rotating machines for the sake of completeness and documentation.

Chapter 3 gives the theory of rotor and bearing modelling. Details of the measurement scheme utilized for the present study on a simple small rig are also discussed.

Chapter 4 gives the details of the three experimental test rigs –two in the Dynamics Laboratory, Department of Mechanical Engineering, University of Wales Swansea (UK) and the third at Aston University, Birmingham (UK), whose measured vibration data were used in the present study.

Chapter 5 gives the theory of the estimation techniques for the foundation model of a flexible rotor-bearing-foundation system using measured vibration data during a machine run-down. The estimation technique involves linear estimation by the least-squares method for the foundation model, followed by model updating of the identified foundation model by non-linear optimization. The theory of the rotor unbalance estimation (both amplitude and phase) and the rotor misalignment of a flexible rotor-bearing-foundation system using measured vibration data during a single machine run-down is also discussed.

Chapter 6 gives an assessment and demonstration of the proposed estimation technique for foundation models through several numerical simulations, as well as on experimental run-down data from two test rigs.

Chapter 7 is concerned with the validation of the proposed rotor unbalance estimation, and both unbalance and misalignment techniques through several numerical simulations and experimental data from three laboratory scale rigs.

Chapter 8 discusses the sensitivity analysis of the proposed rotor unbalance estimation method by introducing perturbations in different modelling parameters to confirm the robustness of the method.

Chapter 9 presents some concluding remarks and also highlights the scope of future work.

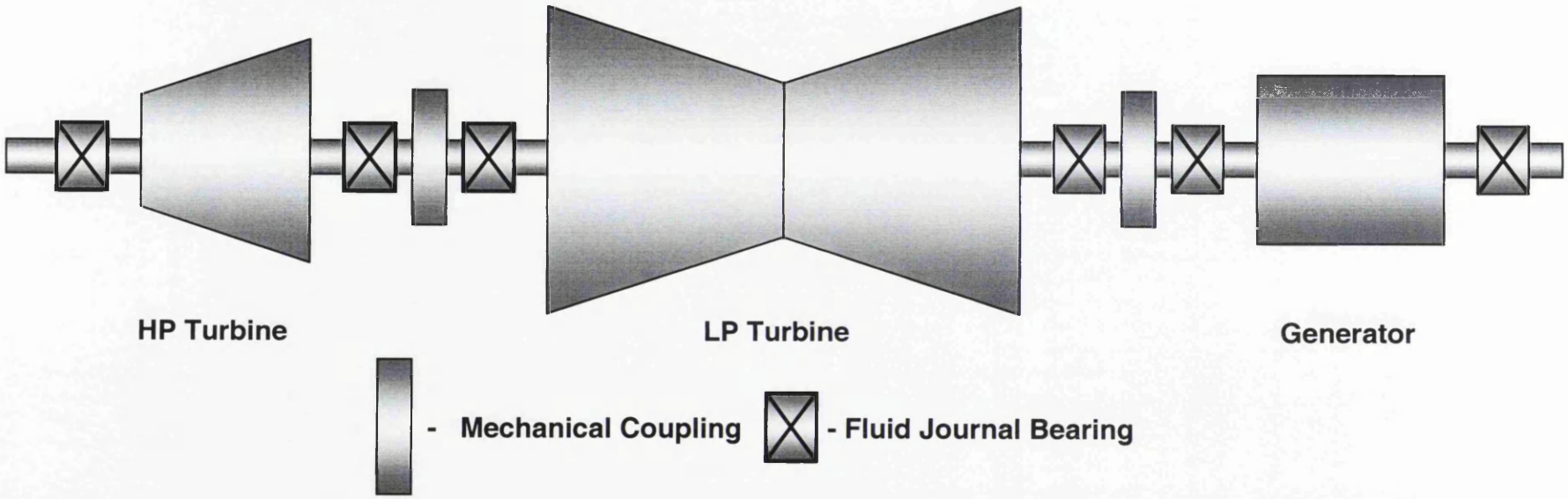

Figure 1.1 Schematic of a simple layout of a TG set

CHAPTER 2

COMPREHENSIVE VIBRATION BASED DIAGNOSIS OF TURBO-GENERATORS: THE STATE OF THE ART

2.0. INTRODUCTION

Condition monitoring requires the continuous observation of various parameters like vibration responses at different locations of the TG sets, and many other process parameters, for example., condenser pressure, bearing fluid pressure and temperature during the machines normal operation. Vibration based condition monitoring is perhaps the most popular and well-recognized in plants, perhaps because the machine vibration response is more sensitive to any small structural or process parameter change. Hence only vibration based condition monitoring is discussed here. There is always two aspects of condition monitoring – *Prediction of faults and their quantification i.e., diagnosis.* In fact the vibration based prediction of faults for rotating machines is now well known and well understood for many known problems of rotating machines. Earlier research studies (Orbit, 1981-2001, Harris, 1988) gave many guidelines to detect faults and are widely used in power plants.

Once a fault is suspected, the machine shutdown can be planned to identify the source of the fault alarm and its solution. However the identified faults like the rotor unbalance, misalignment in the shaft, etc. the quantification of these faults are important to undertake remedial action. The conventional methods (without using mathematical model of the system) to quantify these faults is very time consuming and needs considerable engineering judgement and experience, and even then is generally found to be not so effective most of the time. Recently many research studies have been carried out to solve these problems more efficiently. They have used the mathematical models of machines – for examples, the research studies by Bachschmid and Pennacchi (2000), Bachschmid *et al.* (2002), and Platz *et al.* (2000). Edwards *et al.* (1998) gave the review of model based fault diagnosis (MFD) in the condition monitoring of rotating machinery. Hence the estimation of foundation model proposed in Chapter 5 to construct a reliable model of a complete rotor system is important for the MFD. The books on rotor dynamics by Vance (1988), Childs (1993), Genta (1993), Lalanne and Ferraris (1998), Rao (1996, 2000), and Friswell *et al.*, (2002) have many aspects involved in rotor dynamics modelling and analysis, and many earlier research references and case histories are also included in these books.

In general installation of condition monitoring systems need the combination of both hardware and software, and the kind of data measured and their storage needs to be considered. The intention of the chapter is to compile vibration based condition monitoring information in a very simplified manner so that condition monitoring can be well understood and implemented directly on the power plants. The organization of the chapter as follows.

(a) Type of Vibration Transducers required.
(b) Processing and management of vibration data.
(c) Different faults.
(d) Diagnosis of faults.
(e) Discussion on the MFD.

2.1. TYPE OF VIBRATION TRANDUCERS

The vibration is generally measured near the bearings in a rotating machine. To aid understanding, a small portion of shaft with a bearing pedestal instrumented with different types of vibration transducers is shown in Figure 2.1. Four types of transducers are shown in Figure 2.1 and they each have a different purpose. Every transducer requires some kind of power input and conditioning of the output signals such as conversion of a charge output into a voltage signal, band pass filtering, etc., shown in a unit for all of the transducers in Figure 2.1. The purpose of these transducers is explained below.

The tacho signal is used to measure the rotor speed and also gives the relative phase reference with the signals from the other transducers. Russell (1997) highlights the importance of phase measurement and its use in diagnosing machinery problems is discussed by Forland (1999). One tacho sensor is sufficient for the rotor of a machine.

The change in vibration amplitude due to a small change in structural or process parameters will be more significant in the horizontal and vertical directions. Hence the vibration measurement in these two directions is important, and is why the

accelerometers and the proximity probes are mounted in both the horizontal (x) and vertical (y) directions. Similarly an optical or laser sensor may be mounted in both directions, however for clarity only one is shown in Figure 2.1. The accelerometers measure the absolute acceleration of the bearing pedestals. The acceleration signal can be converted into a velocity and displacement signal. However the proximity probe measures the relative displacement of the rotor with respect to the bearing pedestal, so obviously this will have more information about the shaft vibration. The absolute vibration of the shaft at the measurement location can be obtained by adding or subtracting the two signals depending upon the phase relation between them (Laws, 1998). Alternatively, the absolute shaft vibration can be directly measured using an optical or a laser sensor. All these signals are generally utilized to identify faults in machinery. The kind of data management and signal processing required for fault diagnosis is discussed below.

2.2. DATA PROCESSING AND STORAGE

The data obtained from all transducers shown in Figure 2.1 are analog signals, and continuously vary with time. A sample of these signals is shown in Figure 2.2, assuming that the response of the system is purely sinusoidal to aid understanding. These online measured analog vibration data can be directly imported to a personal computer (PC) through suitable hardware and software by sampling the analog data at a sufficiently high sampling rate. However the storage of these data from all of the bearing locations during a normal machine operation, and transient operations like run-up and run-down, would need a huge storage capacity, and the data handing and retrieval would be difficult. The normal practice is to process the data to get the information required for machine health monitoring and then store the processed data for future use, and to identify a fault is becoming worse.

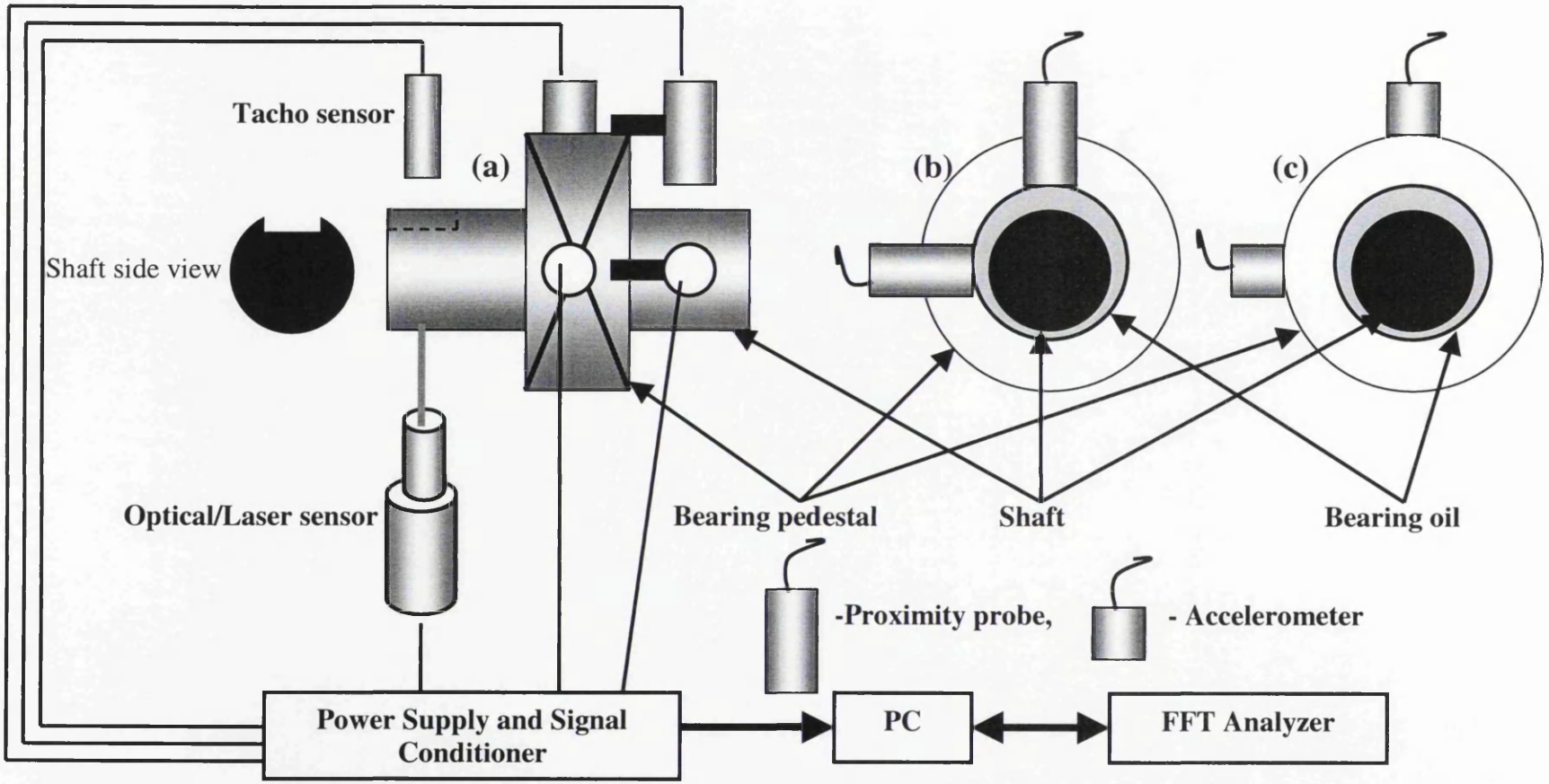

Figure 2.1 Mounting of different types of vibration transducers. (a) Front view of a bearing and shaft, (b) Side view –Accelerometers not shown for clarity, and (c) Side view – Proximity probes not shown for clarity.

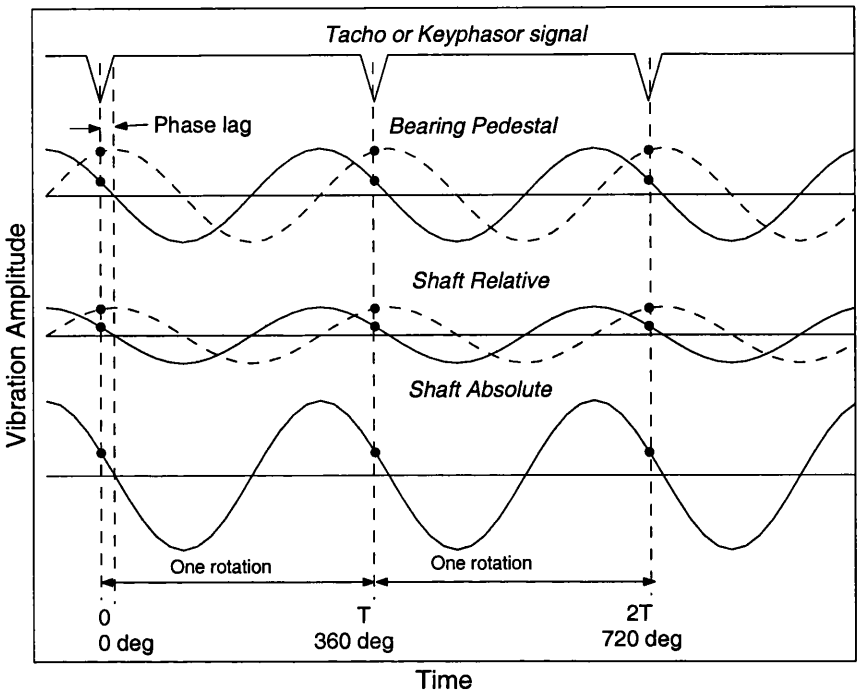

Figure 2.2 Time waveform measured from different transducers (_____ Horizontal direction, _ _ _ Vertical direction)

2.2.1. Normal Operation Condition

During normal machine operation the measurement of the following data at predetermined intervals are important.

2.2.1.1. Overall Vibration Amplitude

The overall vibration amplitude can be stored in term of acceleration, velocity or displacement. These values are specified in three ways – root mean square (*rms*), 0 to peak (*pk*) or peak-to-peak (*pk-pk*). For simple illustration, a displacement sine wave of 50Hz, indicating the meaning of *rms*, *pk*, and *pk-pk* values is shown in Figure 2.3(a). The time waveform shown in Figure 2.3(b) consists of both sub-harmonic and higher harmonics of 50Hz in the displacement signal. The *rms* value of a sine wave is equal to 0.707 times the *pk* value, however for any other kind of time waveform such as shown in Figure 2.3(b), the *rms* needs to be computed numerically.

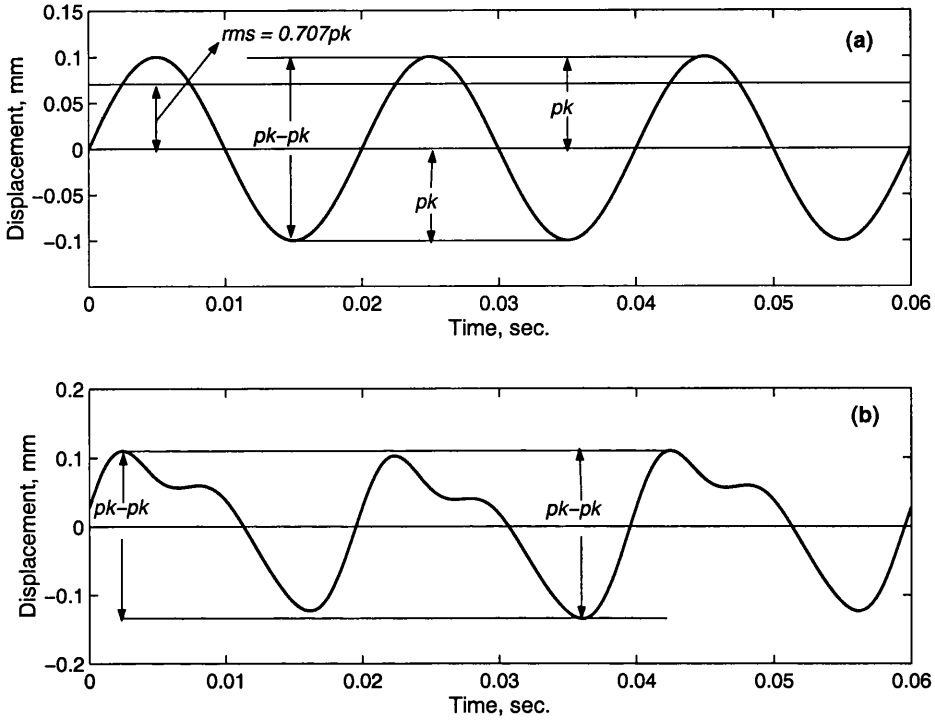

Figure 2.3 Time waveforms marked with peak, peak to peak, and rms amplitude of vibration

2.2.1.2. Vibration Spectrum

The time domain vibration signals should be converted into the frequency domain (Bendat and Piersol, 1980). The plots of vibration amplitude versus frequency (known as the spectrum) must be stored for comparison of day-to-day behaviour of machine performance. The vibration spectra of the time waveforms in Figure 2.3 are shown in Figure 2.4. Since the machine speed was assumed to be 3000RPM, the vibration amplitude at 50Hz is referred as 1X, 25Hz as 0.5X, 100Hz as 2X and so on as indicated in Figure 2.4. Change in the amplitude at these frequencies should be monitored, as these changes may be related to some kind of fault development.

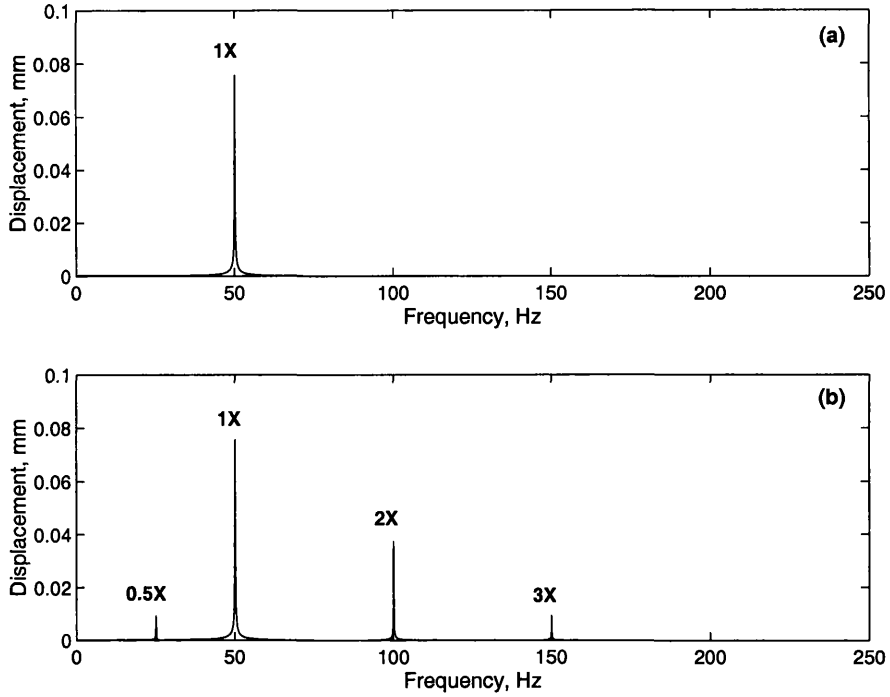

Figure 2.4 Vibration spectra of the time waveforms in Figure 2.3

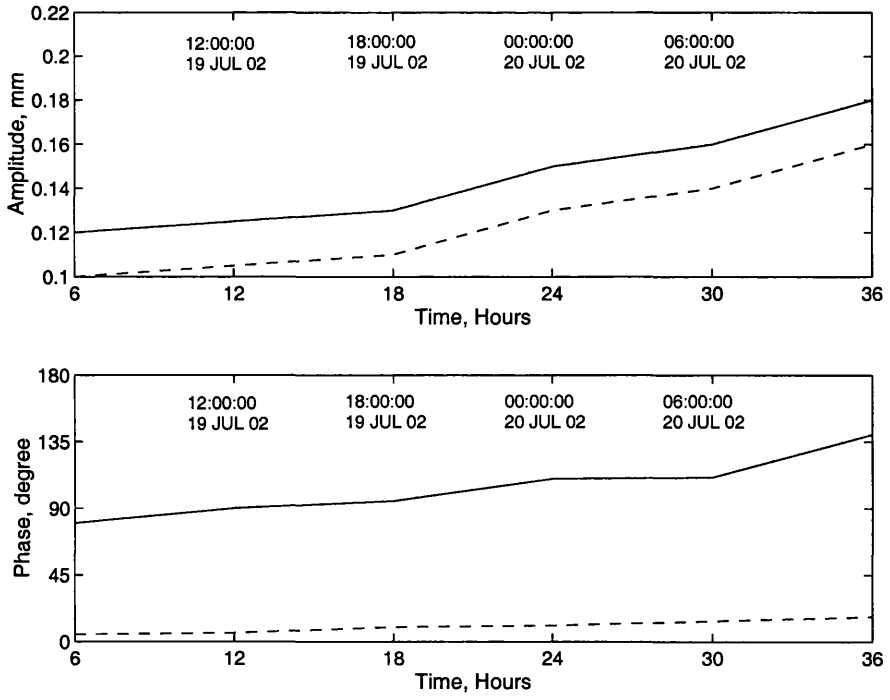

Figure 2.5 Variation of amplitude and phase of 1X component of shaft relative displacement with time (_____Horizontal, _ _ _ Vertical)

2.2.1.3. The Amplitude – Phase versus Time Plot

The 1X (or 2X, 3X,...) vibration amplitude and its phase relative to the tacho signal may be potted as a function of time for both the horizontal and vertical vibration at a bearing. A typical example of such a plot of 1X component for the vertical and horizontal shaft relative displacement with respect to the bearing housing and the phase as a function of the time of machine operation is shown in Figure 2.5.

2.2.1.4. The Polar Plot

Figure 2.5 can also be presented in a more compact way in polar coordinates as shown in Figure 2.6, which is called a polar plot. Thus only one polar plot for each bearing is sufficient to give the required information.

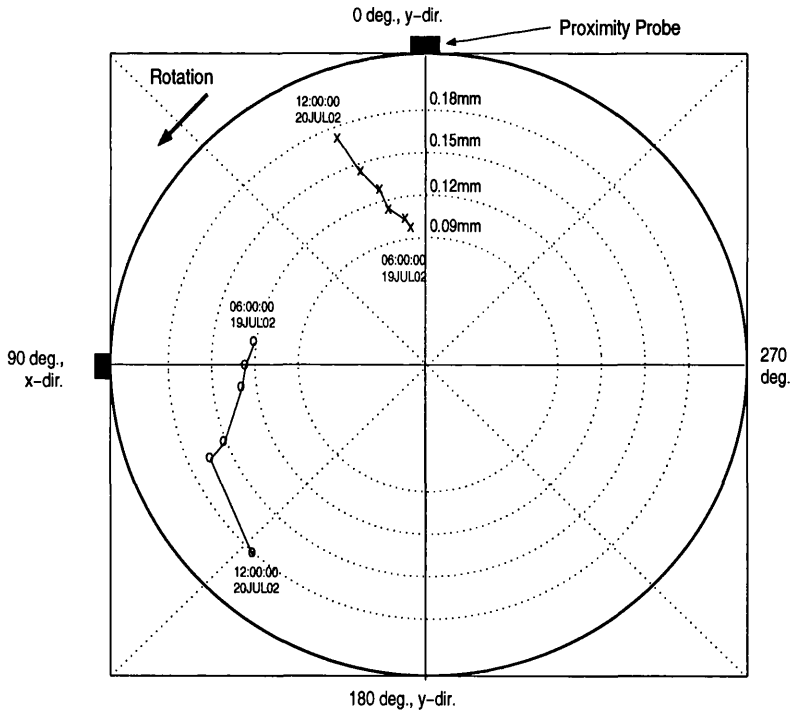

Figure 2.6 Polar representation of Figure 2.5 (o- Horizontal, x- Vertical)

2.2.1.5. The Orbit Plot

The *x-y* proximity probes shown in Figure 2.1 are used to measure the relative shaft displacement to the stationary bearing pedestal. The signal from such a non-contacting proximity probe consists of the following two components.

(a) A *dc signal* that is proportional to the average shaft position relative to the probe mounting. The *x-y* proximity probes give the shaft position in the bearing, and a change in shaft position during normal operation would indicate a load change or maybe bearing wears.

(b) An *ac signal* corresponding to the shaft dynamic motion relative to the probe mounting. The *x-y* probe signals give the shaft centerline's path as the shaft vibrates. For illustration, Figure 2.7 is shows an orbit plot obtained from the time waveform in Figure 2.2 for the shaft relative displacement measured by *x-y* probes. Perfect circlular orbit plot indicates that the supporting foundation stiffness is the same in the vertical and horizontal directions, and the rotor response is at 1X only. This plot is the forward orbit plot as the path of the rotor oscillation is in the direction of rotor rotation with respect to the keyphasor, otherwise it maybe a reverse orbit plot.

The orbit plot can be plotted either for the unfiltered time waveform or for the filtered component of 0.5X, 1X, 2X, etc. for each revolution of shaft. The shaft position and the orbit plots provide useful information about shaft malfunctions. Jordan (1993) discusses the usefulness of the orbit plots and the shaft position in the diagnosis of faults.

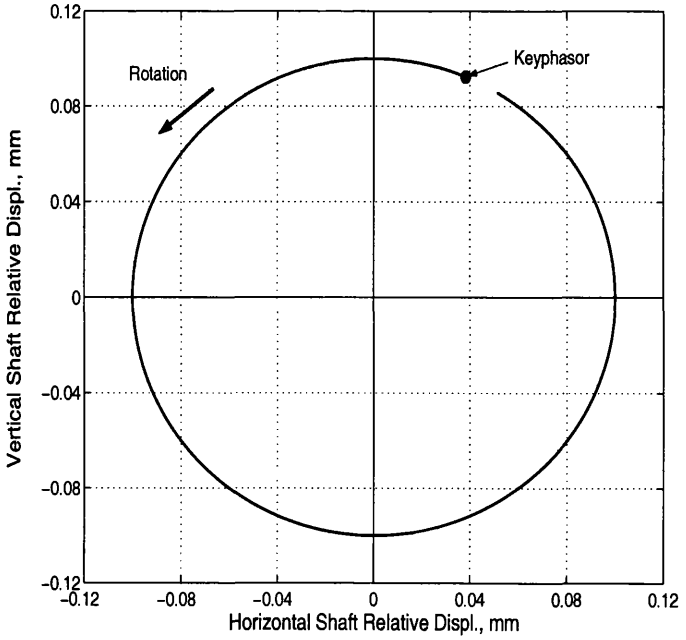

Figure 2.7 The orbit plot

2.2.2. Transient Operation Conditions

The start-up and run-down of a machine are considered as transient operation conditions. The measured data during this condition are very useful for confirming a fault identification and its subsequent diagnosis. Thomas (1995) gave the importance of transient data analysis. The time domain data for complete transient operation must be stored and the following data analysis should be performed.

2.2.2.1. The 3D Waterfall plot of Spectra

A 3D waterfall plot is a plot of the spectra of the *x-y* proximity probes at a bearing with shaft rotating speeds on the third axis. A simple such plot for a machine start-up from 700 RPM to 3000 RPM for the vertical (*y*) proximity probe is shown in Figure 2.8. The appearance or disappearance of any frequency components (multiples of 1X) or even a small abnormal change in the vibration amplitude at any frequency component can be recognized easily from this 3D waterfall plot of the spectra.

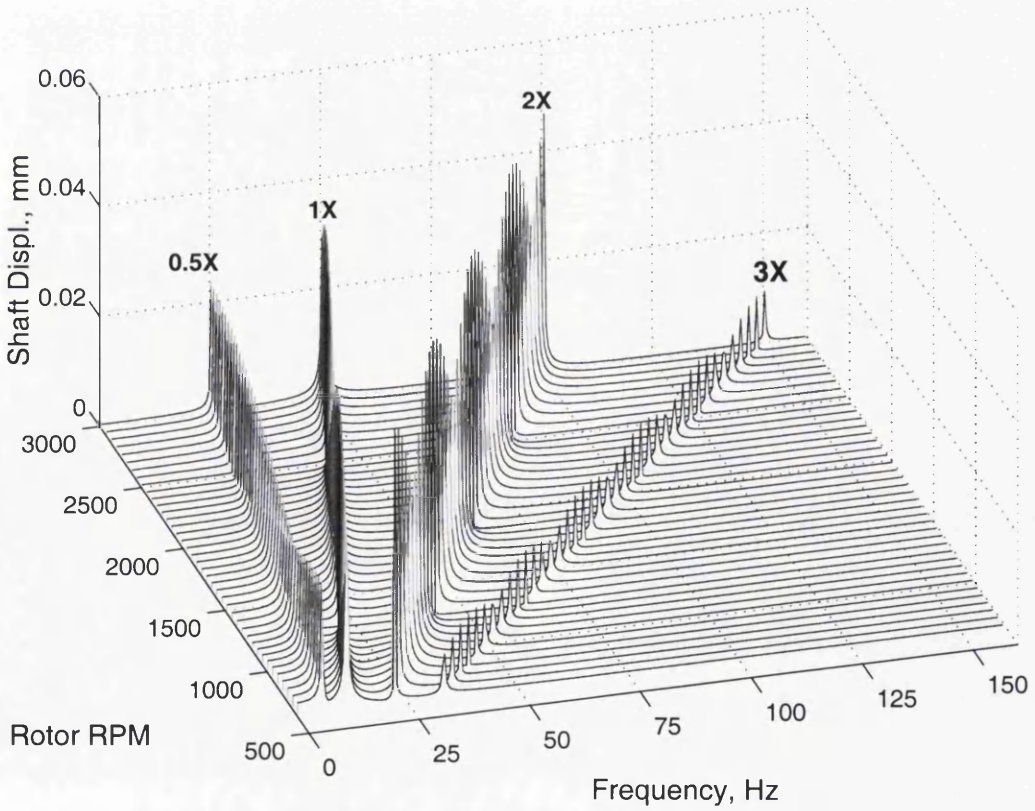

Figure 2.8 The Waterfall plot of spectra during machine run-up

2.2.2.2. The Shaft Centerline Plot

The plotting of *dc signals* of the x-y proximity probes at a bearing with machine rotating speed gives the shaft average centerline. This is useful for identifying changes in bearing load and bearing wear, as well as for calculating the average eccentricity ratio and the rotor position angle. The measured eccentricity helps in the understanding of fluid induced stability and is a parameter that can be directly used in the reliable mathematical modelling of fluid bearings. An assumed shaft centerline plot during machine start-up is shown in Figure 2.9. In Figure 2.9 the vertical and horizontal bearing diametral clearance is 0.44mm and at the start of the machine rotation the rotor was resting at bottom (180 degree) and then slowly moves up to 0.10mm with an angle 225 degree. This indicates that the rotor is rotating in counter clockwise (ccw) direction and the eccentricity (ε) of journal centre to bearing centre is 0.12mm.

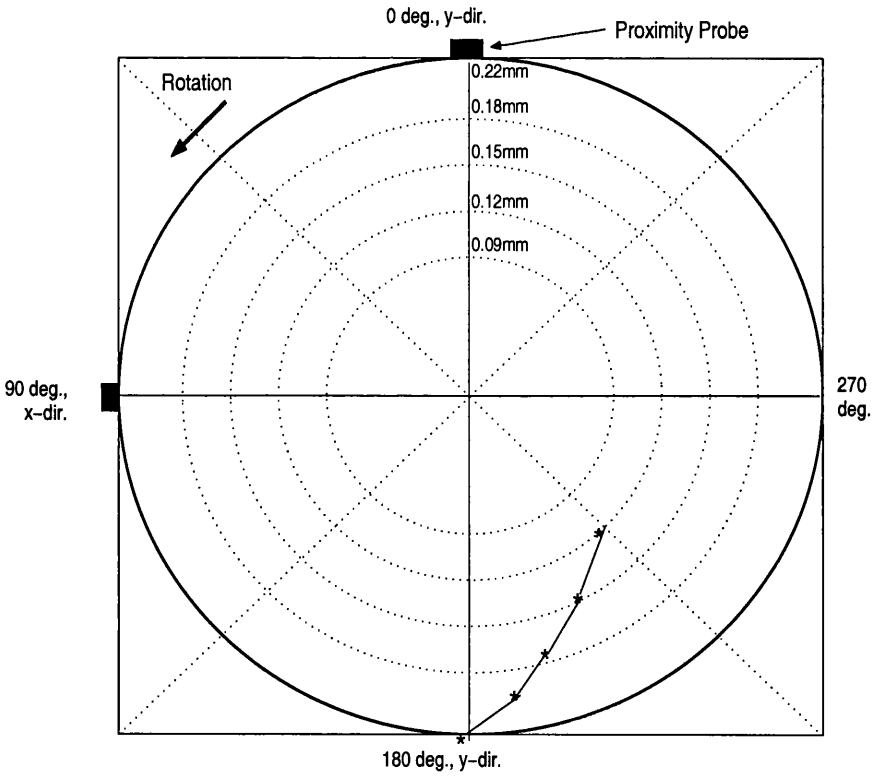

Figure 2.9 The shaft centreline plot

2.2.2.3. The Orbit Plot

The observation of orbit plots, both raw (unfiltered) and filtered 0.5X, 1X, 2X, etc. signals, with the change in machine speed during transient operation is important.

2.2.2.4. The Bode Plot

The measured data have to be order tracked (Bossley *et al.*, 1999, Fyfe and Munck, 1997) to extract the 1X and higher harmonics. The order tracking gives the vibration amplitude-phase relationship of 1X, 2X, etc. with the change in the machine's rotating speed. The plot of vibration amplitude and its phase with speed is known as the Bode plot. A typical Bode plot of 1X frequency component for an assumed machine, run-down from 2400RPM to 360RPM, is shown in Figure 2.10. As can be seem from Figure 2.10 for 1X, the plot is analogous to the frequency response function of standard modal tests (Ewins, 2000). The change in the rotor speed during a run-down is in fact similar to swept-sine excitation to the system from an external shaker. There are a total of four resonant peaks –two in the vertical and two in the horizontal direction in the run-down frequency range. These resonant peaks are known as machine critical speeds. The change in phase at these critical speeds is generally depends on the unbalance phase. But in case of pure unbalance problem, the phase shift would be 90 degree at the critical speeds in one direction (vertical) and in other direction (horizontal) by 180 degree. Changes in phase at the critical speeds are also indicative of the development of some faults.

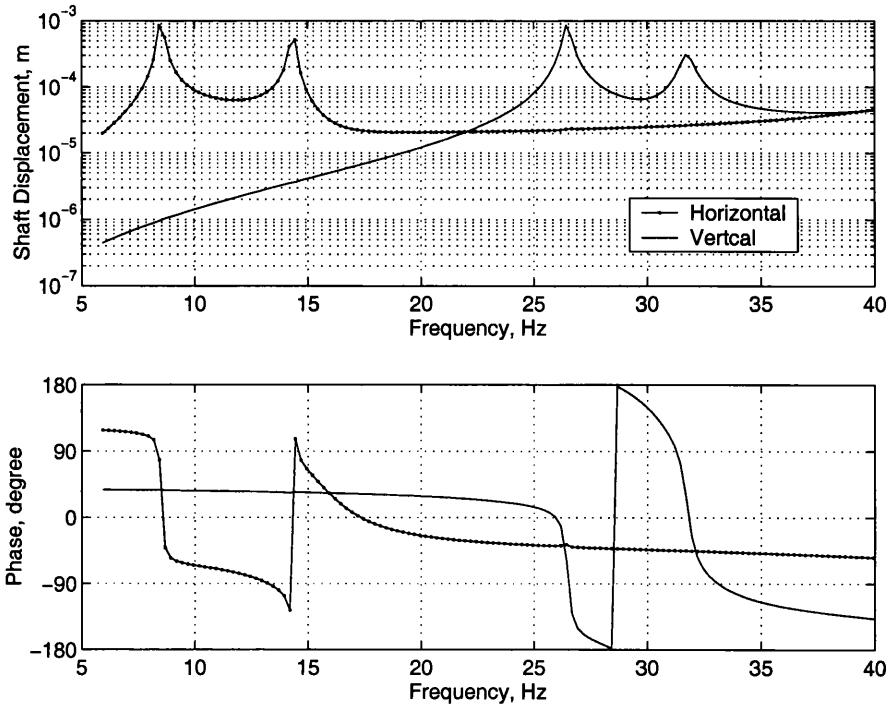

Figure 2.10 The Bode plot of 1X shaft displacement for a machine run-down

2.3. INSTRUMENTING TG SETS FOR CONDITION MONITORING

Considering the safety aspects of TG sets, the accepted practice in most modern power stations is to permanently install different vibration transducers at all possible locations in the TG set to monitor the vibration signals indicative of the machine performance during its normal and transient operations. A simplified diagram of a TG set instrumented with different types of transducers is shown in Figure 2.11. The installation of the accelerometers, proximity probes or any other transducers at a bearing should be similar to that shown in Figure 2.1.

It is well known that the vibration measurements near the bearings are generally indicative of the rotor status. But experience shows that the vibration of turbine blades in different stages generally does not affect the vibration measurements near the bearings. In particular the monitoring of the blades in the last stage of an LP turbine is important, because their fundamental frequency are usually as low as 2 to 3 times the machine rotating speed, and may be excited by small fluctuations in machine output power and/or operating condition. Indeed the catastrophic breakdown of TG sets observed in many power plants in the past was due to the failure of the last stage blades. However these blades could not be removed as they contribute approximately 10% of the total output of any LP turbine which is a significant contribution and cannot be overlooked. Better design is needed and, in fact the manufacturers have been in a constant search of better designs. Apart from design modification it is also important to monitor the last stage blade vibration so that their failure leading to a catastrophic breakdown of the machine, can be avoided. The best option is to install a pressure transducer on the casing near to the periphery of the last stage blades, but the transducer installation would not be easy. In the recent study by Rao and Sinha (2000), the monitoring of the last stage blade vibration is possible by measuring the vibration at the casing near the last stage blades of the LP turbine. Hence one accelerometer mounted on the casing in Figure 2.11 is for monitoring the last stage blade vibration of the LP turbine.

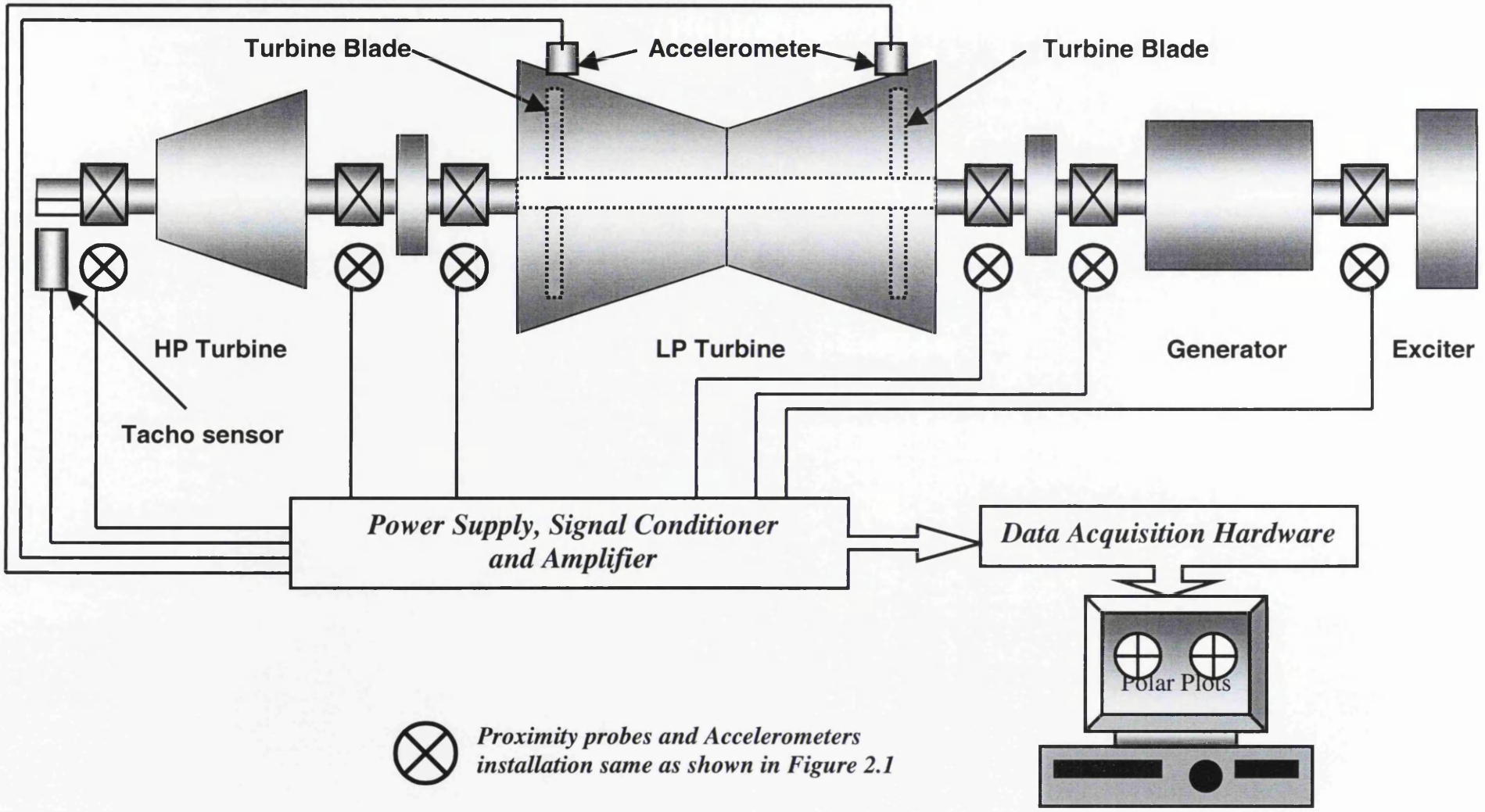

Figure 2.11 Schematic of Transducers installed on a TG set for condition monitoring

A variety of these transducers are available commercially and the selection of the correct transducers is important, depending upon the application. The selection of the transducers generally depends on the frequency range of the vibration measurement and the amplitude level. Although some guidelines for transducer selection is discussed by Laws (1998), there are no absolute rules for the selection and requires considerable experience in vibration measurement.

The measured signals should be processed as discussed in Section 2.2 and stored. The hardware and software required for data acquisition, management, processing, display and storage can be either developed in house or a commercially available system used. The advantage of the user's developed code is that the code can be modified to meet any proposed or required modification in the future. In fact a smart system for handling, processing the measured data and pattern recognition through a training the program for automatic online detection of the faults may be designed.

2.4. TYPES OF FAULTS

There can be many faults that develop or keep developing in a rotating machine during its operation. However the failure of machines in last few decades has always identified the probable cause for the failure in the post-failure study. Many failures have related to the system design and many others to human error – deviation in assembly and inaccuracy in manufacturing, as well as variation in the machine operation conditions. So there have been consistent efforts for many years on design modifications and the development of fault identification tools, so that the problems can be solved in the minimum possible time if a fault is identified. The machine performance shows that there has been a significant improvement in design as machines rarely fail due to design problems now-a-days. However other kinds of problems due to human error and deviation in operative conditions need to be avoided. The well recognized faults resulting from the other kind of errors than the design are listed below.

(a) Mass Unbalance.

(b) Shaft bow or bend.

(c) Misalignment and Preloads.

(d) Crack.

(e) Shaft rub.

(f) Fluid induced instability.

2.5. IDENTIFICATION OF FAULTS

The non-destructive and non-intrusive identification of these faults is discussed in this section. Many studies, both by experiment and numerical simulation, have been carried out to characterize faults. In experiments, faults have been introduced one by one in a laboratory scaled rotating rig by researchers to study the effects on different parameters. Many researchers have numerically simulated these experimental observations or behaviours of several industrial problems of rotating machines to understand the mechanism of the system malfunction, known as MFD. Goldman and Muszynska (1999) and Harris (1988) briefly discuss the state of art for the detection of faults. These identification procedures are outlined here.

2.5.1. Mass Unbalance

In practice, rotors are never perfectly balanced because of manufacturing errors such as porosity in casting, non-uniform density of material, manufacturing tolerances, and loss or gain of material (e.g., scale deposit on blades of steam turbines) during operation (Wowk, 1991). Obviously these will result in a high amplitude of rotor vibration. So the control of machinery vibration is essential in today's industry to meet the requirement for rotating machinery vibration to be within specified levels of vibration during machine operation.

Generally a predominant 1X component of the shaft relative or absolute displacement during normal operation may be an indicative of rotor unbalance. The polar plots of the 1X component for both horizontal and vertical direction near all of the bearings may show some increase in amplitude without any significant change in phase with

time. The Bode plot of the 1X component for the machine run-down (transient operation) should look similar to Figure 2.10.

2.5.2. Shaft Bow or Bend

Bent or bowed shafts may be caused in several ways, for example due to creep, thermal distortion or a previous large unbalance force. The forcing caused by a bend is similar, although slightly different, to that caused by mass unbalance. The shaft vibration spectra are generally dominated by the 1X component, but the 1X amplitude and its phase in polar plots (or Amplitude-Phase versus Time plots) may vary significantly with time during normal machine operation unlike mass unbalance. The best way to detect the presence of the shaft bow through the transient operation of machine. There may be a significant change in the 1X amplitudes and phases when machine passes through the critical speeds during machine transient operation. These changes in general depend on the shaft bow angle.

One of the first extensive investigations into shaft bow was made by Nicholas *et al.* (1976a) on the unbalance response by both experiment and analysis. Since then many studies on the shaft bow response have been carried out. Prominent among these studies are those by Flack *et al.* (1982), Parkinson *et al.* (1984), Meacham *et al.* (1988), Edward (1999), and Rao and Sharma (2000).

2.5.3. Misalignment and Preloads

The preload and the misalignment in rotor system are inter-related (Southwick, 1994). The most general source of the preload is a unidirectional steady state force acting on the fluid bearings in rotor systems due to the shaft self weight. Other sources of preloads are due misalignment in the shaft at coupling locations, or relatively small off-sets in the bearings position. In practice the shaft misalignment may be of three types – parallel, angular or coupled misalignment. It is generally accepted that a significant 2X vibration response of the shaft relative displacement is a major feature of misalignment (Jordan, 1993) and the orbit plot consisting of 1X and 2X signals may be close to the shape of a *'figure eight'* if misalignment causes excessive loads. The affect on 1X vibration behaviour is generally believed to be small. There is some analytical evidence and some limited experiments to justify these observations. Gibbsons (1976) attempted to simulate the shaft misalignment behaviour analytically

assuming that misalignment causes forces and moments at the shaft coupling. This concept has been followed by many researchers - Simon (1992), Xu and Marangoni (1994a, b) and Sekhar and Prabhu (1995). In the present study the estimation of misalignment based on this concept has been suggested and discussed in Chapters 5 and 7. Ehrich (1992b), and Dewell and Mitchell (1984) gave reviews of the potential existence of 2X vibrations.

2.5.4. Crack

If a crack develops in the shaft, the stiffness of the shaft will vary from high-to-low-to-high in a complete revolution of the shaft due to the breathing (opening and closing) of the crack due to the rotor self weight (Mayes and Davies, 1984). This behaviour of the crack shaft also generates a 2X component similar to shaft misalignment. But unlike the misaligned shaft, both the amplitude and phase of the 1X and 2X components change with the time of machine operation due to the propagation of the transverse crack. This can be observed in either the polar plots or the amplitude-phase versus time plots (Bently, 1982). The orbit plot consisting of 1X and 2X components may change from a single loop to double loops like a *'figure eight'*. However during transient operation of the machine, the shaft vibration may be very high when the machine speed will be passing through nearly half of the machine critical speed. At this particular moment the shape of the orbit plot will change from a *figure eight* to a loop containing a small loop inside indicating a significant change in the phase and amplitude of the 2X vibration which is close to the system natural frequency (Bently, 1986, Bently and Werner, 1990). Recent experimental observations on a cracked shaft supported on a rigid foundation during machine run-up are similar to above and are shown in Figure 2.12. As can be seen from Figure 2.12, a single loop (with small distorted shape) in the orbit plot at lower speeds has changed to the *figure eight* as the speed increases and then to a *loop containing another loop* when the rotor rig speed reaches nearly half of the critical speed. Analytically such an observation has been shown by Jun *et al.* (1992), and Yang *et al.* (2002).

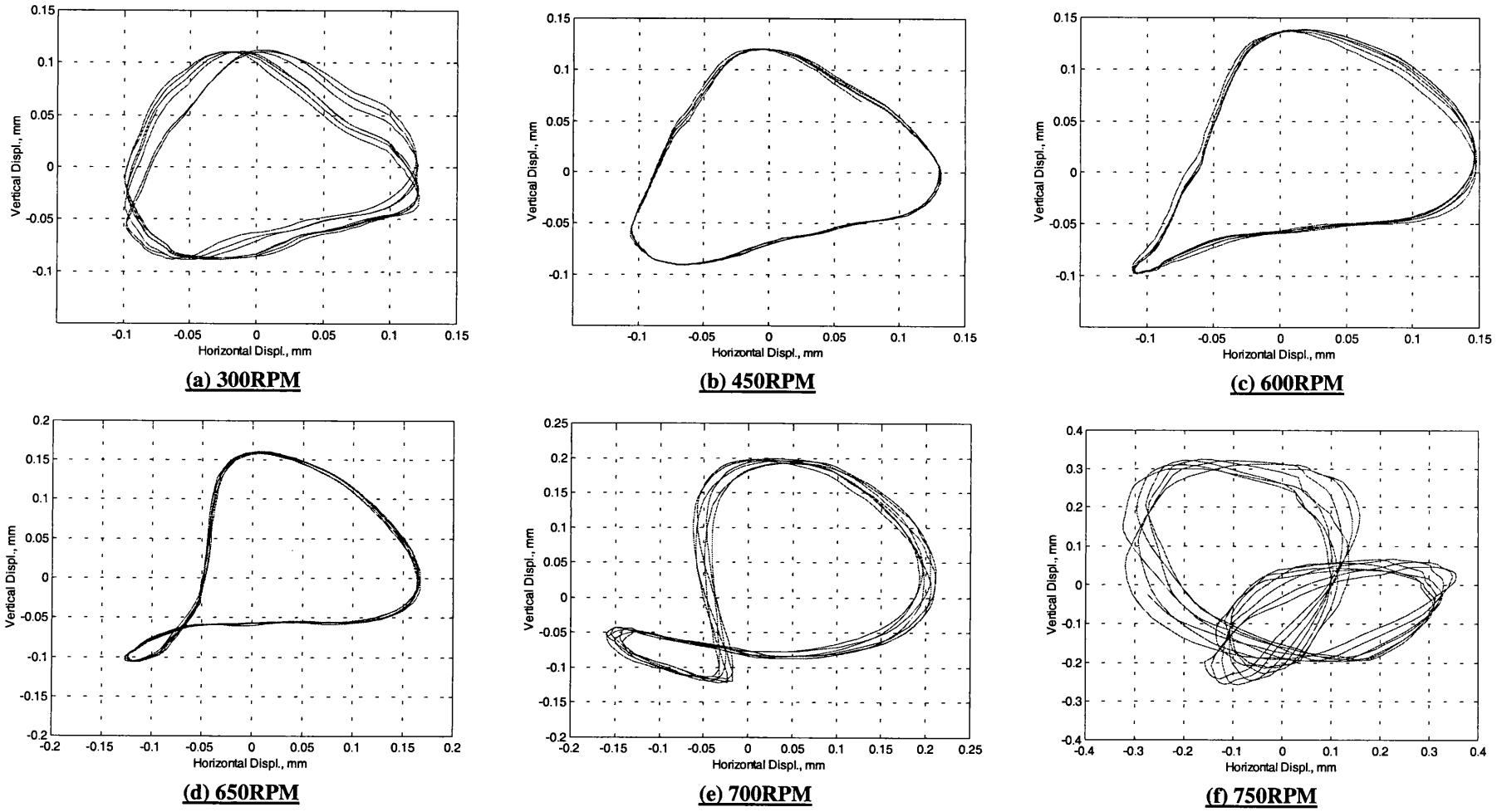

Figure 2.12 Orbit plots at different rotor speed during the small rig run-up

2.5.5. Asymmetric Shaft

In many industrial applications an asymmetric shaft is used. In such cases the shaft stiffness varies in a similar way to a cracked shaft during rotation. Hence such shafts would also generate 2X vibration, but the amplitudes and the phases at 1X and 2X are expected to be constant with time for the rotor system having asymmetric shaft. So it is important to know the difference in the 1X and 2X behaviour of a cracked shaft, shaft misalignment and an asymmetric shaft. The ratio of 1X and 2X components, both amplitudes and phases, will not change with time for an asymmetric shaft, change in both components will occur for cracked shaft if crack propagates with time, and 1X may be invariant but 2X may change with time in the case of shaft misalignment. Furthermore 2X components of shaft vibration would appear right from the start of machine operation in the case of an asymmetric shaft and misalignment. Thus it is important to measure the vibration response when the shaft is aligned, especially for a machine with an asymmetric shaft, to distinguish if the 2X component is due to an asymmetric shaft or misalignment.

2.5.6. Shaft Rub

Rotating machine rubs that occur when a rotor contacts the machine stator. Rubs are generally classified as a secondary malfunction as they may typically be caused by primary malfunctions like a poorly balanced rotor, turbine blade failure, defective bearings and/or seals, rotor misalignment, bowed shaft either mechanical or thermal, deformed casing, etc. The shaft rub may be of two types – partial or full annular rub. Partial rubs are often of the "hit and bounce" type behaviour of a rotor in its bearings. A partial rub usually precedes a full rub causing an increase in the rotor stiffness and the friction force. The behaviour of the system during this period is highly non-linear and may also be chaotic.

Bently (1983a, 1994) and Forland (1999) gave the basis for the detection of partial and full annular rubs based on the experimental observations. Since it is a complex phenomenon it is necessary to use orbit plots, shaft centreline position plots, polar plots and spectrum plots. The general observation is that the rub generates subharmonic X/2, X/3 components of shaft displacement in the vibration spectrum plots, and it should be followed by other checks to confirm the rub existence, such as the polar, orbit and shaft centreline position plots during normal machine operation.

The abnormal change in amplitude and phase of the 1X component with time in the polar plots may be indicative of the rub transition phase from a partial to a full annular rub. The unfiltered orbit plot may change from a multi-loops orbit at a partial rub to an orbit plot where the radius equals the bearing clearance at a full annular rub. The shaft centerline plots may help in identifying the nearest rub location. The presence of subharmonic (X/2 or X/3) along with the 1X and orbit plots may be observed during run-up and run-down that to be similar to normal machine operation. However sometimes in case of a full annular rub, self-excited rotor response occurs due to the increase in friction forces (counter acting the machine forward torque) at the rub at a rotating speed just near the first critical speed and remains locked to a low speed during the run-down or a high speed during the run-up. The 1X component may not be observed in such cases. A typical example of such a phenomenon is shown in Figure 2.13. Other than the presence of a subharmonic component in the standard spectrum plots, the spectrum computed by principal component analysis and an autoregressive technique (PCAT) is suggested as an efficient method for rub detection (Zhengjia *et al.*, 1990).

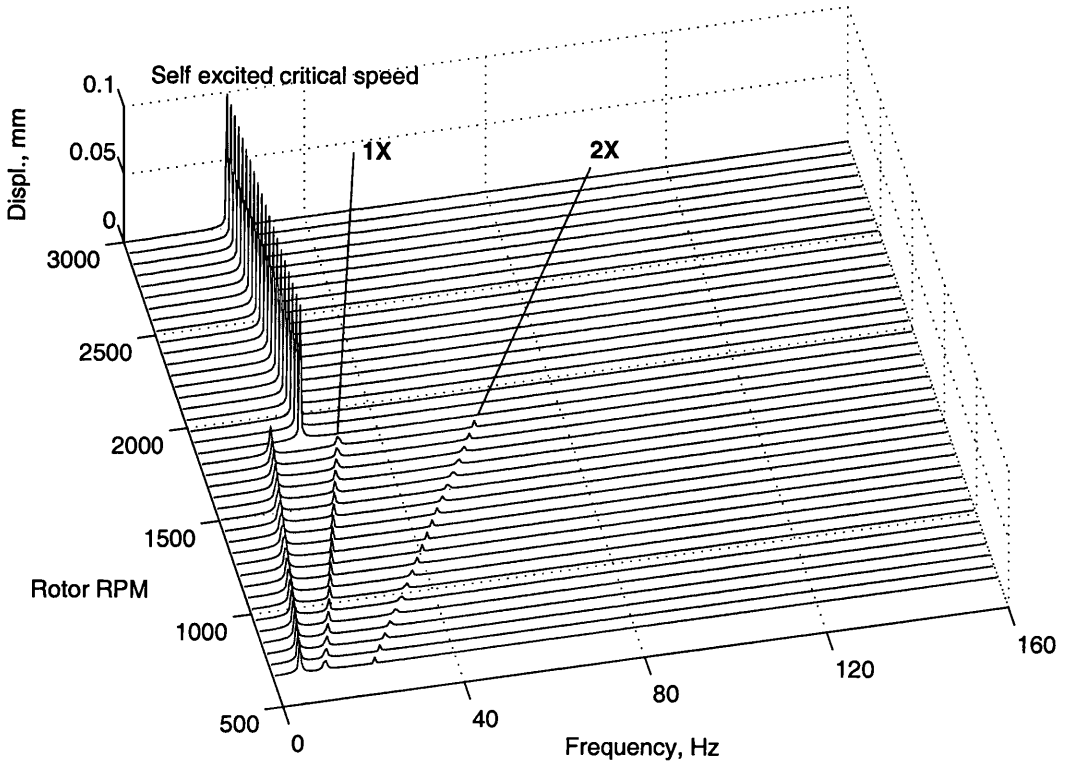

Figure 2.13 A typical case of a full annular rub during a run-up

Many research studies have considered rubs but most of them are oriented towards the development and improvement of mathematical models so that the rubbing phenomenon could be accurately understood. Muszynska (1989) wrote a thorough review of the topic. Muszynska (1993) then demonstrated the effect of the thermal/mechanical rotor-to-stator rubbing in a heavy rotating machine through a simple mathematical model. Ehrich (1988) demonstrated the presence of subharmonic frequency components due to a rub, that leads to chaotic responses in his analytical study (Ehrich, 1992a). Goldman and Muszynska (1994a, b) have successfully showed numerical simulations of several experimentally observed rubbing behaviours. Edwards *et al.* (1999) examined the influence of torsional flexibility on the rotor-stator rubbing in their analytical study.

2.5.7. Fluid Induced Instability

A fluid induced instability is commonly referred as *Oil whip* which is resulting from *Oil whirl* and they are typically occur in fluid bearings. This is actually a fluid induced self-excited phenomenon leading to lateral shaft vibration. When the shaft rotates in the bearing the fluid surrounding the journal also rotates at some circumferential speed ($\lambda\Omega$) relative to the shaft speed (Ω), where λ is known as the fluid average velocity ratio. The ratio λ is generally a non-linear function of the fluid bearing radial stiffness, which depends upon the shaft eccentricity ratio (Muszynska and Bently, 1989, 1996, Southwick, 1993). It has been observed experimentally and analytically that the fluid bearing radial stiffness increases with the journal radial deflection and the velocity ratio λ decreases from maximum to zero i.e., journal is in direct contact with the wall of bearing. The fluid resonance frequency of the fluid in the bearing during shaft rotation is normally slightly less than the half of the shaft rotating speed, say 0.48Ω. If during machine operation or start-up the fluid circumferential speed comes close to the fluid resonance frequency an instability of the shaft occurs that is known as *Oil whirl*. This is generally identified by the presence of a λX (usually 0.45-0.48X or less) component in the spectrum and the forward circular orbit plot for the filtered λX component irrespective of the asymmetric stiffness in the vertical and horizontal direction (Jordan, 1993). If the rotor system natural frequency is equal to the fluid resonance then the system would be completely unstable. The orbit plot may then be of the order of the bearing clearance. This

phenomenon is known as *Oil whip*. *Oil whip* can occur at the first lateral mode as well as at higher modes of the rotor. *Oil whip* generally occurs during machine start-up, that initiates with *Oil whirl* and then gets locked to the *Oil whip* when the shaft speed passes through a critical speed. A typical example during a machine start-up is shown in Figure 2.14.

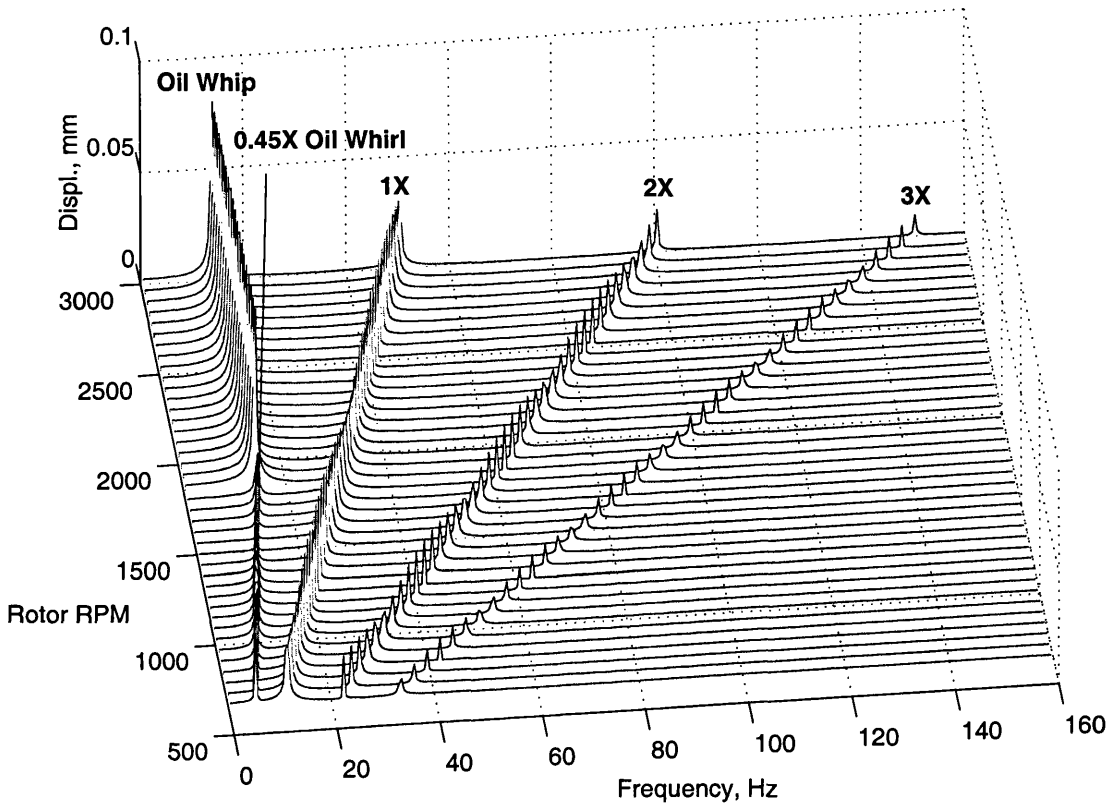

Figure 2.14 A typical case of Oil Whirl – Oil Whip during a machine run-up

Rotor systems like TG sets have many fluid bearings, and if a fluid-induced instability is observed during machine operation it important to identify the bearing that is causing such instability. Forland (1999) indicated that the phase relation at the frequency of instability (λX) of the shaft relative displacement between the measurements at all the bearings can be used to identify the bearing. The bearing which may be suspected as the source of instability, its shaft relative displacement at the λX frequency component will have a phase lag with respect to the shaft relative displacement at other bearings.

Several research studies have been carried out using both experiments and analysis to understand the fluid induced instability. The papers by Muszynska (1986a, 1988) may be useful in understanding this phenomena.

2.5.8. Mechanical Looseness

Bolts joints and the bearing assembly may loosen over a period of normal machine operation. This looseness generates sub-harmonics (X/2 or X/3) and higher harmonics of the shaft displacement during normal operation of machines (Harris, 1988, Mitchell, 1978).

2.5.9. General Comments

The identification procedures for known faults in rotating machines are explained above. However it is often observed that more than one fault appears simultaneously so the identification may not be straightforward and it may require considerable experience in condition monitoring.

2.6. CONDITION MONITORING

Estimating the modal parameters of the machine before any condition monitoring begins would be better and will help in understanding the dynamic behaviour of the machine. These modal data can be obtained by conducting modal tests (Ewins, 2000). Several research studies (Muszynska, 1986b, Ewins, 1998) give more specific procedures for modal testing and parameter identification related to the rotating machines but so far it has not been done on the real machines. As discussed earlier in Section 2.0. that there is always two aspects in condition monitoring – *Prediction of faults and their quantification* so that the remedial action can be planned. The prediction part has already been described in Section 2.5. and their possible quantification is being discussed here. However when discussing the condition monitoring of Steam TG sets, or any other machines, the information gathered from the measured vibration data needs to be classified into different categories to address the different kind of plant personnel. Different groups in a plant may not be familiar with the machines (other than machine operation) and the vibration based diagnostic

techniques but their primary objective is to achieve optimum productivity without affecting the safety of the plant. So the coordination or sharing of information among them is very important. To meet this requirements vibration based information is generally divided into the following three category (Bently, 1983b, Sabin, 1997).

2.6.1. Operational Personnel

These are the people who are concerned with productivity, so for them the information required is whether to run the machine or not. The International Standard Organization has recommended vibration severity limits for machines during normal machine operation and the code *ISO 2372* (1974) gives general guidelines for rotating machines with operating speeds ranging from 10 to 200 rev/s. The codes *ISO 3945* (1980) and *ISO 7919* (1986) provide vibration amplitude limits for steam TG sets. A brief review of these codes can be found in the handbook by Harris (1988). These codes recommend maximum overall vibration amplitudes measured at the recommended locations of machines. The code *ISO 3945* (1980) gives a vibration severity criteria for rotating machines like TG sets supported on rigid or flexible foundations but it assumes a rigid rotor. It recommends the maximum value of the *rms velocity* of vibration amplitude measured at the bearing pedestals in the frequency band of 10Hz to 1000Hz. The vibration severity values as per *ISO 3945* are listed in Table 2.1, and shows that the recommended vibration limits as per this code are independent of the machine operating speed. The recent code *ISO 10816* has been revised to make it suitable for large rotating machines and gives the vibration severity limits at the machine operating speed (Parkinson and McGuire, 1995). The vibration limits as per this code are listed in Table 2.2. These codes are concerned with the vibration of non-rotating parts i.e., bearing pedestals of rotating machines. However the code *ISO 7919* (1986) is directly related to the vibration of the rotating shaft and is applicable to a flexible rotor supported on a flexible foundation. Part 1 of *ISO 7919* gives the measurement guidelines that apply to shaft vibration, measured close to the rotor bearings under normal operating conditions. It recommends both the relative as well as the absolute shaft displacement. The code *ISO 7919 Part 2* (1986) gives the charts for the vibration severity limits to compare measured values and assess the machine overall condition. Parkinson and McGuire (1995) gave an excellent review of the ISO codes related to rotating machines. So for the operational personnel the trend of overall vibration values are sufficient.

Table 2.1 Vibration Severity Limits as per ISO 3945

RMS Velocity (*mm/s*)	Rigid Foundation	Flexible Foundation
0.44 0.71 1.12 1.80	GOOD	GOOD
2.80	SATISFACTORY	
4.60		SATISFACTORY
7.10	UNSATISFACTORY	
11.20		UNSATISFACTORY
18.00	UNACCEPTABLE	
28.00 46.00 71.00		UNACCEPTABLE

Table 2.2 Vibration Severity Limits at Bearing Pedestal for Large Steam TG sets as per ISO 10816-Part 2 (Parkinson and McGuire, 1995)

RMS Velocity (*mm/s*)	ROTOR RPM			
	1500	1800	3000	3600
2.80	A	A	A	A
3.80	B	B		
5.30			B	B
7.50	C	C		
8.50			C	C
11.80	D	D		
			D	D

Zone A – Good, B – Satisfactory, C- Unsatisfactory, and D – Unacceptable

2.6.2. Plant Maintenance Engineers

Plant maintenance engineers are responsible for overall plant safety. They may not be the experts in vibration based diagnosis but they can be trained to understand and observe several things during machine normal operation such as the trend of the overall vibration, spectra, Polar or Amplitude-Phase versus Time plots, Orbit plots (filtered and unfiltered). Any change in the amplitude and phase at 1X and its subharmonics or higher harmonics can be noticed, and if these changes are persistent

or increasing with time then a shutdown may be planned and the machine experts called to identify and solve the problems. It is also likely that the maintenance personnel will develop the required skills over a period of involvement in vibration monitoring that enables them to solve the problems without consulting the machine experts.

2.6.3. Machine Experts

Machine experts usually look at previous vibration data during normal machine operation and the vibration data during transient operations to identify the faults accurately as per the features outlined in Section 2.5. Their quantification and the remedial actions required to solve the problems are discussed below.

2.6.3.1. Mass Unbalance

Several researchers have proposed many methods for balancing the rotor to reduce the machine vibration. Some comprehensive reviews are given by Darlow (1987), Parkinson (1991), Foiles *et al.* (1998), and Zhou and Shi (2001). The recent review by Zhou and Shi. (2001) is, in fact, on the techniques for the active balancing and vibration control of a rotor system. An automatic balancing system to control the machine vibration would be good, but it is still a research topic and will require many more years to mature for plant use. However there are many other methods which have been in use for many years to reduce the machine vibration. Broadly these methods can be categorized into two classes – balancing using measured 1X responses only (known as *Experimental Balancing Approach*), and balancing using both measured 1X responses and a mathematical (often FE) model of the rotor or machine.

The experimental balancing method (Eisemann, 1997) is the most popular and accepted conventional approach used in power plants. In this method several runs of the machine are required to know the influence coefficients of added trail mass at different planes, so that the corrective mass for different unbalance planes can be estimated. This method has a long history of development since the early 1930s, from two plane balancing using two sensors at a single machine speed (Thearle and Schenectady, 1934, Baker and Evansville, 1939, Hopkirk, 1940) to multi-plane balancing using multiple machine speeds (transient operation) and measurement

locations (Goodman, 1964, Tessarzik *et al.*, 1972, Pilkey and Bailey, 1979, Pilkey *et al.*, 1983). The most recent study by Zang *et al.* (2002) has used a single sensor for multi-plane balancing of a rotating machine. The method requires a number of machine run-downs for the calculation of the influence coefficients, but it is useful for the case where the number of available measurement locations is small.

The other class of balancing methods is of two types – the Modal Balancing method, and the Direct Balancing method. Both methods are based on a mathematical model of machine along with the measured responses. These approaches generally require fewer machine runs with trail masses added to balance disks compared to the earlier method. Thus these methods will reduce the downtime of the machine. The modal balancing method was first proposed by Grobel (1953) and this concept has been further followed/improved by by Bishop and Gladwell (1959), Bishop and Parkinson (1972), Saito and Azuma (1983), and Morton (1985). In this approach each mode in the range of the machine run-down or run-up is balanced with a set of masses at a time in different unbalance planes. Hence it requires N-planes for N-modes. Darlow (1987) has suggested an unified balancing approach by utilizing the advantages of both the influence coefficient and modal balancing methods. However for accurate unbalance mass estimation a good FE model of the rotor system is important as the method uses analytically computed mode shapes of the rotor. As brought out earlier in Chapter 1, usually an accurate FE model is the rotor and fairly accurate model of fluid bearings may be constructed, but it is often impossible to construct a reliable FE for the foundation. Hence the implementation of this approach may not be straightforward.

On the other hand the direct method for rotor unbalance estimation developed recently by Lees and Friswell (1997) seems to have potential for fast and reliable unbalance estimation in a quicker manner. The method uses the measured vibration data during a single run-down (one transient operation only) of a machine along with a model of the rotor and fluid bearings only to estimate the multi-plane unbalance in a single step. The foundation parameters are estimated as by-product, and hence the method accounts for the dynamics of the foundation also. So the inaccuracy in the FE model of the complete rotor system due to the foundation is overcome. The method has been demonstrated on a simple experimental rig (Edwards *et al.*, 2000) and has been further

modified to suit the plant conditions (Sinha *et al.*, 2001, 2002b). The method was also observed to be robust to the presence of the modelling (Lees *et al.*, 2002). The modification in the method, its usefulness and the robustness of the method has been discussed in details in Chapters 5, 7 and 8.

A brief review of most of the methods with their advantages and limitations has been discussed. All the above methods will more or less serve the purpose of reducing the machine unbalance but may require some user experience during the balance estimation.

2.6.3.2. Shaft Bow or Bent

If a bend is suspected in the rotor, the bent profile of the shaft along with the rotor unbalance estimation can be estimated using the measured 1X responses by the method proposed by Edwards (1999) and Edwards *et al.* (2000). The bend can be corrected and after the rotor has been rebalanced the machine can be put back to the operation. Alternately if the bend is small and the correction is costly, then the estimated corrective masses may be added to the respective planes without bothering about the bend in the shaft. This will reduce the machine vibration at the operating speed but may not be balanced at all frequencies in the machine run-down speed range. Many researchers (Nicholas *et al.*, 1976b, Parkinson *et al.*, 1984, Meacham *et al.*, 1988) have advocated such an approach for reducing the machine vibration for a bent shaft.

2.6.3.3. Misalignment or Preloads

Several analytical simulations have been performed to understand the reason for the presence of 2X components in shaft relative displacement but unfortunately no analytical tool has been developed earlier that can directly estimate the amplitude of the shaft misalignment at the coupling of multi-shafts within the rotor. If misalignment is detected in the rotor then it needs to be aligned, and this may be time consuming process because of unknown locations and amplitudes of misalignment in the rotor. Campbell (1993) discusses different alignment methods used in practice.

In the present study a method is developed to estimate both rotor unbalance and misalignment using measured response at the bearing pedestals during a single

machine run-down which is discussed in Chapters 5 and 7. Hence the method is expected to reduce the rotor alignment time drastically.

2.6.3.4. Crack

Wu and Huang (1998) have suggested a method for on-line detection of crack size and location in a shaft using 2X components of shaft displacement through a simple numerical model. The practicality of this approach needs to be investigated as the breathing of a crack during shaft rotation and the dynamics of a flexible foundation may complicate the problem.

However the offline identification of crack size and location may be relatively simple. Doebling *et al.* (1996, 1998) gave an extensive survey on the detection of crack size and location in structural system from their vibration properties. Wauer (1990) and Gasch (1993) considered the dynamics of cracked rotors. Sinha *et al.* (2002c) gave a broad survey of previous modelling approaches for cracks before proposing their own simplified model for crack modelling and detection. Penny and Friswell (2002) have further advocated the usefulness of this simplified model for cracks in condition monitoring.

2.6.3.5. Shaft Rub

There is no simple rule to directly diagnose if a shaft rub is detected or confirmed and in fact, a through investigation is required. The shaft centreline plots may help in identifying the rub location. Since a rub is generally caused by some primary malfunction of the shaft, the following probable reasons should be checked and the system to be rectified accordingly.

(a) Earlier vibration data to know whether the rub is due a primary malfunction of the shaft such as unbalance, bow, misalignment, blade failure, etc. or not.
(b) Bearing lubrication.
(c) Alignment of all of the bearing housings.
(d) Bearing seals.

2.6.3.6. Fluid Induced Instabilities

In practice this effect is usually considered while designing the systems to avoid the occurrence of such phenomena. The important factors are short and stiff shafts and better designs of the bearings, instead of plain cylindrical bearings. Perhaps the scope of modifying the shaft design may be limited, however improvement in the fluid bearing may be possible and significant improvements have been achieved in bearing design. These improvements are the use of elliptical or lemon-shaped bearings with grooves and multi-lobes, rough journal surfaces, and bearings with mobile parts (such as a tilting pad bearings), option of fluid anti-swirl injections in bearings instead of just plain cylindrical bearings, to avoid the increase in the fluid circumferential velocity (Muszynska and Bently, 1996). These types of fluid bearings are generally used in machines. However there is always a possibility of some system failure causing drop in a fluid pressure, leakage, and/or human error during bearing assembly that may lead to fluid-induced instability. If such situation arises that can be identified and solved accordingly.

2.6.3.7. Blade Vibration

There is little literature on the measurement of blade vibration in condition monitoring and absolutely no rule on of vibration severity limits. Considerable engineering judgement is required for the person involved in the condition monitoring to interpret or utilized these data. One possibility is to observe and record the vibration level at the blade natural frequency and its frequency during machine normal operation so that these can be compared. Hence any significant change in vibration amplitude or a shift in natural frequency in future should be investigated to avoid any failure.

If the amplitude relation between the actual vibration amplitude of the blade and the amplitude measured at turbine casing can be established, either through analysis or experimental simulation on laboratory scale model, then the maximum alternating stress of the blade can be estimated and compared with the endurance limit. The fatigue failure life of the blade may then be estimated. Rao *et al.* (2001) gave a comparison of different cumulative damage theories for blade life estimation.

2.7. COMMENTS ABOUT MODEL BASED FAULT DIAGNOSIS (MFD)

Most numerical simulations by researchers have assumed very simple rotating machine models to understand the machine malfunctions. The foundation models for such numerical simulations have been in general assumed to be either rigid or a simple model. Hence such an approach is good for understanding the rotor system phenomenon only. However to really understand the machine faults and its solution it is necessary to have or develop a good mathematical model of that machine e.g., models of the rotor, the fluid bearings and the foundation (often flexible) for TG sets. Inclusion of the foundation model is very important as it is observed that the dynamics of the flexible foundation also contributes significantly to the dynamics of the complete machine.

As discussed in Chapter 1 that the construction of a reliable FE model for the foundation is difficult due to many practical limitations and hence the estimation of a model of the foundation directly from measured vibration data has now considered as a most promising approach. Many of the earlier studies (Lees, 1988, Zanetta, 1992, Feng and Hahn, 1995, Vania, 1996, Provasi *et al.*, 2000, Smart *et al.*, 2000, Sinha *et al.*, 2002a) can be referred for such a foundation model estimation. The recent method by Sinha *et al.* (2002a) has been discussed in detail in Chapters 5 and 6.

Once a good model of the complete machine is known the malfunction in the machine can be simulated accurately by including a suitable fault model, for example – the definition of forces due to unbalance and misalignment as discussed in Chapter 5 for a machine expected to have both the problems. Similarly fault model for the rub, crack, etc. can be included in the system model for their quantification. Such MFD will provide sufficient information for solving the problem quickly and reliably.

2.8. SUMMARY

An overview of vibration based condition monitoring of TG sets used in power plants has been discussed. A brief comment is also made on the recent trends in MFD for all kind of faults and the use of a reliable FE model of the foundation along with the models of the rotor and the fluid bearings in MFD is also discussed.

CHAPTER 3

A FLEXIBLE ROTATING MACHINE: MATHEMATICAL MODELLING & VIBRATION MEASUREMENTS

3.0. INTRODUCTION

As described in Chapter 1 and 2 that the condition monitoring and diagnosis of faults in rotating machines relies on measured machine vibration data and accurate dynamic models (often finite element (FE) models) of the machine. Rotating machines such as TG sets in general consist of three major parts – the rotor, the fluid journal bearings and often a flexible foundation. It is also known that often a good FE model of the rotor and a reasonably reliable model of the fluid journal bearings may be constructed. However, reliable FE models for the foundation are difficult, if not impossible, to construct due to a number of practical difficulties (Lees and Simpson, 1983). Considering the limitation of reliable modelling of foundations, the models of the rotor and the bearings have been used for the present research study on identification of faults in machines, along with measured vibration responses at bearings pedestal only. Hence this chapter discusses about the theory of the modelling of the rotor and fluid bearings, vibration measurements and the processing of the measured vibration data.

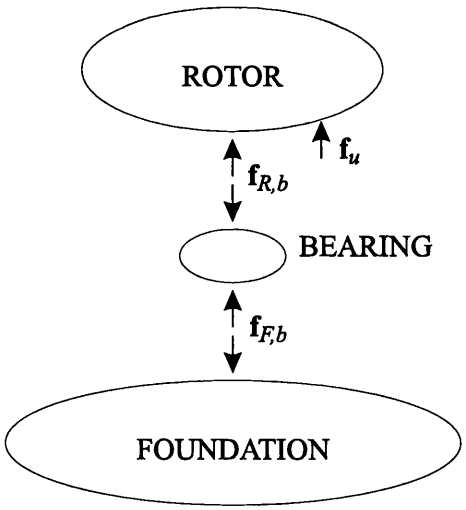

Figure 3.1 The abstract representation of a rotating machine

3.1. MODELLING OF THE MACHINE

Figure 3.1 is the abstract representation of a machine, whereby a rotor is connected to a flexible foundation via oil-film journal bearings. Let us assume that the dynamic stiffness matrices of the rotor, the bearing and the foundation are $\mathbf{Z}_R$, $\mathbf{Z}_B$, and $\mathbf{Z}_F$

respectively. The expression $\mathbf{Z}(\omega) = -\omega^2\mathbf{M} + i\omega\mathbf{C} + \mathbf{K}$ is the frequency dependent dynamic stiffness matrix where **M**, **C** and **K** are the mass, damping and stiffness matrices of the structural system.

3.1.1. FE Modelling of the Rotor ($\mathbf{Z}_R$)

The rotor generally consists of a shaft and balancing disks. The *Timoshenko beam* approach is used to model the shaft. To understand the modelling of the complete shaft for simulation of the lateral vibration (for both vertical and horizontal directions perpendicular to shaft axis), the system matrices of one disk and one shaft element are explained (Friswell *et al.*, 2002).

3.1.1.1. Balance Disk Element

Let us assume that the rotor axis is along x-direction and the disk is symmetric, the element mass and gyroscopic matrices for the disk corresponding to DoF $[u \quad v \quad \theta \quad \psi]^T$ can be written as

$$\mathbf{M}_{d,e} = \begin{bmatrix} m_d & 0 & 0 & 0 \\ 0 & m_d & 0 & 0 \\ 0 & 0 & I_d & 0 \\ 0 & 0 & 0 & I_d \end{bmatrix} \text{ and } \mathbf{G}_{d,e} = \begin{bmatrix} 0 & 0 & 0 & 0 \\ 0 & 0 & 0 & 0 \\ 0 & 0 & 0 & -I_p\Omega \\ 0 & 0 & I_p\Omega & 0 \end{bmatrix}, \qquad (3.1)$$

where the DoF ($u \quad v \quad \theta \quad \psi$) are the transverse displacements in the vertical (z) and horizontal (y) directions and rotations about the y and z axes. m_d is the mass of the disk and (I_p, I_d) are the polar moment of inertia about the rotor axis and the diametral moment of inertia about any axis perpendicular to the rotor axis respectively. Ω is the rotational speed (rad/s) of the rotor.

3.1.1.2. Shaft Element

For a symmetrical solid shaft, the system matrices for a two node *Timoshenko beam* element of length (ℓ) and radius (r) corresponding to DoF $[u_1 \quad v_1 \quad \theta_1 \quad \psi_1 \quad u_2 \quad v_2 \quad \theta_2 \quad \psi_2]^T$, as shown in Figure 3.2, can be written as below.

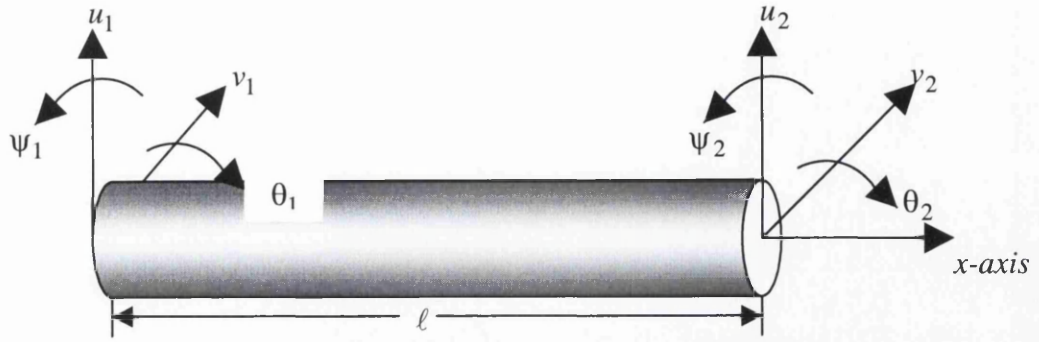

Figure 3.2 Schematic of the two node beam element

Mass matrix: The element mass matrix, $\mathbf{M}_{s,e} = \mathbf{M0}_{s,e} + \mathbf{M}i_{s,e}$, (3.2)

where the consistent mass matrix is,

$$\mathbf{M0}_{s,e} = \frac{\rho_s A_s \ell}{840(1+\Phi)^2}\begin{bmatrix} m1 & 0 & 0 & m2 & m3 & 0 & 0 & m4 \\ 0 & m1 & -m2 & 0 & 0 & m3 & -m4 & 0 \\ 0 & -m2 & m5 & 0 & 0 & m4 & m6 & 0 \\ m2 & 0 & 0 & m5 & -m4 & 0 & 0 & m6 \\ m3 & 0 & 0 & -m4 & m1 & 0 & 0 & -m2 \\ 0 & m3 & m4 & 0 & 0 & m1 & m2 & 0 \\ 0 & -m4 & m6 & 0 & 0 & m2 & m5 & 0 \\ m4 & 0 & 0 & m6 & -m2 & 0 & 0 & m5 \end{bmatrix}$$

and the rotary inertia effects in the mass matrix are,

$$\mathbf{M}i_{s,e} = \frac{\rho_s I_{d,s}}{30(1+\Phi)^2 \ell}\begin{bmatrix} m7 & 0 & 0 & m8 & -m7 & 0 & 0 & m8 \\ 0 & m7 & -m8 & 0 & 0 & -m7 & -m8 & 0 \\ 0 & -m8 & m9 & 0 & 0 & m8 & m10 & 0 \\ m8 & 0 & 0 & m9 & -m8 & 0 & 0 & m10 \\ -m7 & 0 & 0 & -m8 & m7 & 0 & 0 & -m8 \\ 0 & -m7 & m8 & 0 & 0 & m7 & m8 & 0 \\ 0 & -m8 & m10 & 0 & 0 & m8 & m9 & 0 \\ m8 & 0 & 0 & m10 & -m8 & 0 & 0 & m9 \end{bmatrix},$$

where the shaft material properties (E_s ρ_s) are the Young's modulus of elasticity and density respectively and $I_{d,s}$ $(=\pi r^4/4)$ is the diametral moment of inertia about any axis perpendicular to the rotor axis, and other terms are defined as

$m1 = 312 + 588\Phi + 280\Phi^2$, $m2 = (44 + 77\Phi + 35\Phi^2)\ell$, $m3 = 108 + 252\Phi + 140\Phi^2$

$m4 = -(26 + 63\Phi + 35\Phi^2)\ell$, $m5 = (8 + 14\Phi + 7\Phi^2)\ell^2$, $m6 = -(6 + 14\Phi + 7\Phi^2)\ell^2$

$m7 = 36$, $m8 = (3 - 15\Phi)\ell$, $m9 = (4 + 5\Phi + 10\Phi^2)\ell^2$, $m10 = (-1 - 5\Phi + 5\Phi^2)\ell^2$

The non-dimensional shear coefficient (Φ) for circular section of beam is defined as (Cowper, 1966)

$$\Phi = \frac{12E_s I_{d,s}}{\kappa G_s A_s \ell^2}, \tag{3.3}$$

where the shear constant, $\kappa = \dfrac{6(1+\nu)(1+\mu^2)^2}{(7+6\nu)(1+\mu^2)^2 + (20+12\nu)\mu^2}$,

where G_s is the shear modulus of elasticity, ν is the poisson's ratio of the shaft material. A_s is the cross-section area and μ is the ratio of outer radius to inner radius of the shaft. Hutchinson (2001) gives the shear coefficient for many other cross-sectional shapes of beam.

Stiffness matrix: The elemental stiffness matrix is,

$$\mathbf{K}_{s,e} = \frac{E_s I_{d,s}}{(1+\Phi)\ell^3}\begin{bmatrix} 12 & 0 & 0 & 6\ell & -12 & 0 & 0 & 6\ell \\ & 12 & -6\ell & 0 & 0 & -12 & -6\ell & 0 \\ & & (4+\Phi)\ell^2 & 0 & 0 & 6\ell & (2-\Phi)\ell^2 & 0 \\ & & & (4+\Phi)\ell^2 & -6\ell & 0 & 0 & (2-\Phi)\ell^2 \\ & & & & 12 & 0 & 0 & -6\ell \\ & & SYM & & & 12 & 6\ell & 0 \\ & & & & & & (4+\Phi)\ell^2 & 0 \\ & & & & & & & (4+\Phi)\ell^2 \end{bmatrix} \tag{3.4}$$

Damping matrix: The proportional damping, $\mathbf{C0}_{s,e} = \beta\mathbf{K}_{s,e}$ can be used, where the constant, β is the proportional factor to stiffness. However for the present study the rotor has been assumed to be very lightly damped and hence no damping was used.

Gyroscopic matrix: The skew-symmetric gyroscopic matrix is,

$$\mathbf{G}_{s,e} = \frac{\rho_s I_{d,s}}{15\ell}\begin{bmatrix} 0 & -36 & 3\ell & 0 & 0 & 36 & 3\ell & 0 \\ 36 & 0 & 0 & 3\ell & -36 & 0 & 0 & 3\ell \\ -3\ell & 0 & 0 & -4\ell^2 & 3\ell & 0 & 0 & \ell^2 \\ 0 & -3\ell & 4\ell^2 & 0 & 0 & 3\ell & -\ell^2 & 0 \\ 0 & 36 & -3\ell & 0 & 0 & -36 & -3\ell & 0 \\ -36 & 0 & 0 & -3\ell & 36 & 0 & 0 & -3\ell \\ -3\ell & 0 & 0 & \ell^2 & 3\ell & 0 & 0 & -4\ell^2 \\ 0 & -3\ell & -\ell^2 & 0 & 0 & 3\ell & 4\ell^2 & 0 \end{bmatrix} \tag{3.5}$$

The dynamic matrix of the complete rotor ($\mathbf{Z}_R$) can now be constructed by assembling the above matrices for each element of the shafts and the disks, and can be written as

$$\mathbf{Z}_R(\omega) = -\omega^2\mathbf{M}_R + i\omega(\mathbf{C}_R + \Omega\mathbf{G}_R) + \mathbf{K}_R \tag{3.6}$$

3.1.2. Modelling of the Fluid Journal Bearing ($\mathbf{Z}_B$)

Figure 3.3 represents a simple fluid journal bearing. A shaft, commonly referred to as a *journal*, rotates within a bearing housing at a speed Ω. The cavity is filled with oil, and as a result of the circular motion of the journal a pressure build-up occurs in the convergent region labelled *h*. This pressure resists the static load *F* acting downwards on the journal. The distance between journal centre *J* and bearing centre *O* is referred to as the *eccentricity* ε and defined as the ratio of the journal displacement to the radial clearance. This eccentricity depends on the static load, running speed, clearance and oil properties.

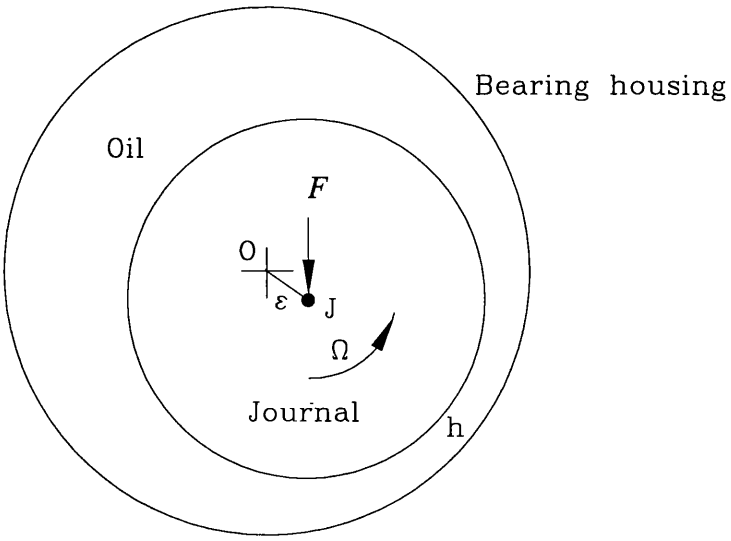

Figure 3.3 Schematic of a simple fluid journal bearing

Since most turbogenerators have bearings with a bearing length (L) to diameter (D) ratio of much less than unity, short bearing theory is used for modelling. The rotating speed dependent stiffness and the damping matrices of a bearing for DoF $[u \quad v]^T$ may be written as (Hamrock, 1994, Smith, 1969)

$$\mathbf{K}_b = \begin{bmatrix} k11 & k12 \\ k21 & k22 \end{bmatrix} \text{ and } \mathbf{C}_b = \begin{bmatrix} c11 & c12 \\ c21 & c22 \end{bmatrix}, \tag{3.7}$$

where

$$k11 = 4A\left(\pi^2\left(2-\varepsilon^2\right)+16\varepsilon^2\right),$$

$$k12 = A\left(\frac{\pi\left(\pi^2\left(1-\varepsilon^2\right)^2-16\varepsilon^4\right)}{\varepsilon\sqrt{1-\varepsilon^2}}\right),\quad k21 = -A\left(\frac{\pi\left(\pi^2\left(1-\varepsilon^2\right)\left(1+2\varepsilon^2\right)+32\varepsilon^2\left(1+\varepsilon^2\right)\right)}{\varepsilon\sqrt{1-\varepsilon^2}}\right)$$

$$k22 = 4A\left(\pi^2\left(1+2\varepsilon^2\right)+\frac{32\varepsilon^2\left(1+\varepsilon^2\right)}{\left(1-\varepsilon^2\right)}\right),\quad A = \frac{F}{c\left(\pi^2\left(1-\varepsilon^2\right)+16\varepsilon^2\right)^{3/2}}$$

$$c11 = B\left(\frac{2\pi\sqrt{1-\varepsilon^2}\left(\pi^2\left(1+2\varepsilon^2\right)-16\varepsilon^2\right)}{\varepsilon}\right),\quad c12 = -8B\left(\pi^2\left(1+2\varepsilon^2\right)-16\varepsilon^2\right),\quad c21 = c12,$$

$$c22 = B\left(\frac{2\pi\left(\pi^2\left(1-\varepsilon^2\right)+48\varepsilon^2\right)}{\varepsilon\sqrt{1-\varepsilon^2}}\right),\quad B = A/\Omega \text{ and } c \text{ is the bearing clearance.}$$

The static load (F) and the eccentricity (ε) can be either measured directly or can be calculated. It is always difficult to calculate the static load accurately (Smart, 1998), however an approximate approach is to estimate this static load from the equation of static. Once the load is know the eccentricity (ε) may be obtained by the following equation (Friswell *et al.*, 2002).

$$\varepsilon^8 - 4\varepsilon^6 + \left(6 - \frac{16-\pi^2}{H}\right)\varepsilon^4 - \left(4 + \frac{\pi^2}{H}\right)\varepsilon^2 + 1 = 0, \tag{3.8}$$

where $H = \left(\frac{8Fc^2}{D\Omega\eta L^3} \right)^2$ is known from for a particular speed (Ω), load (F) and oil viscosity (η). These speed dependent stiffness and damping matrices can be combined to obtain the dynamic stiffness matrix of the bearings at any rotating speed assuming that the effect of fluid inertia is negligible. However the fluid inertia (El-Shafei, 1995) can be included if required.

3.1.3. Modelling of the Foundation (Z_F)

Deriving a reliable model representing the actual behaviour of the foundation by the conventional FE method is difficult. The estimation of a reliable model for the foundation has been the topic of the present research study. This has been derived using measured vibration data during machine run-down and is discussed in detail in Chapter 5.

3.2. VIBRATION MEASUREMENTS

The schematic of a simple rotating rig similar to the experimental rotating rig is shown in Figure 3.4. The rig consists of a rotor having two balance disks which is supported on the flexible foundation through two bearings. The rotor is coupled to the motor through a flexible coupling. The vibration measured at the bearing pedestals in both vertical and horizontal directions during machine run-down has been used for the present study. Only the kind of measured data required for the present research studies is discussed here.

3.2.1. Measurement Scheme

Four accelerometers (2 accelerometers at one bearing pedestal) and one tacho sensor for speed and phase reference were used for the measurements, as shown in Figure 3.4. The charge signals from the accelerometers were converted into the voltage signals using the charge amplifiers. These acceleration responses at the bearing pedestals and the tacho signals are directly stored in the PC using a National Instruments Data Acquisition card during the experiments. The software programme ***FlexiDaq***, developed by Edwards (1999) during his PhD study, controls the motor

run-down speed, data acquisition hardware and stores the accelerometer and tacho signals in the PC. A photograph of the small experimental rig used here, instrumented with accelerometers, tacho sensor and the related cables, hardware and the PC, is shown in Figure 3.5.

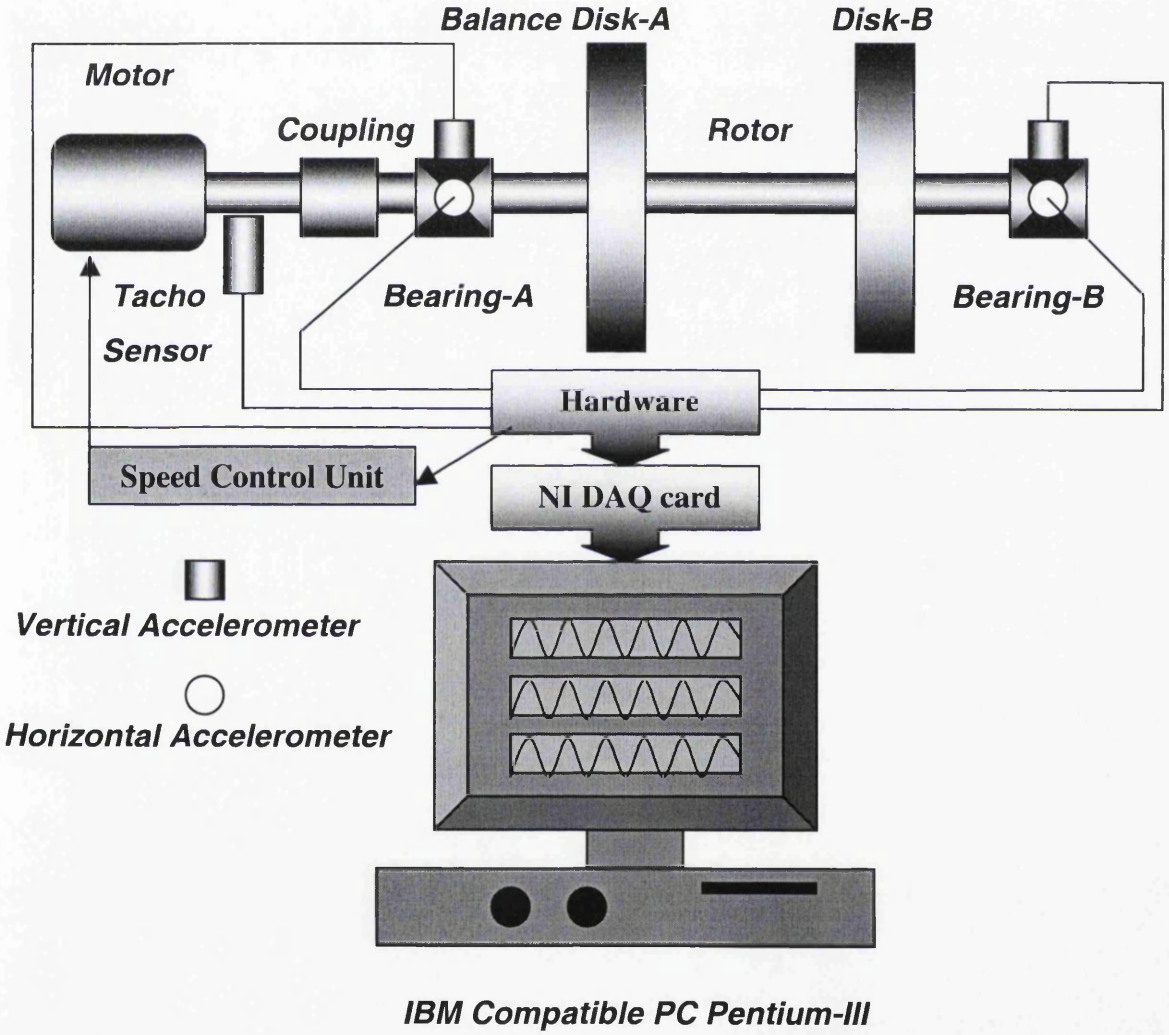

Figure 3.4 Schematic of the rig with vibration data measurement scheme

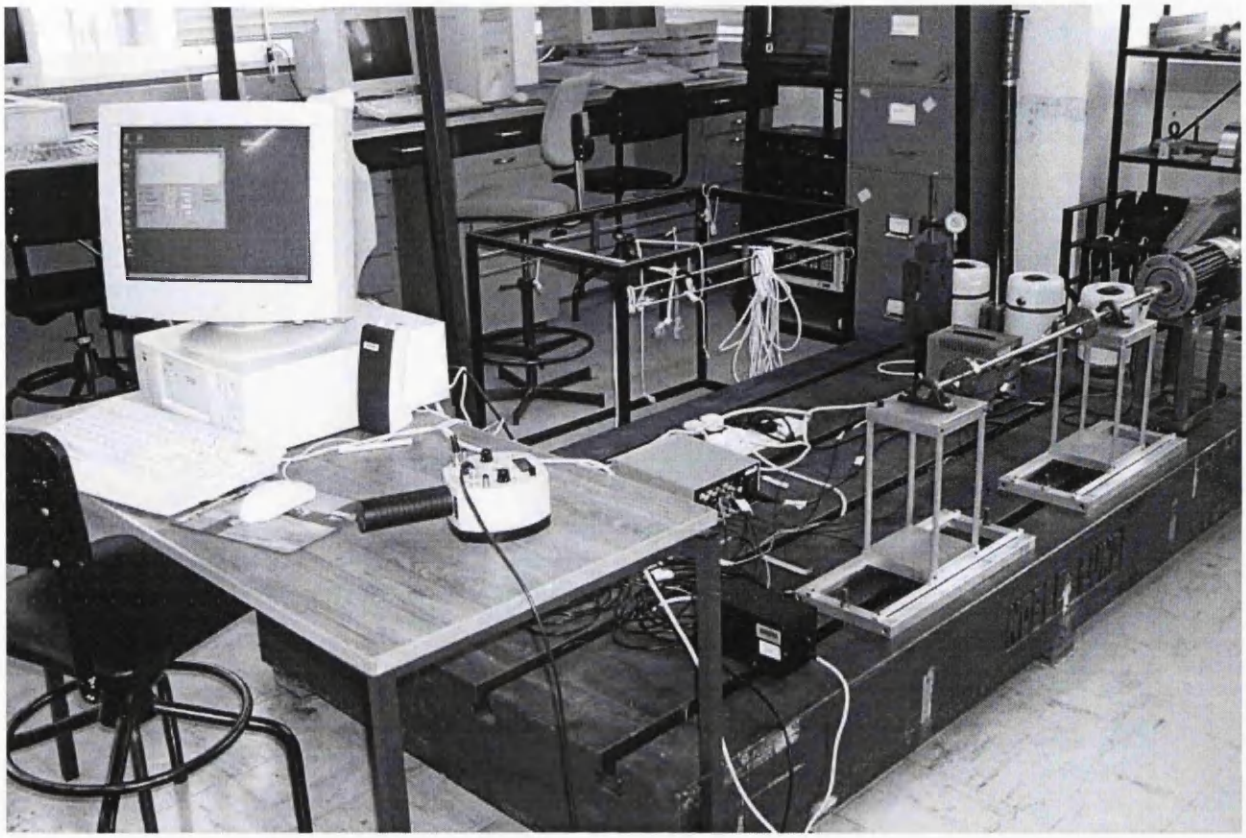

Figure 3.5 Photograph of the small rig instrumented with vibration sensors and related hardware

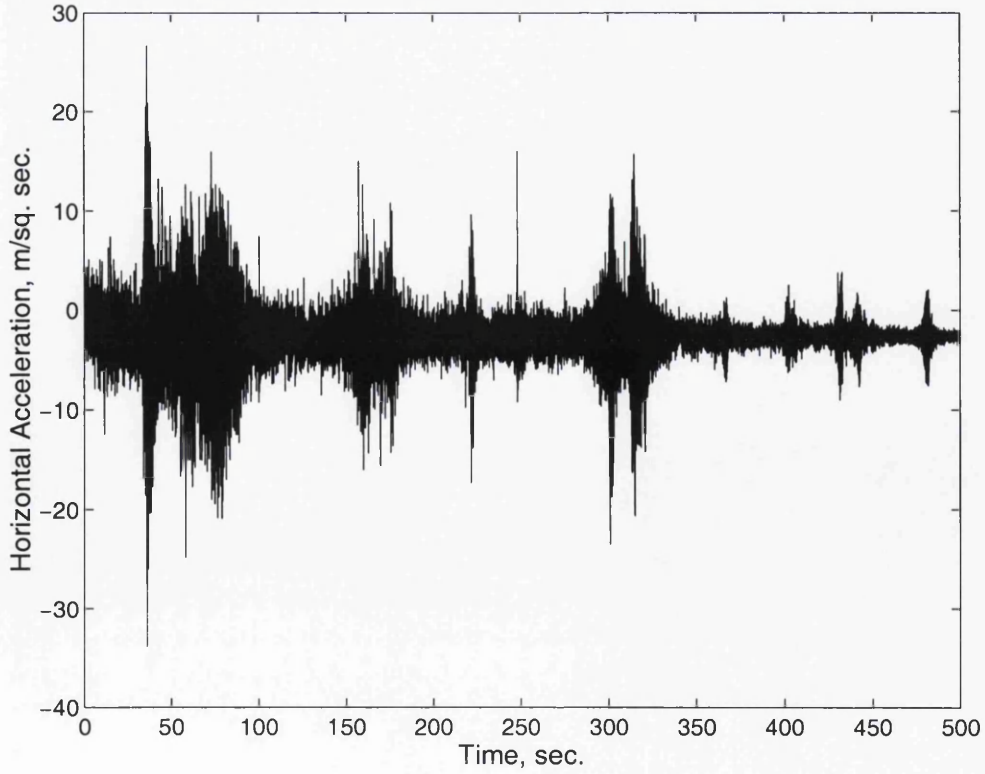

Figure 3.6 A typical run-down acceleration response of a machine

3.2.2. Run-down Experiments

Different unbalance masses at different phases were added to the balance disks for different run-down experiments. Each run-down was carried out from a machine rotating speed of 2500RPM to 300RPM and lasted 500 seconds. The measured signal from each sensor was collected at the rate of 2500 sample per second and stored in the PC. One such typical run-down acceleration response is shown in Figure 3.6.

3.2.3. Order Tracking of Run-down Data

The 1X component of the run-down data in the frequency domain has been used for the unbalance and foundation model estimation. Hence the run-down time domain data needed to be order tracked to get the 1X data. Fyfe and Munck (1997) and Bossley *et al.* (1999) gave the theory of order tracking. Either a computational program can be written for order tracking or any commercially available software code or hardware can be used for this purpose. Here the software code ***VSI Rotate 2.0*** from Vold Solutions (2000) has been used for data order tracking. The order tracked response (1X component) of the run-down data in Figure 3.6 is shown in Figure 3.7.

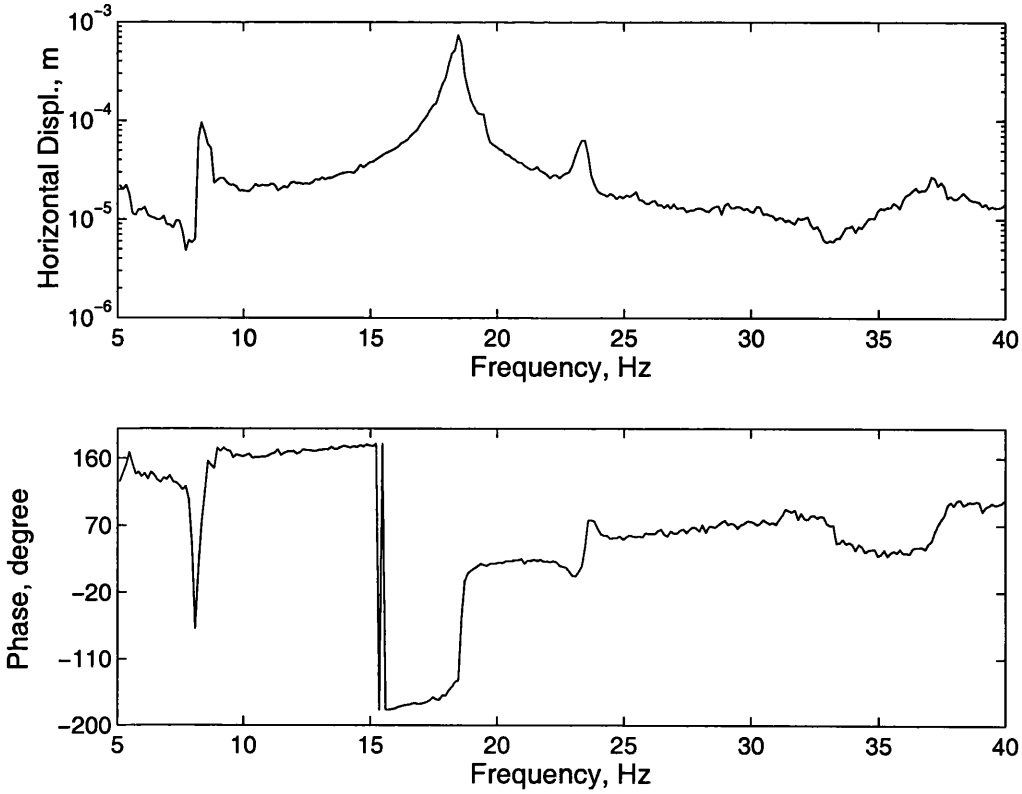

Figure 3.7 The first order (1X) response of the run-down data in Figure 3.6

3.3. SUMMARY

The rotor FE modelling and the modelling of the fluid bearings has been discussed. A computational code in MatLab software has been developed using the above theory for modelling of the rotors and bearings of the experimental rigs. The vibration measurements, data collection and the data processing to get the required information for further study has also been discussed through a simple example of a rotating rig.

CHAPTER 4

THE EXPERIMENTAL RIGS

4.0. INTRODUCTION

Three laboratory scale experimental rotating rigs were used for the present study. Two rigs which have been designed, fabricated and installed in the Dynamics Laboratory of Department of Mechanical Engineering, University of Wales Swansea (UK) for the present study. These rigs are named ***Small Rig*** and ***New Small Rig***. Third rig is relatively much bigger compared to other rigs and is installed at the Aston University, Birmingham (UK). Some run-downs vibration data from this rig were used in the present study. This rig is called as the ***Aston rig*** throughout in the thesis. Details of these rigs are discussed here.

4.1. THE SMALL RIG

The small rig consists of a 12 mm OD (d) steel shaft of 980 mm length connected to two flexible supports and coupled with a motor through a flexible coupler. Both flexible supports are made of aluminium and physically identical. One flexible foundation is connected at 10 mm and other at 760 mm from the left end of the shaft through self-lubricating ball bearings. The shaft also carries two identical balancing disks made of steel and placed at 135 mm and 635 mm from the left end of the shaft. The balancing disk dimensions are 75 mm OD, 12 mm ID and 15 mm thickness (see Figure 4.1). Each balance disk has 16 holes of diameter 2 mm at a pitch circle diameter of 60 mm and each holes are separated by a 22.5 degree angle. These holes are deliberately made on the balance disk for adding the unbalance masses at different phase angles. The modulus of elasticity (E) and density (ρ) of the rotor are 200 GN/m^2 and 7800 kg/m^3 respectively. The photograph of the rig is shown in Figure 4.2. The dynamic characterization was carried out for the following components by both modal tests and FE analysis.

4.1.1. Rotor alone

The first three free-free bending modes of the rotor with balance disks were calculated to be 47.29Hz, 129.93Hz and 281.31Hz.

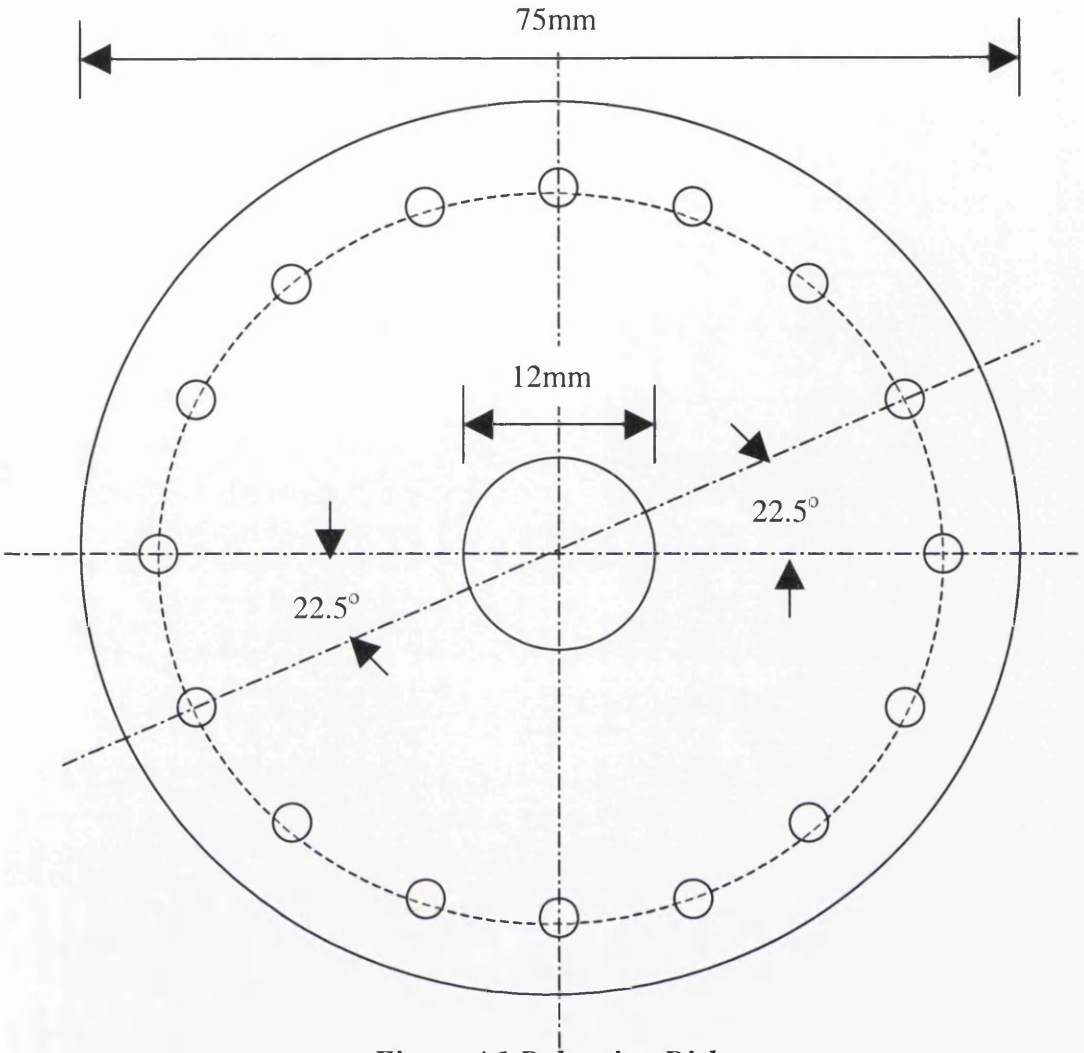

Figure 4.1 Balancing Disk

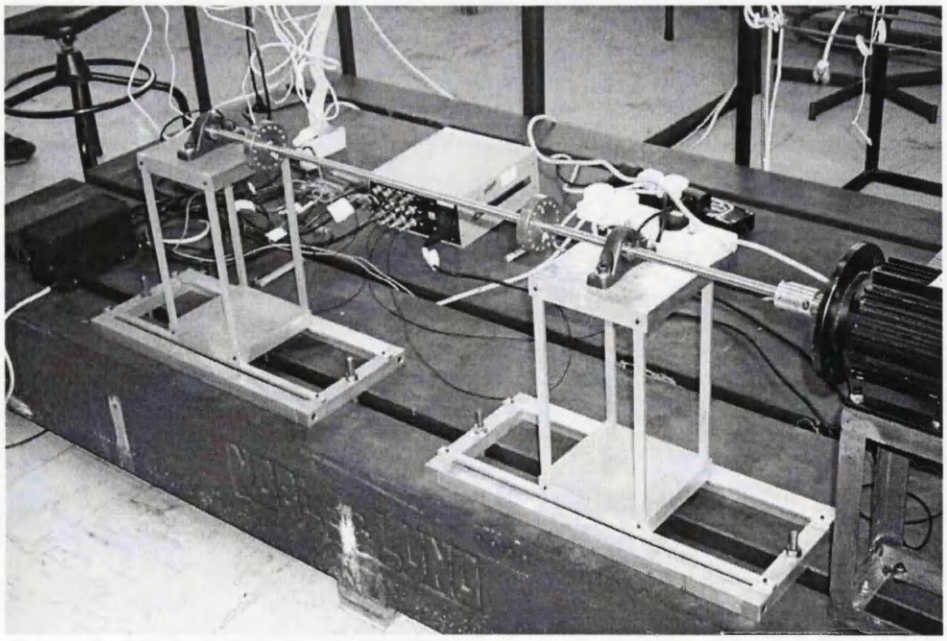

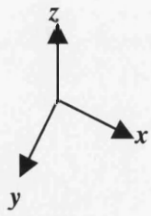

Figure 4.2 Photograph of the Small rig in Swansea (UK)

4.1.2. Foundation alone

Each foundation represents typical frame type structure and is made of aluminium and shown in Figure 4.3. The frame was designed such that it has a few modes in both vertical and horizontal directions in the machine run-down speed range. The frame consists of two horizontal beams (6.52mm x 12.8mm x 496mm), four vertical beams (6.52mm x 12.8mm x 300mm) and 2 plates (25.88mm x 169mm x 159mm). The connections of all beams are shown in Figure 4.3. The horizontal beams are bolted to the bottom frame that is rigidly connected to the massive base plate as seen in Figure 4.3.

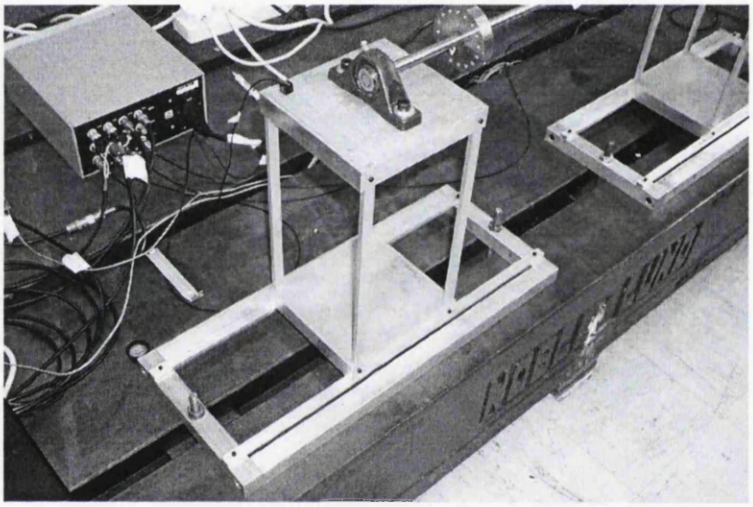

Figure 4.3 Photograph of the foundation alone

Modal tests (Ewins, 2000) were carried out using a small-instrumented hammer and a tiny 3.5g accelerometer. The identified modes are listed in Table 4.1 with their mode interpretation. An FE model was developed using two node Euler-Bernoulli beam elements for the horizontal and vertical beams and 4-node *quad4* plate elements for the top and bottom plates using the MatLab Structural Dynamics Toolbox (Balmes, 2000). The ends of both the horizontal beams were assumed to be rigid in the initial FE model. The FE model is shown in Figure 4.4. The computed natural frequencies are also listed in Table 4.1 for comparison with the experimental results.

The small deviation in the computed natural frequencies from those obtained by experiment could be because the initial assumption of rigid end supports for the horizontal beams is not correct. These supports may allow some rotation in the

horizontal and vertical directions. The FE model has been further modified by replacing the rigid support assumption by two rotational stiffnesses (k_y and k_z) with zero translation at supports. Using these two updating parameters the initial model was updated by the gradient based sensitivity model updating (Friswell and Mottershead, 1995). It was observed that the computed natural frequencies in the lateral and vertical directions are close to experiment for k_y = 2 kNm/rad and k_z=10 kNm/rad. These frequencies are also listed in Table 4.1.

Table 4.1 Natural frequencies of the foundation alone

Modes	Experiment data	FE model	Updated FE model	Remarks
1st	10.00 Hz	12.83 Hz	9.986 Hz	Bending in y-dir of vertical frame
2nd	19.75 Hz	22.99 Hz	22.527 Hz	Bending in x-dir of vertical frame
3rd	32.125 Hz	34.34 Hz	32.777 Hz	Bending in z-dir of horizontal 2 beams
4th	57.50 Hz	55.63 Hz	55.631 Hz	Twisting of vertical frame

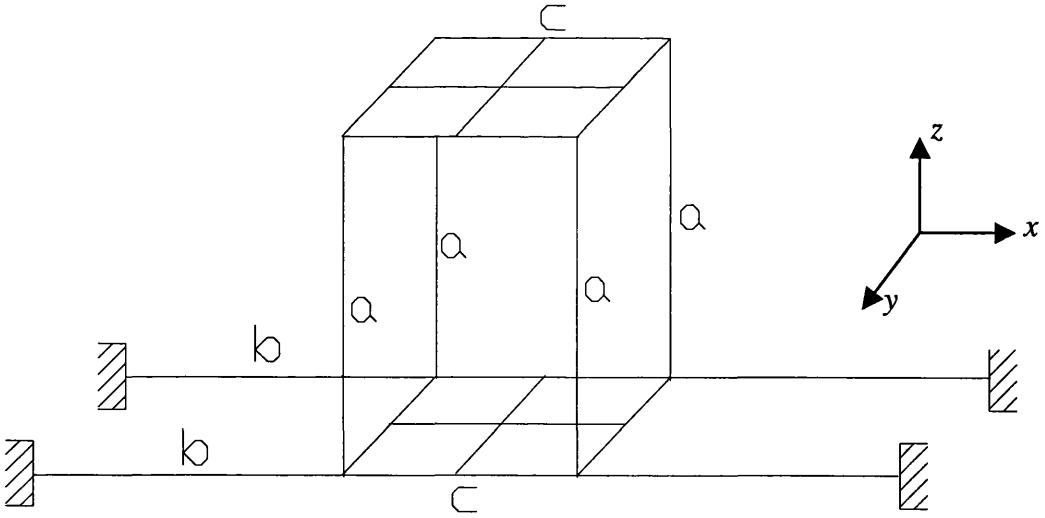

Components ***a*** and ***b*** - modelled using Beam elements, Component ***c*** – modelled using *quad4* Plate elements.

Figure 4.4 FE model of the foundation alone

4.1.3. Complete Rig not coupled to Motor

Initially the modal tests were conducted on the foundations of the rig without the motor coupling. An FE analysis was also carried out using the above updated FE model of the foundation along with the rotor and disks model. The FE model

developed in MatLab for the rotor using two node Euler-Bernoulli beam elements is shown in Figure 4.5. Since the rotor is supported on the flexible foundations through the ball bearings so the rotor connection to the foundation at bearing locations is modelled as pinned connections. Hence the translational DoF of the rotor FE model was rigidly connected to the translational DoF of the updated foundation FE model at bearing locations. The measured and the computed natural frequencies in Table 4.2 and the computed mode shapes for the rotor are shown in Figure 4.6.

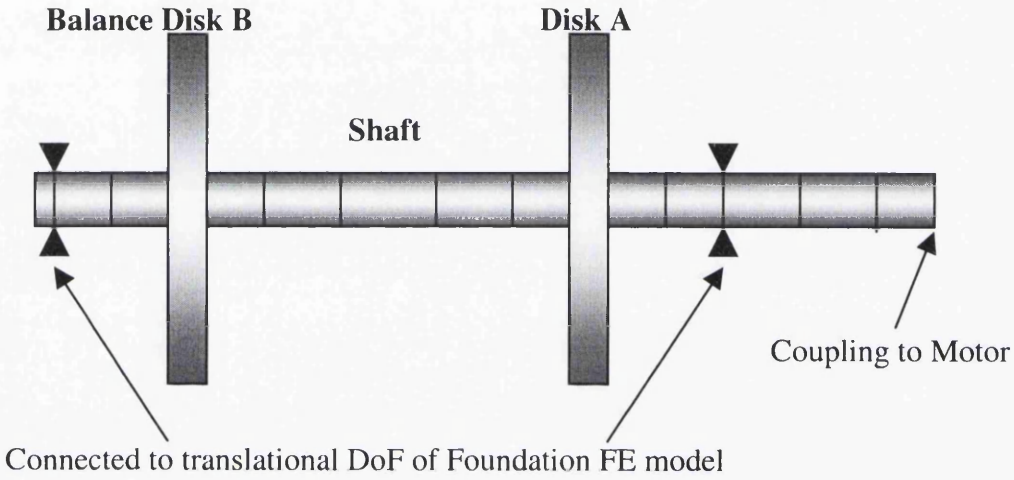

Figure 4.5 FE model of the rotor of the Small rig

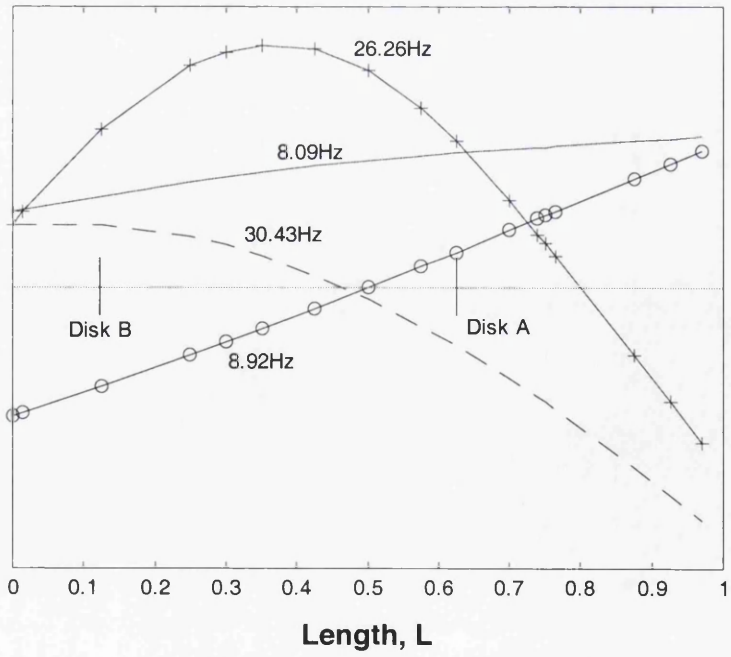

Figure 4.6 Computed mode shapes for the rotor in the Small rig when the motor is not connected

Table 4.2 Small rig natural frequencies when the rotor not coupled to the motor

Modes	Experiment data	FE model	Remarks
1st	8.25 Hz	8.099 Hz	Lateral mode (y-dir.)
2nd	9.00 Hz	8.922 Hz	Lateral mode (y-dir.)
3rd	26.25 Hz	26.262 Hz	Vertical mode (z-dir.)
4th	30.00 Hz	30.431 Hz	Vertical mode (z-dir.)

4.1.4. Complete Rig coupled to Motor

The above FE model of the rig is close to the experimental setup of the rig. The rig rotor was then connected to the motor, required to rotate the rotor at different RPM, through a flexible mechanical coupler. The photograph of the complete setup is shown in Figure 4.2. The modal tests were again conducted on this arrangement of the rig. The tests were conducted at different shaft RPM. The experimentally identified natural frequencies are listed in Table 4.3.

Table 4.3 Small rig natural frequencies when the rotor coupled to the motor

Modes (Hz)	Experiment Modal data at different rotor RPM				Updated FE model
	Static 0 RPM	372 RPM	1320 RPM	2424 RPM	Static
1st	8.625	8.500	8.500	8.500	8.537
2nd	14.375	14.375	14.500	14.500	14.341
3rd	26.250	26.500	26.500	26.750	26.550
4th	31.375	31.375	31.125	31.250	31.753
Remark	Coupling stiffnesses realized during FE model updating are k_t = 27 kN/m and k_θ = 25 Nm/rad				

As can be seen from Table 4.3 the change in rig frequencies are negligible at different rotor speed so there is little gyroscopic effect in the shaft. However a small change in the rig frequencies is seen after flexible coupling to the motor. Using the measured frequencies and the FE model without coupling, the coupling stiffnesses, both translational (k_t) and rotational stiffness (k_θ), were estimated by the gradient based sensitivity model updating method (Friswell and Mottershead, 1995). The estimated coupling stiffnesses are k_t = 27 kN/m and k_θ = 25 Nm/rad and the computed natural frequencies are also close to the experimental results. But the changes in the rotor

mode shapes shown in Figure 4.7 are quite significant compared to the rig without motor coupling. A good FE model of the complete rig including the rotor, the bearings, the foundation and the flexible coupling is now known. Hence any accurate simulation is possible.

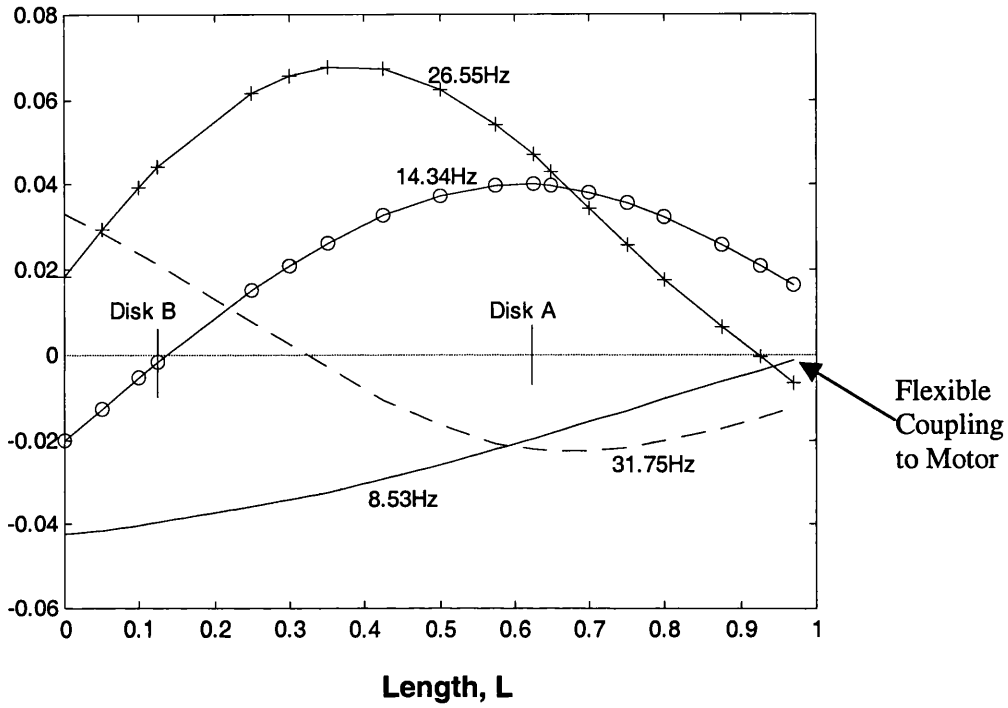

Figure 4.7 Computed mode shapes for the rotor in the Small rig when the motor is connected

4.2. THE NEW SMALL RIG

The photograph of the rig is shown in Figure 4.8. The rig is similar to the *Small rig* and the only difference is the foundation. Each foundation of this rig, shown in Figure 4.9, consists of a horizontal beam (500mm x 25.5mm x 6.4 mm) and a vertical beam (322mm x 25.5mm x 6.4mm) made of steel. The horizontal beam is bolted to the massive base plate and the vertical beam to the bearing assembly as seen in the photograph. A layer of acrylic foam (315mm x 19mm x 1mm) was bonded between the vertical beam and thin layers of metal sheet (315mm x19mm x 350μm) to increase the damping. In fact the modal experiment confirms that the damping of the foundation increased to 1.4% from a value of 0.6% at the first lateral mode. A 12 mm OD (*d*) steel shaft of 980 mm length connected to this flexible supports and coupled with a motor through a flexible coupler. One flexible foundation is connected at

15 mm and other at 765 mm from the right end of the shaft through self-lubricating ball bearings. The shaft also carries two identical balancing disks shown in Figure 4.1 and placed at 140 mm and 640 mm from the right end of the shaft. Disk A is near to the Motor. In a similar way to the *Small rig* modal tests and an FE analysis were carried out for this rig and their results were compared. These are summarized in Tables 4.4 to 4.6.

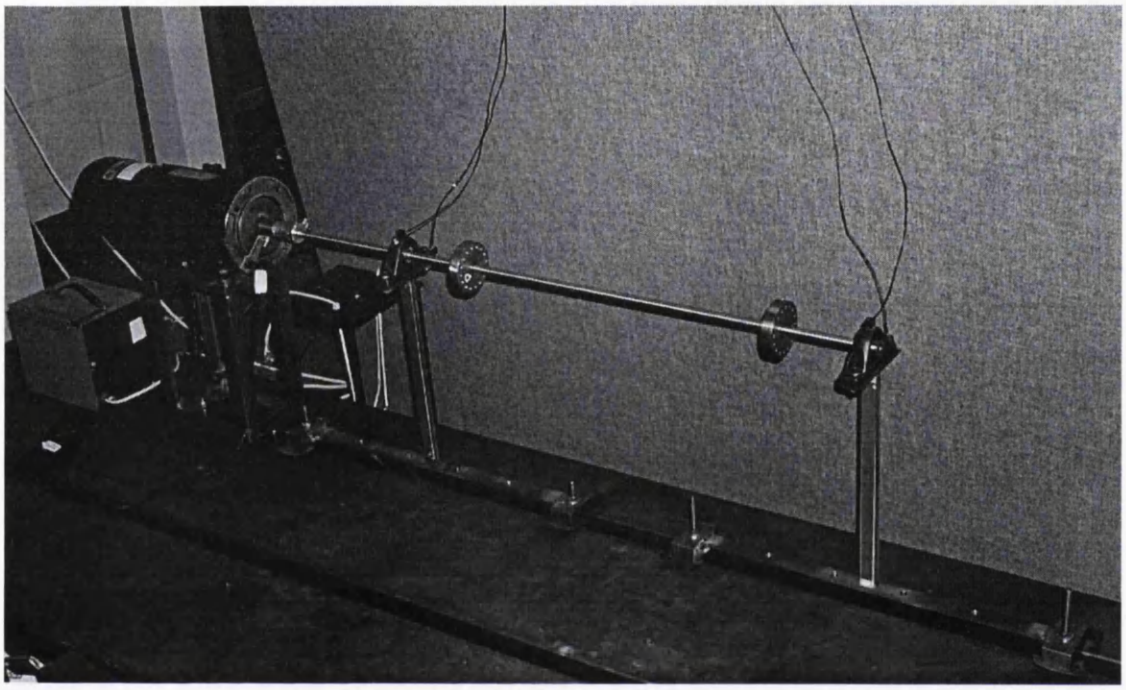

Figure 4.8 Photograph of the New small rig in Swansea (UK)

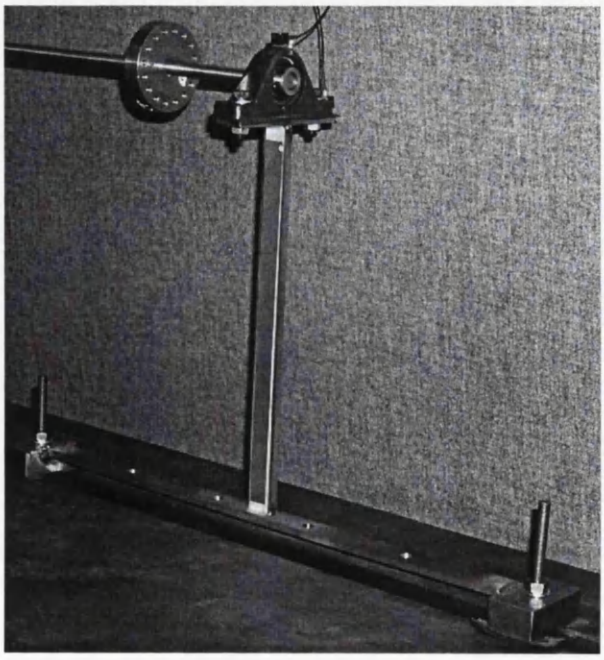

Figure 4.9 Photograph of the foundation of the New small rig in Swansea (UK)

Table 4.4 Natural frequencies of the rotor alone for the New small rig

Mode	Rotor without balance disks		Rotor with two balance disks	
	Experiment data	FE model	Experiment data	FE model
1st	56.563 Hz	56.323 Hz	48.125 Hz	48.014 Hz
2nd	154.688 Hz	255.262 Hz	129.688 Hz	129.889 Hz
3rd	304.063 Hz	304.401 Hz	278.438 Hz	279.212 Hz

Table 4.5 Natural frequencies of the foundation alone for the New small rig

Mode	Foundation alone		Foundation with bearing assemby		Remarks
	Experiment data	FE model	Experiment data	FE model	
1st	22.188 Hz	22.438 Hz	12.34 Hz	13.22 Hz	Lateral mode (y-dir.)
2nd	50.313 Hz	50.444 Hz	29.25 Hz	30.62 Hz	Axial mode (x-dir.)
3rd	72.813 Hz	72.892 Hz	58.25 Hz	57.63 Hz	Vertical mode (z-dir.)

Table 4.6 Natural frequencies of the New small rig

Mode	Rotor not coupled to Motor		Rotor coupled to Motor		Remarks
	Experiment data	FE model	Experiment data	FE model	
1st	7.875 Hz	8.865 Hz	8.750 Hz	9.590 Hz	Lateral mode (y-dir.)
2nd	10.563 Hz	10.562 Hz	18.250 Hz	18.223 Hz	Lateral mode (y-dir.)
3rd	20.937 Hz	20.655 Hz	23.500 Hz		Axial mode (x-dir.)
4th	36.500 Hz	36.950 Hz	36.625 Hz	37.182 Hz	Vertical mode (z-dir.)
5th	41.238 Hz	39.825 Hz	59.313 Hz	55.076 Hz	Lateral mode (y-dir.)
6th	47.750 Hz	47.357 Hz	49.813 Hz	49.752 Hz	Vertical mode (z-dir.)

4.3. THE ASTON RIG

The photograph of the test rig at Aston University, Birmingham is shown in Figure 4.10. The rig consists of a solidly coupled, two-shaft system mounted on four oil lubricated journal bearings. The bearings sit on flexible steel pedestals bolted onto a large lathe bed which rests on a concrete foundation. The rotor itself consists of two steel shafts 1.56 m and 1.175m long, each with a nominal diameter of 38 mm and

coupled through flanges of 150 mm long and 100 mm diameter at the connecting end of both shafts. The dimensions of the rotor at each station of the rig are given in Table 4.7. Young's modulus of elasticity and the density of rotor material are 200 GN/m^2 and 7850 kg/m^3 respectively.

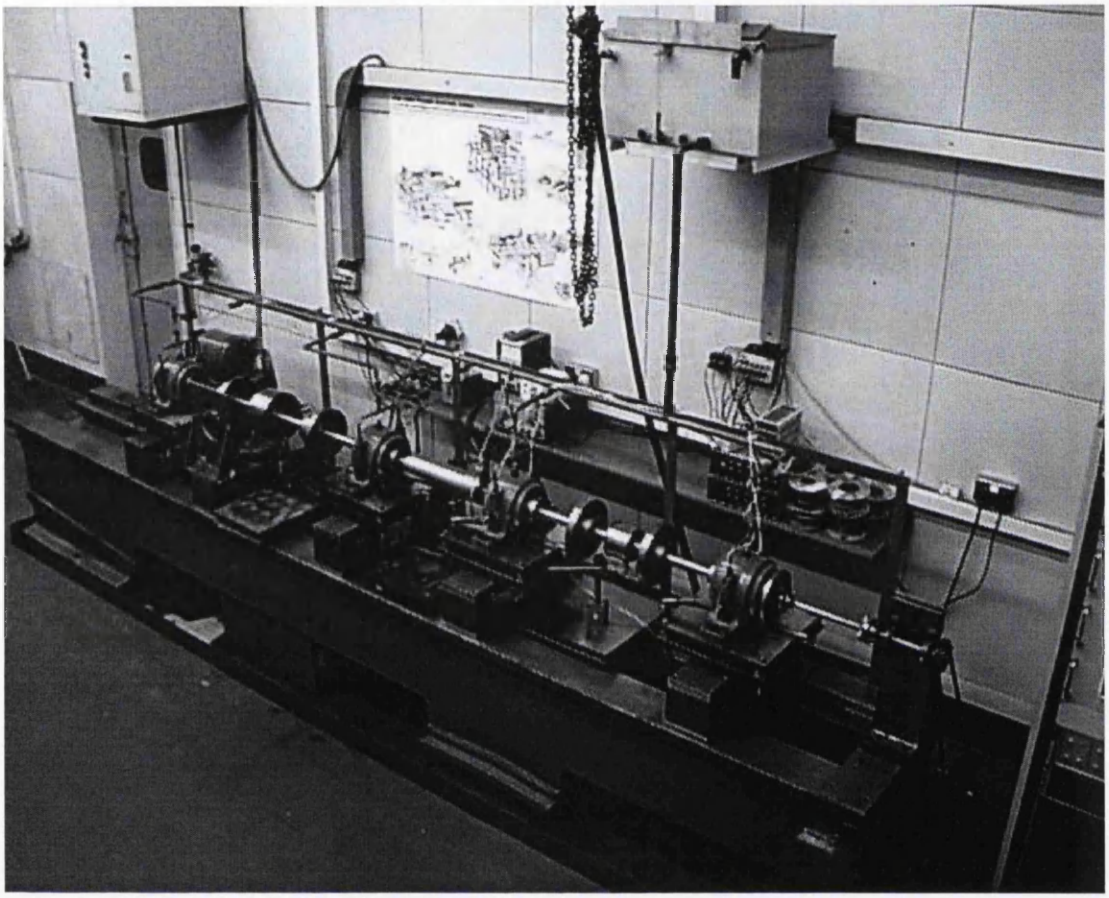

Figure 4.10 Photograph of the Aston rig

At either end of the shafts are journals of diameter 100 mm, and in the centre of the shafts are machined sections which take balancing disks, three for long rotor and two for the short rotor. Each balancing disk is made of steel and is 203.2mm diameter and 25.4mm thickness. Constructional detail is similar to the balance disk shown in Figure 4.1. The balance disks were placed at 457.2mm, 746.8mm, 1016mm, 2351mm and 2630mm from the left end of the shaft. The bearings are circular, have a length to diameter ratio of 0.3, a radial clearance of 150 μm and contain oil of viscosity 0.0009Ns/m^2. One bearing is located at either end of the shaft and the remaining two bearings were located at 1372mm and 2046mm from the left end.

Table 4.7 The physical dimensions of the rotor of the Aston rig

Long Rotor Properties			Short Rotor Properties		
Station	Length (mm)	Diameter (mm)	Station	Length (mm)	Diameter (mm)
1	203.2	100	14	6.35	38.1
2	203.2	38.1	15	25.4	77.57
3	101.6	103	16	50.8	38.1
4	177.8	38.1	17	203.2	100
5	101.6	109	18	177.8	38.1
6	177.8	38.1	19	50.8	116.8
7	101.6	117	20	76.2	38.1
8	203.2	38.1	21	76.2	109.7
9	203.2	100	22	76.2	38.1
10	50.8	38.1	23	50.8	102.9
11	25.4	78.1	24	177.8	38.1
12	12.7	38.1	25	203.2	100
13	Coupling between the two rotors through coupling flanges (see Figure 4.10) of 300 mm length and 100 mm diameter.				

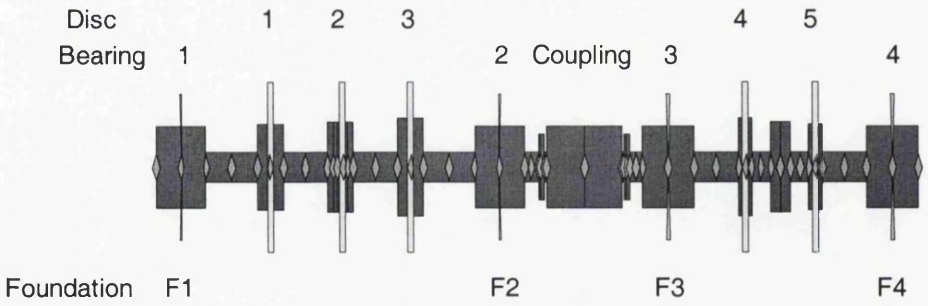

Figure 4.11 FE model of the rotor of the Aston rig

An FE model shown in Figure 4.11 was created for the rotor with 51 two noded Timoshenko beam elements, each node with two translational and two rotational DoFs. The computed free-free bending modes of the coupled shaft having all balance disks are 12.30Hz, 27.40Hz, 57.76Hz and 101.70Hz. These are close to the measured

values of 12.0Hz, 27.5Hz, 55.9Hz and 99.0Hz (Smart, 1998). Similarly the measured natural frequencies for the foundation alone (without rotor) are 15.6Hz, 17.3Hz, 26.9Hz, 45.2Hz, 51.2Hz & 57.7Hz in horizontal direction, and 46.6Hz, 48.4Hz, 53.0Hz & 58.1Hz in vertical direction. Smart (1998) gave a more detailed description of the rig and its dynamic characterization carried out by modal tests.

4.4. SUMMARY

The physical, material properties and the constructional details of all the experimental rigs used are discussed here. They are used in the numerical simulations and for the experimental cases in the present study.

CHAPTER 5

ESTIMATION THEORY AND COMPUTATIONAL IMPLEMENTATION

5.0. INTRODUCTION

The requirements of the foundation model, the rotor unbalance and misalignment estimation have been brought out in Chapter 1. This chapter is concerned with the theory of modelling a flexible foundation, and the estimation of the unbalance and misalignment of a rotating machine, say a TG set. The theoretical concept and the complete computational implementation required for the estimation are presented here.

5.1. EQUATION OF MOTION OF A ROTATING MACHINE

Figure 3.1 in Chapter 3 is the abstract representation of a turbogenerator, whereby a rotor is connected to a flexible foundation via oil-film journal bearings. The dynamic stiffness matrix of the system may be written as (Smart, 1998, Smart *et al.*, 2000);

$$\begin{bmatrix} \mathbf{Z}_{R,ii} & \mathbf{Z}_{R,ib} & \mathbf{0} & \mathbf{0} \\ \mathbf{Z}_{R,bi} & \mathbf{Z}_{R,bb}+\mathbf{Z}_B & -\mathbf{Z}_B & \mathbf{0} \\ \mathbf{0} & -\mathbf{Z}_B & \mathbf{Z}_B+\mathbf{Z}_{F,bb} & \mathbf{Z}_{F,bi} \\ \mathbf{0} & \mathbf{0} & \mathbf{Z}_{F,ib} & \mathbf{Z}_{F,ii} \end{bmatrix} \begin{Bmatrix} \mathbf{r}_{R,i} \\ \mathbf{r}_{R,b} \\ \mathbf{r}_{F,b} \\ \mathbf{r}_{F,i} \end{Bmatrix} = \begin{Bmatrix} \mathbf{f}_u \\ \mathbf{0} \\ \mathbf{0} \\ \mathbf{0} \end{Bmatrix}, \tag{5.1}$$

where $\mathbf{Z}$ is the dynamic stiffness matrix which is defined in Chapter 3. The subscripts b and i refer to bearing and internal (connection) DoF respectively, and the subscripts F, R, and B refer to foundation, rotor and bearings. $\mathbf{r}$ are the responses and $\mathbf{f}_u$ the unbalance force, which is assumed to be applied only at the rotor internal DoF.

Since measurements are taken at the bearings and not at the internal DoF of the foundation, only a reduced foundation model $\overline{\mathbf{Z}}_F$ can be estimated which, using the last row of equation (5.1) to eliminate the internal foundation DoF, is

$$\overline{\mathbf{Z}}_F = \mathbf{Z}_{F,bb} - \mathbf{Z}_{F,bi}\mathbf{Z}_{F,ii}^{-1}\mathbf{Z}_{F,ib} \tag{5.2}$$

Therefore equation (5.1) may be written as

$$\begin{bmatrix} \mathbf{Z}_{R,ii} & \mathbf{Z}_{R,ib} & \mathbf{0} \\ \mathbf{Z}_{R,bi} & \mathbf{Z}_{R,bb}+\mathbf{Z}_B & -\mathbf{Z}_B \\ \mathbf{0} & -\mathbf{Z}_B & \mathbf{Z}_B+\overline{\mathbf{Z}}_F \end{bmatrix} \begin{Bmatrix} \mathbf{r}_{R,i} \\ \mathbf{r}_{R,b} \\ \mathbf{r}_{F,b} \end{Bmatrix} = \begin{Bmatrix} \mathbf{f}_u \\ \mathbf{0} \\ \mathbf{0} \end{Bmatrix} \tag{5.3}$$

The solution of equation (5.1) to eliminate $\mathbf{r}_{R,i}$ and $\mathbf{r}_{R,b}$ gives the following relation

$$\overline{\mathbf{Z}}_F \mathbf{r}_{F,b} = \mathbf{Z}_B(\mathbf{P}^{-1}\mathbf{Z}_B - \mathbf{I})\mathbf{r}_{F,b} - \mathbf{Z}_B\,\mathbf{P}^{-1}\mathbf{Z}_{R,bi}\mathbf{Z}_{R,ii}^{-1}\mathbf{f}_u\,, \tag{5.4}$$

where $\mathbf{P} = \mathbf{Z}_{R,bb} + \mathbf{Z}_B - \mathbf{Z}_{R,bi}\mathbf{Z}_{R,ii}^{-1}\mathbf{Z}_{R,ib}$

5.1.1. Definition of Unbalance Force, $\mathbf{f}_u$

Although the unbalance will be distributed throughout the rotor, this is equivalent to a discrete distribution of unbalance, provided there are as many balance planes as active modes. Suppose the unbalance planes are located at nodes $n_1, n_2, \ldots, n_p$, where p is the number of planes. The associated amplitude of unbalance (defined as the unbalance mass multiplied by distance between the mass and geometric centres) and phase angles are $[u_{n_1}, u_{n_2}, \ldots, u_{n_p}]^{\mathrm{T}}$ and $[\theta_{n_1}, \theta_{n_2}, \ldots, \theta_{n_p}]^{\mathrm{T}}$ respectively. These amplitudes and phase angles can be expressed, for the i th balance plane, as the complex quantity $u_{n_i}\exp\left(\mathrm{j}\theta_{n_i}\right) = e_{r,n_i} + \mathrm{j}\,e_{i,n_i}$. Hence, the unbalance forces, $\mathbf{f}_u$, in the horizontal and vertical directions, can be written as

$$\mathbf{f}_u = \omega^2 \begin{Bmatrix} \mathbf{0} \\ e_{r,n_1} + j\,e_{i,n_1} \\ -j\,e_{r,n_1} + e_{i,n_1} \\ \mathbf{0} \\ \vdots \\ \mathbf{0} \\ e_{r,n_2} + j\,e_{i,n_2} \\ -j\,e_{r,n_2} + e_{i,n_2} \\ \mathbf{0} \\ \vdots \end{Bmatrix}, \tag{5.5}$$

where the positions in the unbalance force vector depend on the nodal locations of the unbalance planes. The expression for the unbalance forces can be further simplified as

$$\mathbf{f}_u = \omega^2 \mathbf{T}\mathbf{e}, \tag{5.6}$$

where $\mathbf{e} = \left[e_{r,n_1} \;\; e_{r,n_2} \;\cdots\; e_{r,n_p} \;\; e_{i,n_1} \;\; e_{i,n_2} \;\cdots\; e_{i,n_p} \right]^{\mathrm{T}}$ and $\mathbf{T}$ is the transformation matrix that is defined such that equations (5.5) and (5.6) are equivalent. Substituting equation (5.6) into equation (5.4) produces,

$$\overline{\mathbf{Z}}_F \mathbf{r}_{F,b} = \mathbf{Z}_B(\mathbf{P}^{-1}\mathbf{Z}_B - \mathbf{I})\mathbf{r}_{F,b} - \omega^2(\mathbf{Z}_B\,\mathbf{P}^{-1}\mathbf{Z}_{R,bi}\mathbf{Z}_{R,ii}^{-1}\mathbf{T})\mathbf{e} \tag{5.7}$$

or, equivalently,

$$\overline{\mathbf{Z}}_F \mathbf{r}_{F,b} = \mathbf{Z}_1 \mathbf{r}_{F,b} + \omega^2 \mathbf{Z}_2 \mathbf{T}\mathbf{e}, \tag{5.8}$$

where the form of $\mathbf{Z}_1$ and $\mathbf{Z}_2$ is clear from equation (5.7). As mentioned earlier in Chapter 3, it is assumed that good models for rotor and bearings ($\mathbf{Z}_R, \mathbf{Z}_B$) are known *a priori* and $\mathbf{r}_{F,b}$ are the measured data.

5.2. FOUNDATION MODEL ESTIMATION

To identify the foundation parameters accurately, the unbalance forces (**e**) are also assumed to be known either from balancing runs, by the difference in the response during two run-downs. Since all other quantities and data in equation (5.8) are known, the foundation model ($\overline{\mathbf{Z}}_F$) can be estimated. The linear least-squares estimation of foundation models from equation (5.8) should be followed by non-linear estimation. These aspects are discussed below.

5.2.1. Linear Least-Squares Estimation

Equation (5.8) can be solved in the linear least-squares sense. The foundation parameters are grouped into a vector $\mathbf{v}$. Let us assume that the foundation dynamic stiffness matrix, $\overline{\mathbf{Z}}_F$, is written in terms of mass, damping and stiffness matrices. If there are n measured degrees of freedom at the foundation-bearing interface, then $\mathbf{v}$ will take the form,

$\mathbf{v} =$

$$\left[\bar{k}_{F,11} \quad \bar{k}_{F,12} \quad \cdots \quad \bar{k}_{F,nn} \quad \bar{c}_{F,11} \quad \bar{c}_{F,12} \quad \cdots \quad \bar{c}_{F,nn} \quad \bar{m}_{F,11} \quad \bar{m}_{F,12} \quad \cdots \quad \bar{m}_{F,nn}\right]^{\mathrm{T}}, \tag{5.9}$$

where the elements in **v** are individual elements of the structural matrices. Such an assumption for the form of the foundation system matrices help to reduce the number of parameters compared to those used by Smart *et al.* (2000). With the present definition of **v**, there is a linear transformation such that

$$\bar{\mathbf{Z}}_F \mathbf{r}_{F,b} = \mathbf{W}\mathbf{v}, \tag{5.10}$$

where **W** contains the response terms at each measured frequency (Sinha *et al.*, 2002b). For the q th measured frequency

$$\mathbf{W}(\omega_q) = \left[\, \mathbf{W}_0(\omega_q) \;\; \mathbf{W}_1(\omega_q) \;\; \mathbf{W}_2(\omega_q) \,\right], \tag{5.11}$$

where, if all parameters of the elements of the foundation mass, damping and stiffness matrices are identified,

$$\mathbf{W}_k(\omega_q) = (\mathrm{j}\omega_q)^k \begin{bmatrix} \mathbf{r}_{F,b}^{\mathrm{T}}(\omega_q) & \mathbf{0} & \cdots & \mathbf{0} \\ \mathbf{0} & \mathbf{r}_{F,b}^{\mathrm{T}}(\omega_q) & & \mathbf{0} \\ \vdots & \vdots & \ddots & \vdots \\ \mathbf{0} & \mathbf{0} & \cdots & \mathbf{r}_{F,b}^{\mathrm{T}}(\omega_q) \end{bmatrix} \tag{5.12}$$

where $k = 0, 1, 2$. Equation (5.8) then becomes

$$\mathbf{W}(\omega_q)\mathbf{v} = \mathbf{Q}(\omega_q), \tag{5.13}$$

where the form of **Q** may be obtained by comparing equations (5.8), (5.10) and (5.13), as

$$\mathbf{Q}(\omega_q) = \mathbf{Z}_1(\omega_q)\mathbf{r}_{F,b}(\omega_q) + \omega_q^2 \mathbf{Z}_2(\omega_q)\mathbf{T}\mathbf{e} \tag{5.14}$$

5.2.1.1. Splitting the Frequency Range

Obviously, the DoF of the estimated foundation model by this method would be equal to the number of measurement locations during machine run-down. Often, especially for large machines, the number of critical speeds of the system in the run-down frequency range, is more than the number of measurement locations. This requires

splitting the entire frequency range into smaller bands and the foundation models have to be estimated for each frequency band (Smart *et al.*, 2000, Sinha *et al.*, 2002a). The splitting of the frequency range may be performed by a visual inspection of the measured responses, together with some experience and a trial and error approach. However, the first trial itself will give a good estimate if the number of frequency peaks seen on the measured responses (both in the vertical and horizontal directions) are less than the total DoF of the foundation model to be estimated in each frequency band.

Suppose that the frequencies at which the response is measured are ω_q, $q = 1,\ldots, N$. Let us assume that the run-down frequency range is split into b frequency bands. The vectors of the foundation parameters are to be identified in each frequency band, and are denoted as $\mathbf{v}_1$, $\mathbf{v}_2,\ldots,$ $\mathbf{v}_b$. For each frequency band an equation similar to equation (5.13) is generated and can be written as

$$\mathbf{W}_{\text{band}\_\ell}\mathbf{v}_\ell = \mathbf{Q}_{\text{band}\_\ell} \tag{5.15}$$

where $\ell = 1, 2, \ldots, b$. Clearly there is an equation of the form of (5.15) for each frequency band. The equations generated may be solved in a least squares sense directly, although the solution via the singular value decomposition (SVD) is more robust. Such an equation error approach does not optimize the error in the response directly, and thus the accuracy of the predicted response is not assured. The great advantage is that the equations are linear in the parameters. However a non-linear optimization (output error) has to be performed, starting with the linearly estimated parameters, if a more accurate prediction of the response is required. Such a non-linear optimization is discussed later.

5.2.1.2. Regularization

Equation (5.15) is a least-squares problem, and its solution is likely to be ill conditioned (Smart, 1998). The following two types of *regularization* were used to solve the least-squares problem.

Regularization Method-1: In solving the least-squares problem, generally two types of scaling, namely row scaling and column scaling, may be applied (Golub and Van

Loan, 1996). Column scaling is necessary because of the different magnitudes of elements of the $\bar{\mathbf{M}}_F$, $\bar{\mathbf{C}}_F$ and $\bar{\mathbf{K}}_F$ matrices, and the scaling factors used here were 1, $\bar{\omega}$ and $\bar{\omega}^2$ respectively, where $\bar{\omega}$ is the mean value of the frequency range. Truncated SVD was used to solve the equations (Hansen, 1994).

Regularisation Method-2: Other physically based constraints may be applied to the foundation model to improve the conditioning including *Regularization Method 1.* For example, the mass, damping and stiffness matrices of the foundation may be assumed to be symmetric, therefore reducing the number of unknown foundation parameters. Other constraints could be introduced, such as a diagonal mass or damping matrix, or block diagonal matrices if bearing pedestals do not interact dynamically.

Depending upon the physical constraints applied to the foundation model, the vector ($\mathbf{v}^*$) of the foundation parameters to be estimated may be reduced and can be defined as

$$\mathbf{v} = \mathbf{T}^* \mathbf{v}^*, \tag{5.16}$$

where $\mathbf{T}^*$ is the Transformation matrix that is defined such that equations (5.9) and (5.16) are equivalent. Substituting equation (5.16) into equation (5.15) produces,

$$\mathbf{W}_{\text{band\_}\ell} \mathbf{T}^* \mathbf{v}^*_\ell = \mathbf{Q}_{\text{band\_}\ell} \tag{5.17}$$

5.2.2. Non-Linear Optimization

The linearly estimated foundation models using both regularization methods were then optimized non-linearly. The output error function is defined as

$$\varepsilon_o = \mathbf{r}_m - \mathbf{r}(\mathbf{v}) \tag{5.18}$$

where $\mathbf{r}_m = \mathbf{r}_{F,b}$ is the measured response and $\mathbf{r}(\mathbf{v})$ is the output of the model i.e., predicted response for the measured quantities which is a function of the foundation parameters $\mathbf{v}$. The responses $\mathbf{r}(\mathbf{v})$ can be calculated from equation (5.8) as

$$\mathbf{r}(\mathbf{v}) = \omega^2 (\bar{\mathbf{Z}}_F - \mathbf{Z}_1)^{-1} \mathbf{Z}_2 \mathbf{T} \mathbf{e} \tag{5.19}$$

The change in the foundation parameters can be found by minimizing the cost function

$$\min \mathbf{J}_o = \sum \varepsilon_o^T \varepsilon_o \tag{5.20}$$

Equation (5.20) is non-linear in the parameters, and as a result an iterative process is required to solve it. The expression for the change in the parameters at each iteration is

$$\delta \mathbf{v} = (\mathbf{S}^T \mathbf{S})^{-1} \mathbf{S}^T (\mathbf{r}_m - \mathbf{r}(\mathbf{v})) \tag{5.21}$$

where $\mathbf{S}$ is the sensitivity matrix. It is the first order derivative of the response with respect to updating parameters, and can be expressed as

$$\mathbf{S} = \left[\frac{\partial \mathbf{r}}{\partial v(1)} \quad \frac{\partial \mathbf{r}}{\partial v(2)} \quad \cdots \quad \frac{\partial \mathbf{r}}{\partial v(p)} \right] \tag{5.22}$$

where $v(1)$, $v(2)$, ..., $v(p)$ are the elements of the foundation parameters vector $\mathbf{v}$. The equation (5.22) may be ill-conditioned and require regularization. Hence the equation (5.22) is regularized by adding a stabilization λ. The expression for the parameter changes may now be written as

$$\delta \mathbf{v} = (\mathbf{S}^T \mathbf{S} + \lambda \mathbf{I})^{-1} \mathbf{S}^T (\mathbf{r}_m - \mathbf{r}(\mathbf{v})) \tag{5.23}$$

The equation (5.23) is the *Levenberg-Marquardt technique* for solving the non-linear least-squares problems (Schoukens and Pintelon, 1991, Gill *et al.*, 1981), which is closely related to the minimum norm constraint in model updating. The regularization parameter, λ, generally helps to improve the solution conditioning if the matrix $\mathbf{S}^T\mathbf{S}$ becomes ill-conditioned and the cost function starts moving towards a saddle point. It also acts to restrain the size of the step change and avoid divergence.

Equation (5.22) for the sensitivity matrix can be further written as

$$\mathbf{S}=\begin{bmatrix} \mathbf{D}_k(\omega_1) & \mathbf{D}_c(\omega_1) & \mathbf{D}_m(\omega_1) \\ \mathbf{D}_k(\omega_2) & \mathbf{D}_c(\omega_2) & \mathbf{D}_m(\omega_2) \\ \vdots & \vdots & \vdots \\ \mathbf{D}_k(\omega_N) & \mathbf{D}_c(\omega_N) & \mathbf{D}_m(\omega_N) \end{bmatrix}, \tag{5.24}$$

where

$$\mathbf{D}_k(\omega_q)=\begin{bmatrix} \frac{\partial \mathbf{r}(\omega_q)}{\partial \bar{k}_{F,11}} & \frac{\partial \mathbf{r}(\omega_q)}{\partial \bar{k}_{F,12}} & \cdots & \frac{\partial \mathbf{r}(\omega_q)}{\partial \bar{k}_{F,nn}} \end{bmatrix} \tag{5.25}$$

$$\mathbf{D}_c(\omega_q)=\begin{bmatrix} \frac{\partial \mathbf{r}(\omega_q)}{\partial \bar{c}_{F,11}} & \frac{\partial \mathbf{r}(\omega_q)}{\partial \bar{c}_{F,12}} & \cdots & \frac{\partial \mathbf{r}(\omega_q)}{\partial \bar{c}_{F,nn}} \end{bmatrix} \tag{5.26}$$

$$\mathbf{D}_m(\omega_q)=\begin{bmatrix} \frac{\partial \mathbf{r}(\omega_q)}{\partial \bar{m}_{F,11}} & \frac{\partial \mathbf{r}(\omega_q)}{\partial \bar{m}_{F,12}} & \cdots & \frac{\partial \mathbf{r}(\omega_q)}{\partial \bar{m}_{F,nn}} \end{bmatrix} \tag{5.27}$$

Each element of equations (5.25) to (5.27) is calculated from equation (5.8). Equation (5.23) is applied to each frequency band as follows

$$\delta \mathbf{v}_\ell = (\mathbf{S}^T_{\text{band}\_\ell}\mathbf{S}_{\text{band}\_\ell} + \lambda_\ell \mathbf{I})^{-1}\mathbf{S}^T_{\text{band}\_\ell}(\mathbf{r}_m - \mathbf{r}(\mathbf{v}_\ell))_{\text{band}\_\ell} \tag{5.28}$$

where $\ell = 1, 2, \ldots, b$. $\mathbf{S}_{\text{band}\_\ell}$ is the sensitivity matrix for ℓ-band. The initial value of the regularization parameter, λ_ℓ, for starting the iteration should be a sufficiently high value. A good approximation may be obtained from the corner λ_ℓ of the *L*-curve (Hansen, 1994) for $\mathbf{S}_{\text{band}\_\ell}$ at starting $\mathbf{v}_\ell$. As brought out earlier the starting values used for $\mathbf{v}_\ell$ are always the linearly estimated values from section 5.2.1.

5.3. STATE OF ROTOR UNBALANCE ESTIMATION

In Section 5.2, the estimation of foundation models directly from the measured vibration data for a flexibly supported turbogenerator was presented. The suggested

method assumed a known unbalance of the rotor. Once a reliable mathematical model of the complete system, namely the rotor, the fluid bearings and the foundations of a TG set, is available the state of the rotor unbalance (both amplitude and phase) at multi-balance planes can be estimated from the measured vibration responses from a single run-down of the machine. However the model of the machine foundation is not readily available for many machines installed on site and the estimation of these parameters may be time consuming. Hence an alternative method is required that can overcome this limitation. The technique suggested by Lees and Friswell (1997) seems to be the most viable alternative.

The method suggested by Lees and Friswell (1997) estimates the rotor unbalance (both amplitude and phase) at multi-balance planes. The method uses the models of the rotor and bearings along with measured vibration response at the bearing pedestals during a single machine run down without affecting the normal setup of the machine, unlike other balancing methods. The method estimates the parameters of the foundation model as a by-product to account for the effects of the foundation dynamics along with the rotor unbalance. The potential of the method was highlighted through a simulated simple example (Lees and Friswell, 1997). Edwards *et al.* (2000) and Edwards (1999) have further demonstrated this approach experimentally on a small test rig during his doctorate study. Lees *et al.* (2000) further applied the method to a real life problem in a large TG unit. The estimated rotor unbalance was also observed to be sufficiently good for the TG unit. However this investigation will further explore the possibility of improvements to the rotor unbalance estimation method.

In the above examples (a simulated example, a small experimental rig and a TG set), the estimation was carried out using the whole frequency range of the run-down in a single band. For large machines, such as a turbogenerator, the number of modes of the flexible foundation in the whole run-down frequency range is likely to be higher than the measured number of DoFs in the foundation model. In such cases, the frequency range should be divided into smaller bands as suggested in Section 5.2 and the corresponding frequency dependent foundation parameters estimated as a by-product. This section gives theory and computational concept for the estimation of the rotor unbalance.

5.3.1. Linear Least-Squares Approach

Equation (5.7) can be written as

$$\bar{\mathbf{Z}}_F \mathbf{r}_{F,b} + \omega^2 \left[\mathbf{Z}_B \, \mathbf{P}^{-1} \mathbf{Z}_{R,bi} \, \mathbf{Z}_{R,ii}^{-1} \, \mathbf{T} \right] \mathbf{e} = \mathbf{Z}_B \left[\mathbf{P}^{-1} \mathbf{Z}_B - \mathbf{I} \right] \mathbf{r}_{F,b} . \tag{5.29}$$

Once again, it is assumed that good models for the rotor and bearings ($\mathbf{Z}_R, \mathbf{Z}_B$) are known *a priori* and $\mathbf{r}_{F,b}$ are the measured data. Since, all the quantities and data of equation (5.29) are known, the unbalance (**e**) along with the foundation model ($\bar{\mathbf{Z}}_F$) can be estimated.

To identify the unbalances along with the foundation parameters in a least squares sense, the equation (5.29) then becomes

$$\left[\mathbf{W}(\omega_q) \quad \mathbf{R}(\omega_q) \right] \begin{Bmatrix} \mathbf{v} \\ \mathbf{e} \end{Bmatrix} = \mathbf{Q}(\omega_q), \tag{5.30}$$

where **e** is unbalance parameters as defined in equation (5.6) and the form of **R** and **Q** may be obtained by comparing equations (5.29) and (5.30), as

$$\mathbf{R}(\omega_q) = \omega_q^2 \mathbf{Z}_B(\omega_q) \mathbf{P}^{-1}(\omega_q) \mathbf{Z}_{R,bi}(\omega_q) \mathbf{Z}_{R,ii}^{-1}(\omega_q) \mathbf{T} \tag{5.31}$$

$$\mathbf{Q}(\omega_q) = \mathbf{Z}_B(\omega_q) \left[\mathbf{P}^{-1}(\omega_q) \mathbf{Z}_B(\omega_q) - \mathbf{I} \right] \mathbf{r}_{F,b}(\omega_q) \tag{5.32}$$

Clearly there is an equation of the form of (5.30) at every frequency. How these sets of equations are combined is addressed below. The equations generated may be solved in a least squares sense directly, although the solution via the singular value decomposition (SVD) is more robust. Such an equation error approach does not optimize the error in the response directly, and thus the accuracy of the predicted response is not assured. The great advantage is that the equations are linear in the parameters. However a non-linear optimization (output error) may be performed, starting with linear estimated parameters, if a more accurate prediction of the response is required. In this chapter, only the equation error approach has been considered in order to concentrate on the influence of frequency range subdivision.

5.3.2. Computational Approach

As earlier it is suppose that the frequencies at which the response is measured are ω_q, $q = 1,\ldots,N$. Then the different methods arise depending on whether the frequency range is split, or not, and whether the unbalance is assumed to be different in each frequency band. Thus the identification can be carried out in three ways.

5.3.2.1. Method 1: Using the Entire Frequency Range as a Singie Band

Here all the measurements are used at once, and only one estimate of the unbalance state and the foundation model is produced. Thus, equation (5.30) is repeated N times to give

$$\begin{bmatrix} \mathbf{W}_0(\omega_1) & \mathbf{W}_1(\omega_1) & \mathbf{W}_2(\omega_1) & \mathbf{R}(\omega_1) \\ \mathbf{W}_0(\omega_2) & \mathbf{W}_1(\omega_2) & \mathbf{W}_2(\omega_2) & \mathbf{R}(\omega_2) \\ \vdots & \vdots & \vdots & \vdots \\ \mathbf{W}_0(\omega_N) & \mathbf{W}_1(\omega_N) & \mathbf{W}_2(\omega_N) & \mathbf{R}(\omega_N) \end{bmatrix} \begin{Bmatrix} \mathbf{v} \\ \mathbf{e} \end{Bmatrix} = \begin{bmatrix} \mathbf{Q}(\omega_1) \\ \mathbf{Q}(\omega_2) \\ \vdots \\ \mathbf{Q}(\omega_N) \end{bmatrix} \tag{5.33}$$

This is the method suggested by Lees and Friswell (1997). However if the number of modes in the run-down frequency range is more than the measured DoF at the bearing pedestals, one set of foundation parameters, **v**, may not be enough and the estimated unbalance and the responses may not be close to the actual values. There could be two possible approaches (***Methods 2*** and ***3***) for solving such limitations, which are discussed below.

5.3.2.2. Method 2: Dividing the Frequency Range into Bands

Often, especially for large machines, the number of critical speeds of the system in the run-down frequency range, is more than the number of measurement locations i.e., measured DoFs. This requires splitting the entire frequency range into smaller bands, as discussed in Section 5.2. The frequency dependent foundation model and the unbalance can be then estimated in each frequency band in a similar manner to ***Method 1***. The estimated unbalance for each band should be the same, however this is unlikely because different modes will influence the response in each of the bands. In this approach there will often be fewer critical speeds in the frequency band than foundation DoF, and regularization using the SVD method has to be applied.

5.3.2.3. Method 3: The Combined Approach

Method 1 estimates only one rotor unbalance state and one foundation model for whole frequency range. It is highly likely that the foundation identification will not be accurate. The foundation model estimated by ***Method 2*** may be accurate enough, but a global estimate of unbalance is not obtained. Hence, a combined approach is suggested combining the expected advantages of the above two methods.

Let us assume that the run-down frequency range is split into b frequency bands. The vectors of the foundation parameters are identified in each frequency band, and are denoted $\mathbf{v}_1, \mathbf{v}_2, \ldots, \mathbf{v}_b$. For each frequency band an equation similar to equation (5.30) is generated, and if the **W**, **R** and **Q** matrices are combined, can be written as

$$\left[\mathbf{W}_{\text{band}\_\ell} \;\; \mathbf{R}_{\text{band}\_\ell}\right]\begin{Bmatrix}\mathbf{v}_\ell \\ \mathbf{e}\end{Bmatrix} = \mathbf{Q}_{\text{band}\_\ell} \tag{5.34}$$

Rather than solving for the parameters for an individual band, as in ***Method 2***, the problem may also be solved in one step using entire frequency range of the run-down as ***Method 1***, giving a global estimate of the unbalance vector **e**. Thus, combining equation (5.34) for all the bands, gives

$$\begin{bmatrix} \mathbf{W}_{\text{band}\_1} & \mathbf{0} & \cdots & \mathbf{0} & \mathbf{R}_{\text{band}\_1} \\ \mathbf{0} & \mathbf{W}_{\text{band}\_2} & \cdots & \mathbf{0} & \mathbf{R}_{\text{band}\_2} \\ \vdots & \vdots & \ddots & \vdots & \vdots \\ \mathbf{0} & \mathbf{0} & \cdots & \mathbf{W}_{\text{band}\_b} & \mathbf{R}_{\text{band}\_b} \end{bmatrix}\begin{Bmatrix}\mathbf{v}_1 \\ \mathbf{v}_2 \\ \vdots \\ \mathbf{v}_b \\ \mathbf{e}\end{Bmatrix} = \begin{Bmatrix}\mathbf{Q}_{\text{band}\_1} \\ \mathbf{Q}_{\text{band}\_2} \\ \vdots \\ \mathbf{Q}_{\text{band}\_b}\end{Bmatrix} \tag{5.35}$$

Equations (5.33) to (5.35) are least squares problems, and their solutions are likely to be ill-conditioned (Smart *et al.*, 2000) and may need some regularization.

5.3.3. Regularization

The kind of regularization required to obtain a useful solution of the above equations generally depends on engineering judgement. However, broadly two types of regularization should be used as described in Section 5.2.3. One is the mathematical treatment (*Regularization Method 1*) of the least squares equations and the other is by imposing physical relations between the system parameters to be estimated including *Regularization 1* (*Regularization Method 2*). Apart from these regularizations, one

more regularization is also important in case of unbalance estimation which is discussed below.

Regularization Method 3: The way the system dynamic matrices have been partitioned in the equation (5.1), the expression $\mathbf{Z}_{R,ii}$ is the dynamic matrix of the rotor with pinned DoFs at the bearing locations of the rotating machinery. It contains natural frequencies of the pinned supported rotor, which do not represent any system dynamics, in the run-down frequency range. At these frequencies the dynamic matrix $\mathbf{Z}_{R,ii}$ would be close to singular and its inverse may result in numerical ill-conditioning particularly for lightly damped rotor. Hence it would be better to remove a small frequency band at these frequencies, from the run-down range, to avoid this numerical ill-conditioning. *Regularization 3* includes *Regularization 2* also.

5.4. ESTIMATION OF BOTH UNBALANCE AND MISALIGNMENT FROM A SINGLE MACHINE RUN-DOWN

In ***Methods 1*** to ***3*** the estimation of unbalance using the measured 1X responses at the bearing pedestals is performed using a single machine run-down. The unbalance estimation may be in error if the multi-coupled rotors have some misalignment, since the misalignment may influence the 1X response. The misalignment in the rotor, which is usually assumed at couplings, is expected to generate forces and moments at the couplings in both the horizontal and vertical directions, as suggested earlier by Gibbons (1976). The magnitude of these forces and moments will depend on the extent of the misalignment. However, the influence of these forces and moments at the rotor coupling on the machine dynamic behaviour is expected to be constant throughout the run-down speed range. Hence the estimation of the forces and moments at rotor couplings along with the unbalance at multi-balance planes has been proposed. The proposed theory is discussed below.

5.4.1. Theory

Equation (5.7) can be written as

$$\bar{\mathbf{Z}}_F \mathbf{r}_{F,b} + \mathbf{Z}_B \mathbf{P}^{-1} \mathbf{Z}_{R,bi} \mathbf{Z}_{R,ii}^{-1} (\mathbf{f}_u + \mathbf{f}_m) = \mathbf{Z}_B \left[\mathbf{P}^{-1} \mathbf{Z}_B - \mathbf{I} \right] \mathbf{r}_{F,b} . \tag{5.36}$$

where the definition of the unbalance force $\mathbf{f}_u$ is same as in the equation (5.6) and $\mathbf{f}_m$ is a vector of forces and moments due to the misalignment.

5.4.1.1. Definition of Misalignment Force, $\mathbf{f}_m$

It has been assumed that the misalignment in the rotor exists at the couplings between the multi-rotors. The nature of the rotor misalignment could be parallel, angular or combined as shown in Figure 5.1, but all of them would generate forces and moments. Let us assumed that there are c couplings in the rotor located at nodes m_1, m_2, ..., m_c. The associated amplitude of forces and moments are $\mathbf{e}_m = [\mathrm{f}_{z,m_1}, \ \mathrm{f}_{y,m_1}, \ \mathrm{M}_{y,m_1}, \ \mathrm{M}_{z,m_1}, \ \mathrm{f}_{z,m_2}, \ \mathrm{f}_{y,m_2}, \ \mathrm{M}_{y,m_2}, \ \mathrm{M}_{z,m_2}, \ \ldots$ $\ldots \ \mathrm{f}_{z,m_c}, \ \mathrm{f}_{y,m_c}, \ \mathrm{M}_{y,m_c}, \ \mathrm{M}_{z,m_c}]^T$, where the subscripts y and z represent the horizontal and vertical directions and f and M are forces and moments respectively. Hence, the misalignment force, $\mathbf{f}_m$, can be written as

$$\mathbf{f}_m = [\mathbf{0} \ \ \mathrm{f}_{z,m_1} \ \ \mathrm{f}_{y,m_1} \ \ \mathrm{M}_{y,m_1} \ \ \mathrm{M}_{z,m_1} \ \ \mathbf{0} \ \ldots \mathrm{f}_{z,m_2} \ \ \mathrm{f}_{y,m_2} \ \ \mathrm{M}_{y,m_2} \ \ \mathrm{M}_{z,m_2} \ \ \mathbf{0} \ \ldots]^T \tag{5.37}$$

This expression can be further simplified as

$$\mathbf{f}_m = \mathbf{T}_m \mathbf{e}_m , \tag{5.38}$$

where $\mathbf{T}_m$ is the transformation matrix that is defined such that equations (5.37) and (5.38) are equivalent. Substituting equations (5.6) and (5.38) into equation (5.36) produces,

$$\overline{\mathbf{Z}}_F \mathbf{r}_{F,b} + \mathbf{Z}_B \mathbf{P}^{-1} \mathbf{Z}_{R,bi} \mathbf{Z}_{R,ii}^{-1} \begin{bmatrix} \omega^2 \mathbf{T} & \mathbf{T}_m \end{bmatrix} \begin{Bmatrix} \mathbf{e} \\ \mathbf{e}_m \end{Bmatrix} = \mathbf{Z}_B \left[\mathbf{P}^{-1} \mathbf{Z}_B - \mathbf{I} \right] \mathbf{r}_{F,b} . \tag{5.39}$$

Since, all the other quantities and data in equation (5.39) are known, the unbalance ($\mathbf{e}$) and the misalignment forces and moments ($\mathbf{e}_m$) along with the foundation model ($\overline{\mathbf{Z}}_F$) can be estimated.

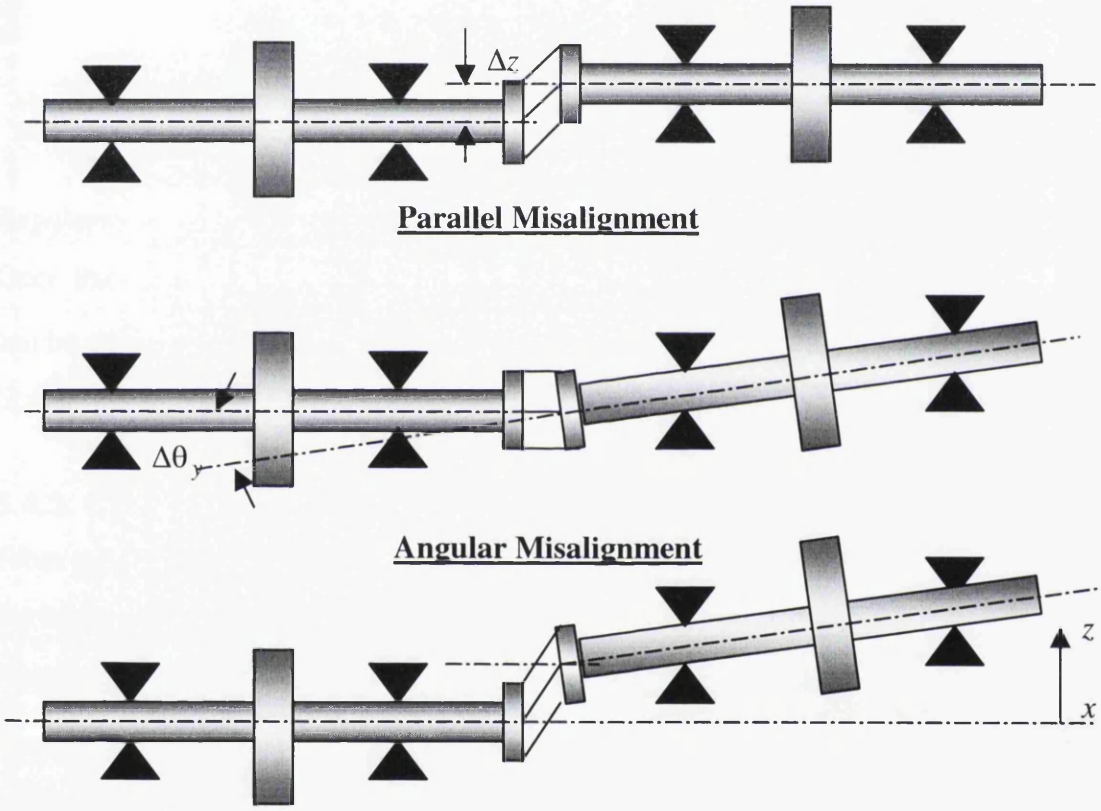

Figure 5.1 Schematic of rotor with misalignment at a coupling

5.4.2. Linear Least-Squares Approach

To identify the unbalance and misalignment in a least squares sense similar to ***Method 3***, equation (5.39) becomes

$$\begin{bmatrix} \mathbf{W}_{\text{band\_1}} & \mathbf{0} & \cdots & \mathbf{0} & \mathbf{R}_{\text{band\_1}} & \mathbf{R}_{m,\text{band\_1}} \\ \mathbf{0} & \mathbf{W}_{\text{band\_2}} & \cdots & \mathbf{0} & \mathbf{R}_{\text{band\_2}} & \mathbf{R}_{m,\text{band\_2}} \\ \vdots & \vdots & \ddots & \vdots & \vdots & \vdots \\ \mathbf{0} & \mathbf{0} & \cdots & \mathbf{W}_{\text{band\_}b} & \mathbf{R}_{\text{band\_}b} & \mathbf{R}_{m,\text{band\_}b} \end{bmatrix} \begin{Bmatrix} \mathbf{v}_1 \\ \mathbf{v}_2 \\ \vdots \\ \mathbf{v}_b \\ \mathbf{e} \\ \mathbf{e}_m \end{Bmatrix} = \begin{Bmatrix} \mathbf{Q}_{\text{band\_1}} \\ \mathbf{Q}_{\text{band\_2}} \\ \vdots \\ \mathbf{Q}_{\text{band\_}b} \end{Bmatrix}, \quad (5.40)$$

where the definition of **W**, **R** and **Q** is same as defined in equations (5.12), (5.31) and (5.32). The form of $\mathbf{R}_m$ may be obtained by comparing equations (5.39) and (5.40), as

$$\mathbf{R}_m(\omega_q) = \mathbf{Z}_B(\omega_q)\mathbf{P}^{-1}(\omega_q)\mathbf{Z}_{R,bi}(\omega_q)\mathbf{Z}_{R,ii}^{-1}(\omega_q)\mathbf{T}_m \quad (5.41)$$

Regularization 1-3 must be used to solve equation (5.40) in a least squares sense. Once the misalignment force ($\mathbf{e}_m$) is estimated the linear and angular misalignment can be calculated as below.

5.4.3. Calculation of Linear and Angular Misalignment

From geometry and the material properties the stiffness matrix for each coupling in the multi-rotors machine can be calculated. Let us assume that the stiffness of an *i*th coupling is $\mathbf{K}_{c,i}$ then the linear misalignment, Δy_i & Δz_i, and the angular misalignment, $\Delta\theta_{y,i}$ & $\Delta\theta_{z,i}$ at the *i*th coupling in the horizontal and the vertical directions can be calculated as (Gibbon, 1976)

$$\begin{Bmatrix} \Delta z_i \\ \Delta y_i \\ \Delta\theta_{y,i} \\ \Delta\theta_{z,i} \end{Bmatrix} = [\mathbf{K}_{c,i}]^{-1} \begin{Bmatrix} \mathrm{f}_{z,i} \\ \mathrm{f}_{y,i} \\ \mathrm{M}_{y,i} \\ \mathrm{M}_{z,i} \end{Bmatrix} \quad (5.42)$$

5.5. SUMMARY

The theory for the estimation of the foundation model directly from the measured vibration data has been presented. The suggested method and two regularization methods have been applied to simulated and experimental examples of rotating machines to bring out their usefulness and potential. This is presented in Chapter 6.

The importance and requirements of the proposed methods for rotor unbalance and misalignment estimation is highlighted. The theory of rotor unbalance and misalignment estimation and its computational concept has been discussed. The advantages and limitations of the proposed estimation methods will be presented in Chapter 7 through the numerical simulations and experimental examples. The sensitivity analysis of the proposed method with respect to errors in the rotor and bearings models is presented in Chapter 8.

CHAPTER 6

FOUNDATION MODEL ESTIMATION: NUMERICAL SIMULATIONS AND EXPERIMENTAL EXAMPLES

6.0. INTRODUCTION

This chapter is concerned with the usefulness and validation of the suggested method (in Chapter 5) for the estimation of foundation models of a rotor-fluid bearing-flexible foundation system like a TG set. A computational program for both linear and non-linear optimization for foundational model estimation using the theory given in Chapter-5 has been developed in MatLab. Options for both the *Regularization Method*s discussed in Chapter 5 are included in the computational code. Initially the suggested method for foundation model estimation is attempted using simulated examples with both *Regularization Method*s. Once the usefulness of the suggested method for the foundation models has been established on the numerical simulations of the rigs, the method is also applied to the Aston rig.

6.1. SIMULATED EXAMPLE 1: THE ASTON RIG

The numerically simulated rig is based on the *Aston rig* shown in Section 4.3 of Chapter-4. The physical dimensions and material properties for the rotor and bearings are exactly the same for this simulated case. A model for the rig foundation connected to the fluid bearings was assumed and the measured responses at bearing pedestals were computed analytically for the assumed foundation.

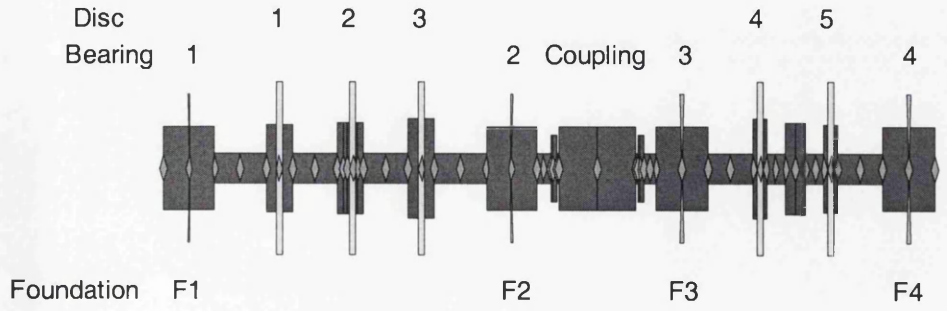

Figure 6.1 The mathematical model of the rotor and fluid bearings of the Aston rig

An FE model was created for the rotor with 51 two-noded *Timoshenko* beam elements, each with two bending translational and two bending rotational DoF. Short bearing theory was used to obtain values for the bearing stiffness and damping (Hamrock, 1994), assuming the static loads acting on bearings 1 to 4 are 400N, 221N, 486N and 461N respectively. The entire rig was assumed to be constrained along the axial direction of the rotor. The mathematical model of the rotor and fluid bearings is shown in Figure 6.1

Since there are four bearings, and only the horizontal and vertical accelerations are measured, there are 8 measured DoF. For the purpose of the simulation, the following mass, damping and stiffness matrices were used for the foundation, assuming no rotational components and the displacement vector of the foundation is ordered as

$$\mathbf{r}_F = [y_1 \quad z_1 \quad y_2 \quad z_2 \quad y_3 \quad z_3 \quad y_4 \quad z_4]^T, \tag{6.1}$$

where y and z are horizontal and vertical directions, and the subscripts refer to the response at the corresponding bearing. The foundation mass, damping and stiffness matrices are taken as

$$\mathbf{M}_F = \text{diag}[52 \quad 52 \quad 50 \quad 50 \quad 52 \quad 52 \quad 50 \quad 50] \text{ kg} \tag{6.2}$$

$$\mathbf{C}_F = \text{diag}[150 \quad 150 \quad 150 \quad 150 \quad 150 \quad 150 \quad 150 \quad 150] \text{ N s/m} \tag{6.3}$$

$$\mathbf{K}_F = \begin{bmatrix} 1.60 & -0.1 & -0.5 & 0.0 & 0.0 & 0.0 & 0.0 & 0.0 \\ & 1.60 & 0.0 & -0.5 & 0.0 & 0.0 & 0.0 & 0.0 \\ & & 1.50 & -0.1 & -0.5 & 0.0 & 0.0 & 0.0 \\ & & & 1.60 & 0.0 & -0.5 & 0.0 & 0.0 \\ & & & & 1.60 & -0.1 & -0.5 & 0.0 \\ & & \text{SYM} & & & 1.60 & 0.0 & -0.5 \\ & & & & & & 1.50 & -0.1 \\ & & & & & & & 1.60 \end{bmatrix} \text{MN/m} \tag{6.4}$$

This foundation model has a similar dynamic stiffness to the actual foundation and has a similar distribution of modes of the foundation in isolation (Smart, 1998). The measured responses associated with the translational degrees of freedom at all four

bearing pedestals were computed using the assumed foundation model and a given unbalance on the rotor, using equation (5.1). Table 6.1 shows the different unbalance configurations used to excite the rotor for the different runs. The machine was run-down from 60 Hz to 1 Hz, with simulated measurements taken at a spacing of 0.5 Hz. Using these measured responses without noise, the identification of the foundation models was then carried out using different *Regularization Methods*.

Table 6.1 The unbalance for the Aston rig simulation without noise

Unbalance Config	Balance Disk	Unbalance (amplitude in g m, phase in degree)	
		Unbalance	Phase
1	3	0.160	45
	4	0.160	150
2	1	0.160	195
	3	0.160	45
3	1	0.160	195
	5	0.160	0
4	1	0.160	195
	3	0.160	45
	4	0.160	150
5	1	0.160	195
	3	0.160	45
	5	0.160	0

6.1.1. Regularization Method 1

Considering the flexible foundation and bearing-rotor system together, the frequency range was divided into four bands, 1Hz to 15Hz, 15Hz to 28Hz, 28Hz to 40Hz and 40Hz to 60Hz. The estimation of the foundation models was carried out for each frequency band in turn. This estimation was carried out by both the linear and the non-linear iterative process starting from the linearly estimated values for the different unbalance configurations listed in Table 6.1. It has been observed that the linearly estimated foundation models produce a close fit to the simulated responses in all cases. Figure 6.2 shows a typical comparison of the estimated and measured responses for unbalance configuration 1. Non-linear estimation further improves the dynamics

of the foundation models, and the estimated responses are now an almost exact fit to the measured responses. This is also shown in Figure 6.2 for comparison.

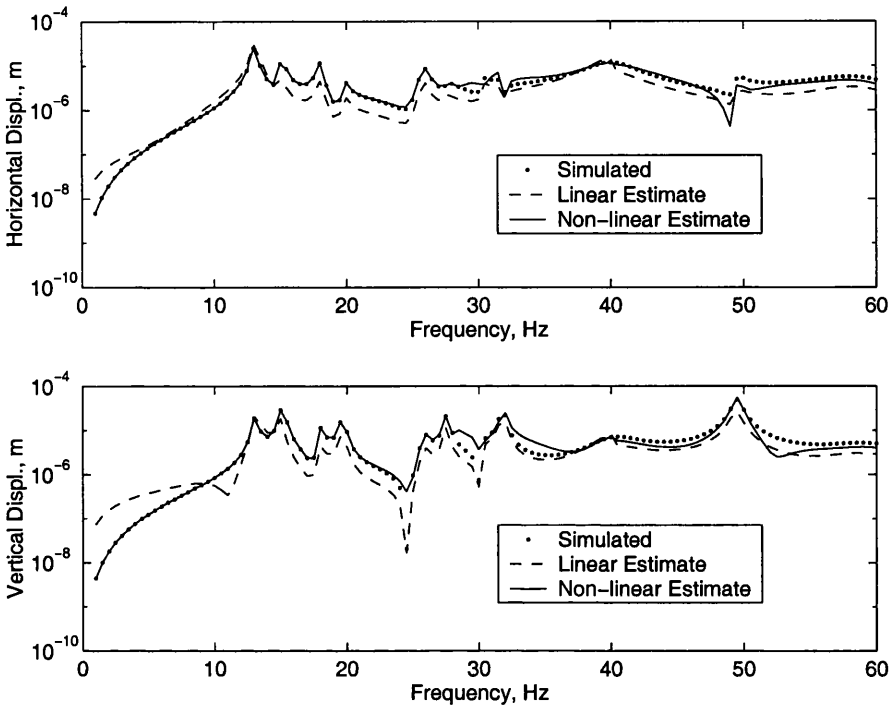

Figure 6.2 Comparison of simulated and estimated responses at bearing 2 using unbalance configuration 1 and Regularization 1 for the Aston rig simulation

6.1.1.1. Results and Discussion

Considering the use of the estimated foundation models for the prediction of faults and condition monitoring of the complete rotating machine, the validation of the estimated foundation models is very important. This validation should test the prediction capacity with respect to different excitations. This exercise was carried out using estimated foundation models with different unbalance configurations of Table 6.1. It was observed that the prediction capability was poor. One such prediction is shown in Figure 6.3. Hence this optimization seems to perform numerical conditioning for a set of known unbalance and the measured responses without any physical meaning and the estimated foundation dynamics may not be useful.

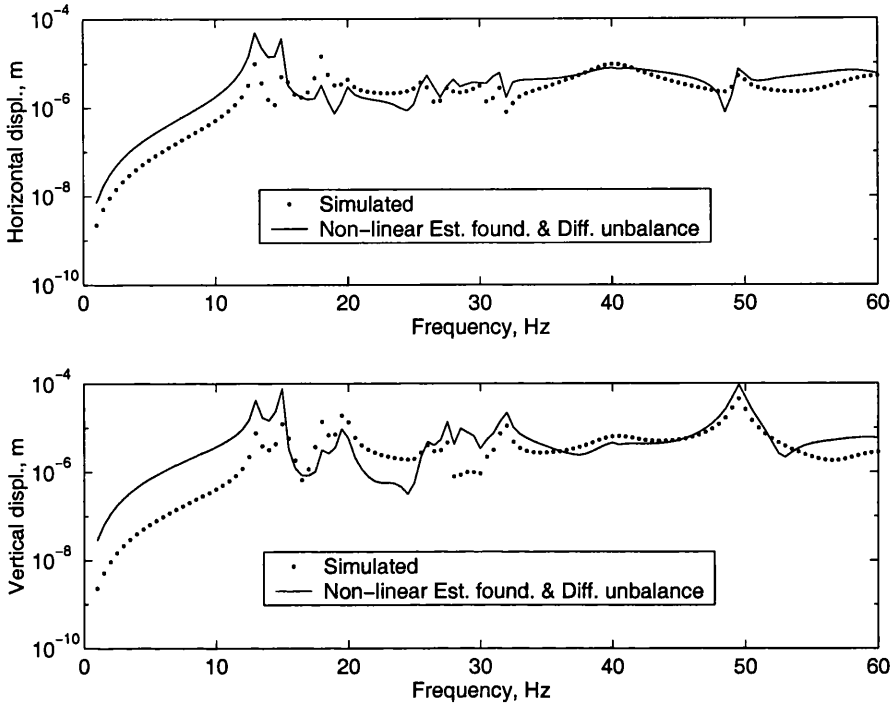

Figure 6.3 Dynamic behaviour (simulated and predicted responses) at bearing 2 of the estimated foundation using unbalance configuration 1 and Regularization 1, by unbalance configuration 3 for the Aston rig simulation

6.1.2. Regularization Method 2

The above exercise was repeated using the method discussed in Section 5.2.1.2. of Chapter 5 by assuming a symmetric stiffness matrix and diagonal damping and mass matrices (with the same mass at a node for vertical and horizontal DoF). This regularization is based on physical meaning, and has reduced the number of foundation parameters to be identified to a much smaller number compared to the earlier regularization. It was observed that the dynamics of the estimated foundation models based on the linear method was worst compared to the earlier *Regularization Method 1*. But the non-linear estimates starting from the linearly estimated values produces foundation models whose dynamics were found to be excellent. Figure 6.4 gives one such comparison of the estimated responses (by both linear and non-linear approaches) and the measured responses.

6.1.2.1. Results and Discussion

As can be seen from Figures 6.2 & 6.4, the linear estimation is poorer for the *Regularization Method 2* but the non-linear estimation is far superior. The prediction capacity of the estimated models with respect to different excitations was also checked. The prediction capability was found to be excellent for a variety of different unbalance configurations listed in Table 6.1. Several such predictions are shown in Figure 6.5. Hence the results obtained by this optimization seem to be useful and encouraging.

This method is again tested on a much simpler simulated example with noise to further strengthen the confidence level in the present optimization approach.

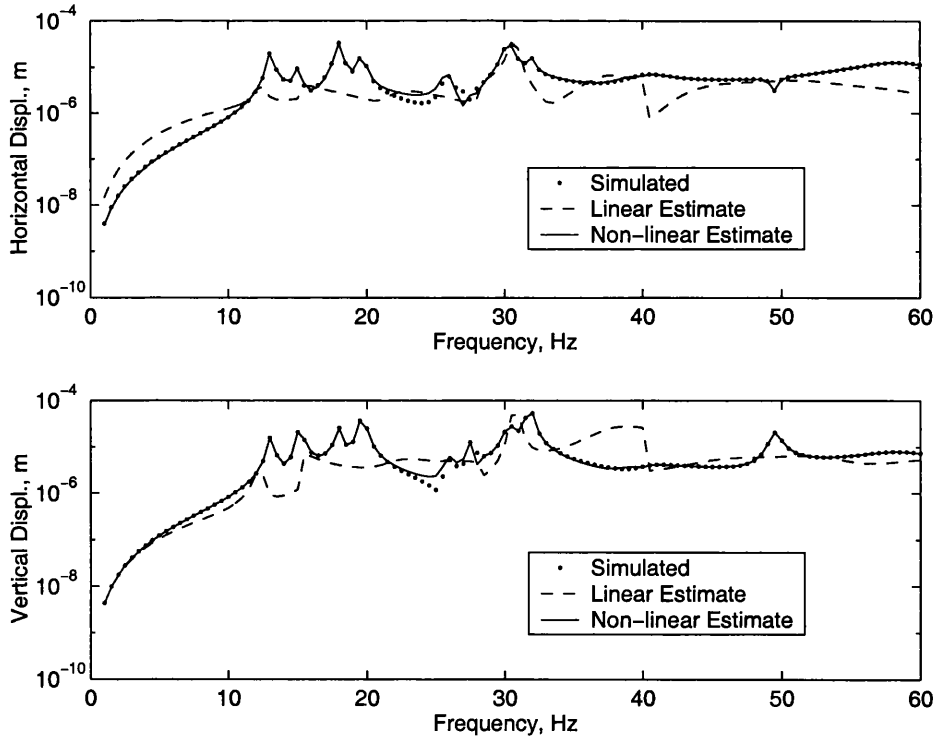

Figure 6.4 Comparison of simulated and estimated responses at bearing 3 using unbalance configuration 1 and Regularization 2 for the Aston rig simulation

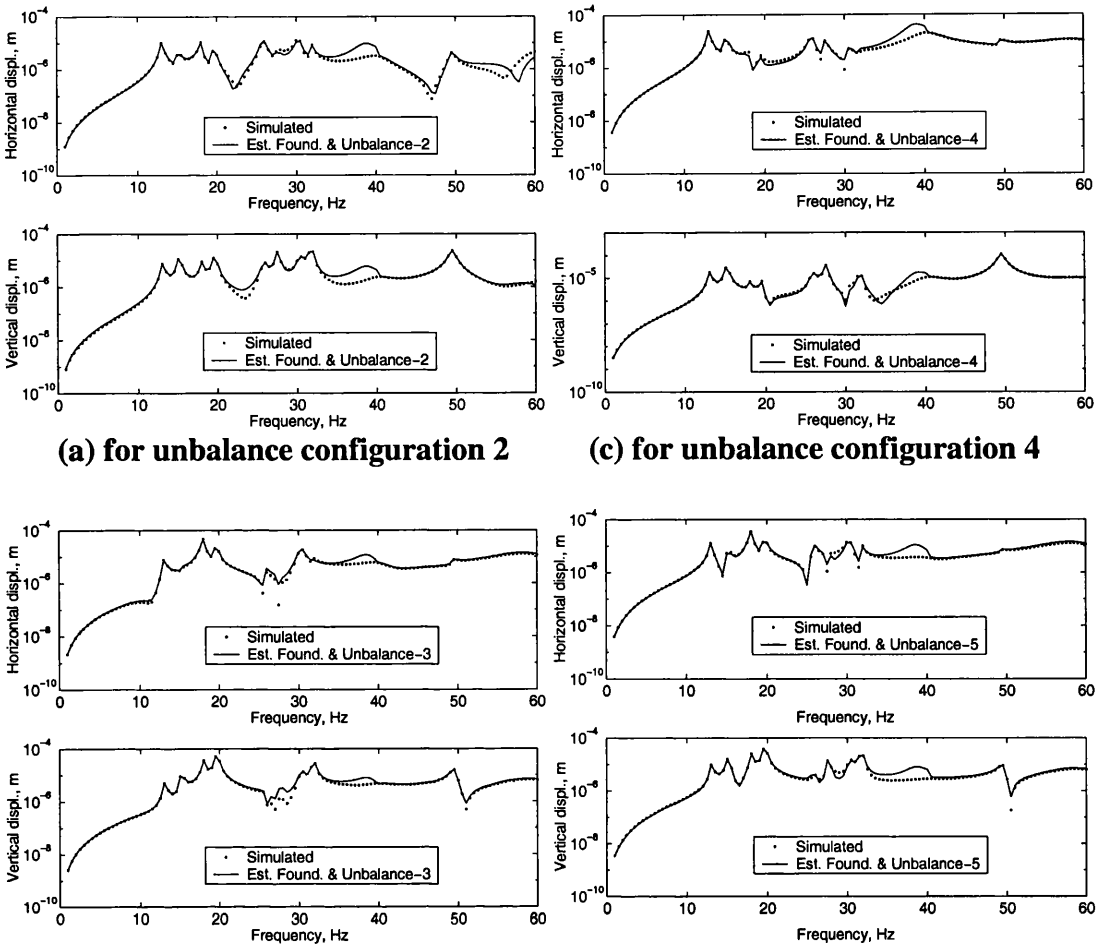

(a) for unbalance configuration 2 **(c) for unbalance configuration 4**

(b) for unbalance configuration 3 **(d) for unbalance configuration 5**

Figure 6.5 Prediction capacity of estimated foundation models using unbalance configuration 1 and Regularization 2, at bearing 3, by different unbalances for the Aston rig simulation

6.2. SIMULATED EXAMPLE 2: THE SMALL RIG

The simulated rig is based on the physical *small rig* at Swansea (UK), as described in Section 4.1. of Chapter 4. For the present simulations, the updated FE model of the foundation from Chapter 4 is used for the computation of measured responses at the bearing pedestals for a given unbalance on the rotor, using equation (5.1). For the simulation, the damping matrix for the foundation model was assumed to be proportional to the mass and stiffness matrices of the updated FE model with the proportional coefficients for the mass and stiffness of 0.9896 and 6.764e-5 respectively. These proportional coefficients result in 1% and 0.94% damping at the foundational natural frequencies of 9.986Hz and 32.777Hz respectively. Since there

are two bearings, and only the horizontal and vertical accelerations are measured, there are 4 measured DoF. The FE model of the rotor is rigidly connected to the foundation through the ball bearings shown in Figure 4.5 of Chapter 4 has been used for the responses computation and subsequent foundation model estimation. Table 6.2 shows the different unbalance configurations used to excite the rotor for different runs. The machine was run-down from 40Hz to 6Hz, with measurements taken at a spacing of 0.25 Hz. In practice the measured data will be contaminated by both structure and measuring instrument noise. To simulate this condition, the computed responses (assumed to be measured) for unbalance configuration-1 were contaminated by normally distributed random noise with zero mean and standard deviation of 2% of the maximum response amplitude (applied to both real and imaginary parts of the response). Using these measured responses the identification of the frequency band dependent foundation models was then carried out using *Regularization Method 2* – symmetric stiffness and damping matrices, and a diagonal mass matrix.

Table 6.2 The unbalance for the Small rig simulation with noise

Unbalance Config	Balance Disk	Unbalance (amplitude in g m, phase in degree)	
		Unbalance	Phase
1	A	5.0e-2	75
	B	5.0e-2	135
2	A	10.0e-2	90
	B	10.0e-2	30
3	A	7.5e-2	180
	B	15.0e-2	0

6.2.1. Linear Estimation

As in the earlier example, the frequency range was divided into two smaller bands, 6Hz to 21Hz and 21Hz to 40Hz. The estimation of the foundation models was carried out for each frequency band in turn using noise-contaminated responses for the rotor unbalance configuration 1. Initially the foundation models were estimated linearly using equation (5.17) of Section 5.2.1 of Chapter 5. The computed responses at bearings A and B are shown in Figure 6.6 and compared with the measured responses.

As usual the dynamic behaviour of the linearly estimated foundation models are poor. Hence non-linear optimization is necessary.

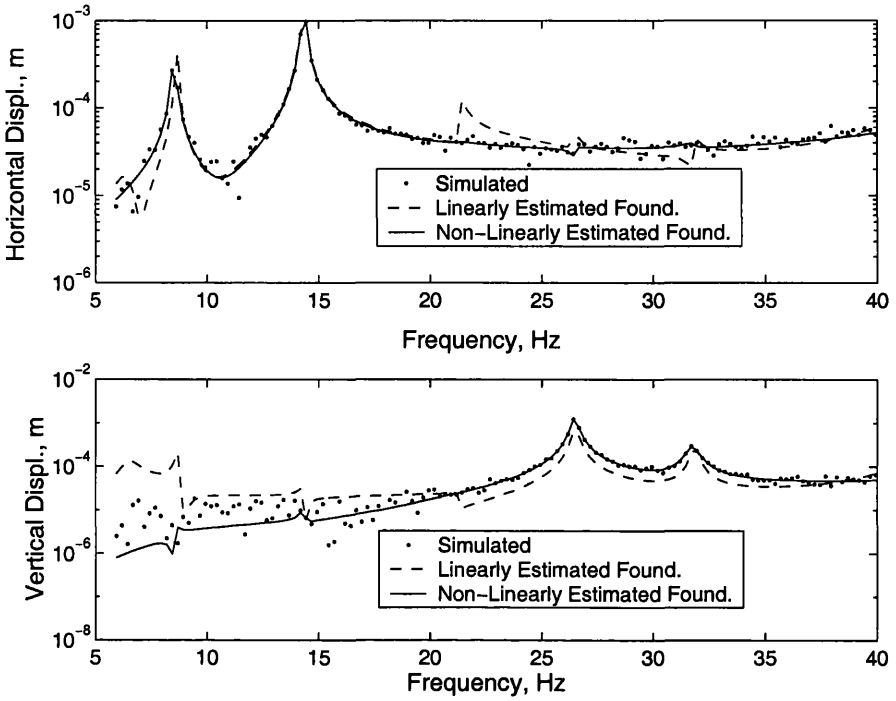

(a) Bearing A responses

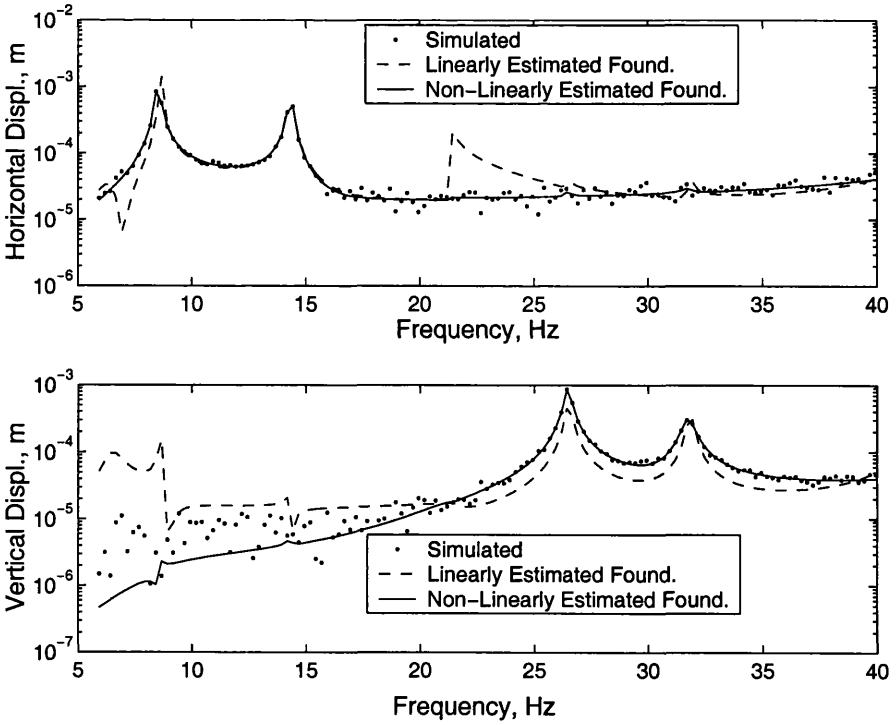

(b) Bearing B responses

Figure 6.6 Comparison of simulated (with noise) and estimated responses using unbalance configuration 1 and Regularization 2 for the Small rig simulation

6.2.2. Non-Linear Optimization

The non-linear optimization starting from linearly estimated foundation models were also carried out as per Section 5.2.2 of Chapter 5. A suitable value of regularization parameter, λ_ℓ (where $\ell = 1, \quad 2$), for starting the iterative process by the *Levenberg-Marquardt technique* for solving the non-linear least-squares problems, is important. As mentioned earlier in Section 5.2.2 (Chapter 5), a good choice is the corner λ_ℓ of *L*-curve for the sensitivity matrix at starting values of the foundation parameters. Figure 6.7 shows the *L*-curve at the start of first iteration for the frequency band 6Hz to 21Hz. As can be seen from the *L*-curve there is no clearly defined corner in the curve. In fact most of the practical optimization problems have similar difficulties that require some user or engineering judgement in choosing the value of λ_1. Alternatively different values of λ_1 can be used to check the convergence. Here the value of λ_1 = 0.000875 was chosen from *L*-curve and the non-linear optimization seems to converged, even though the measured responses were corrupted with noise. The dynamics of the non-linearly estimated foundation models are also shown in Figures 6.6.

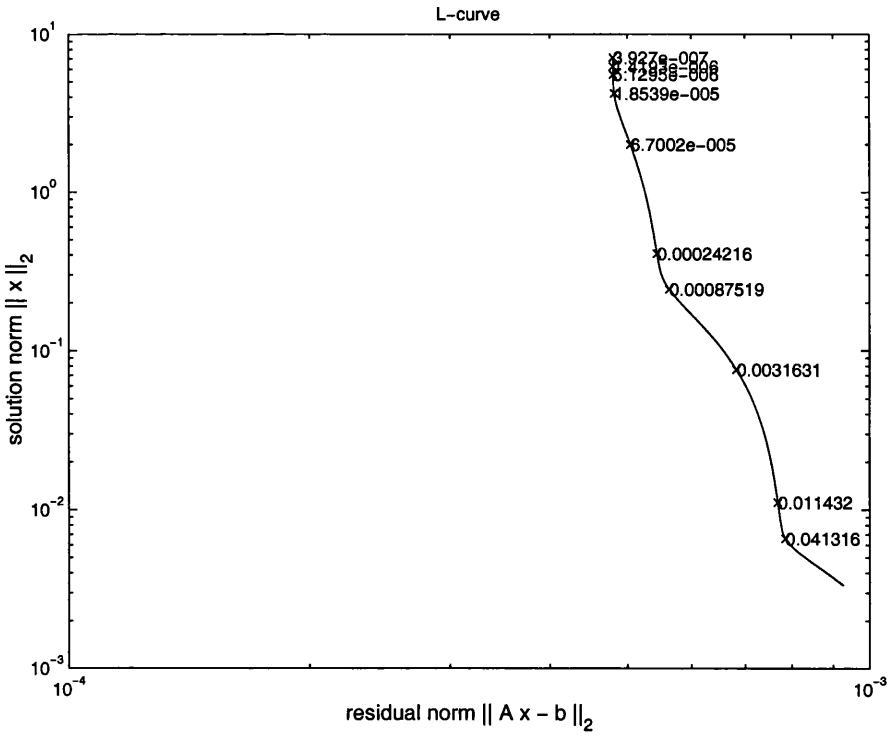

Figure 6.7 L-curve

6.2.3. Results and Discussion

As can be seen from Figure 6.6, although the measured responses in the frequency region other than the machine critical speeds range, both in horizontal and vertical directions, are very low in amplitude (perhaps only noise), the non-linear optimization seems to be promising. The prediction capacity of the estimated foundation models with respect to different excitations was also checked. The prediction capability was found to be excellent for a variety of different unbalance configurations listed in Table 6.2. Few typical predictions are shown in Figures 6.8. The predicted responses, both amplitudes and phases, are excellent in the machine critical speed range. Some deviation in the amplitudes and phases away from the critical speed range should not be any cause of concern as the displacement amplitudes are very small. Hence the suggested method for the foundation model estimation can be considered a robust method.

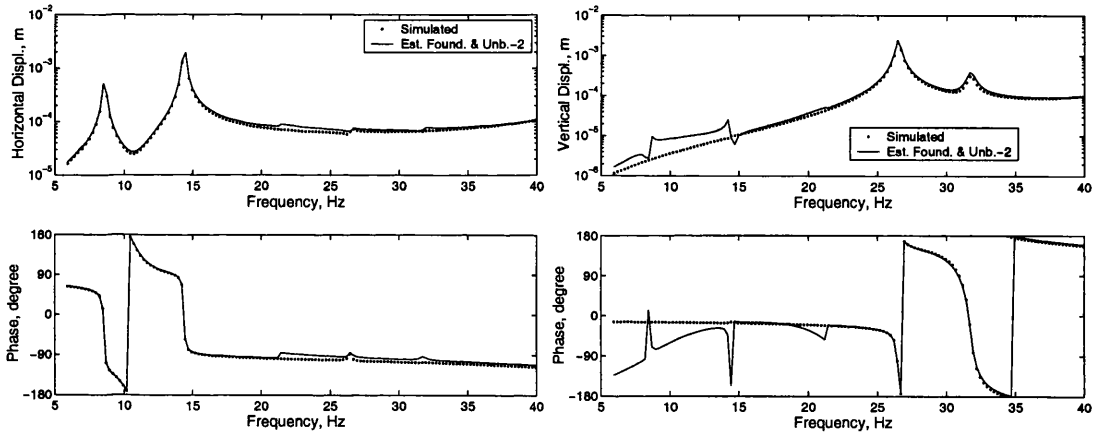

(a) For unbalance configuration 2

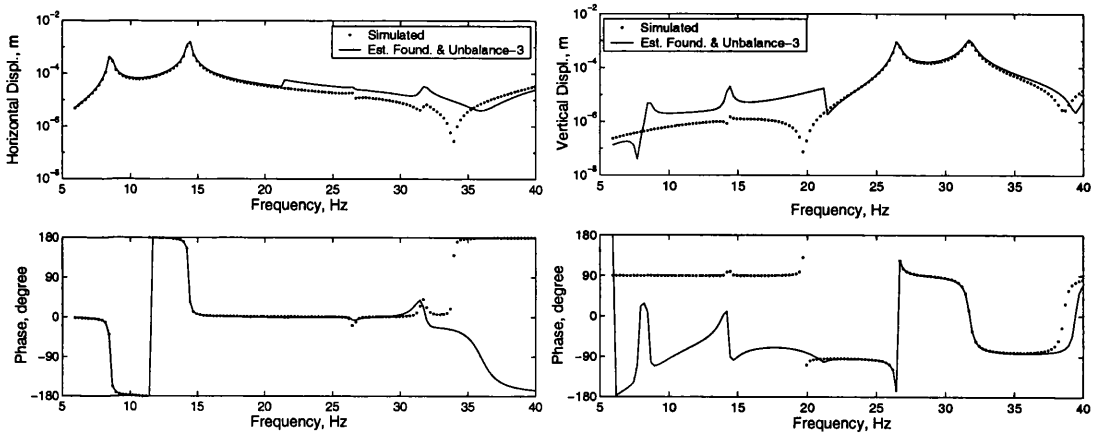

(b) For unbalance configuration 3

Figure 6.8 Prediction capacity of estimated foundation models using unbalance configuration 1 and Regularization 2, at bearing A, by different unbalances for the Small rig simulation

Having established the suggested method with *Regularization Method 2* for the foundation model estimation on the numerically simulated examples with and without noise, the method is now applied to the experimental examples of the *New small rig* and the *Aston rig*. The measured responses are generally contaminated with some structural and instrument noise.

6.3. EXPERIMENTAL EXAMPLE 1: THE NEW SMALL RIG

Details of the *New small rig* are given in Section 4.2 of Chapter 4. Different run-down experiments were performed with the rotor speed reducing from 2500 RPM to 300 RPM for different combinations of added masses to the balance disks A and B listed in Table 6.3. Runs 1 and 4 were the residual runs-down i.e., without any added mass to the disks. The order tracking was performed such that each set of the run-down data consisted of the 1X component of the displacement responses in the frequency range from 5.094Hz to 40.969Hz in steps of 0.125Hz. The linear system behaviour has also been confirmed by comparing the difference in the responses of run 2 and run 1 with the difference of run 3 and run 2.

Table 6.3 Different sets of the experimental run-downs for the New small rig

Run	Disk A (g @ deg.)	Disk B (g @ deg.)
1	Residual	Residual
2	0.76 @ 180	0.76 @ 0
3	1.52 @ 180	1.52 @ 0
4	Residual	Residual
5	0.76 @ 45	0.76 @ 225

The resulting responses from the subtraction of runs 3 and 1 have been used for the foundation model estimation for the known unbalance and the rotor FE model. The run-down responses contain total four critical speeds. These critical speeds consist of two lateral modes, one vertical mode and one axial mode of the rig. The appearance of these modes in both the horizontal and vertical responses indicates that the directions are coupled. Hence the frequency range was divided into four small bands, 5.094Hz to 12.094Hz, 12.094Hz to 20.969 Hz, 20.969Hz to 29.696Hz, and 29.696Hz to 40.969Hz, and *Regularization Method 2* was used by assuming symmetric stiffness, damping and mass matrices for the foundation. Figure 6.9 compares the measured and the estimated responses for unbalance run (3-1). The estimation is excellent though

the measured responses were noisy. The prediction capacity of the estimated foundation models with respect to different unbalances listed in Table 6.3 was also checked, and the predicted responses, both amplitude and phase, were found to be excellent. A few typical predictions are shown in Figure 6.10.

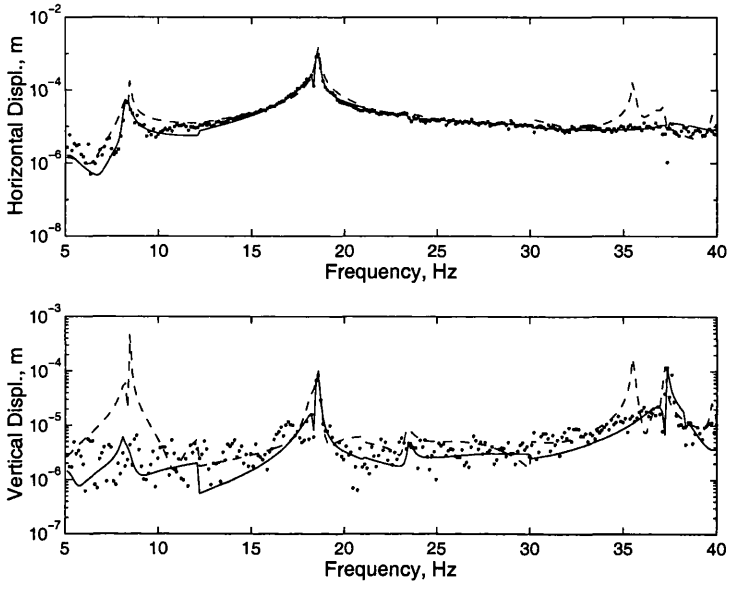

(a) Bearing A responses

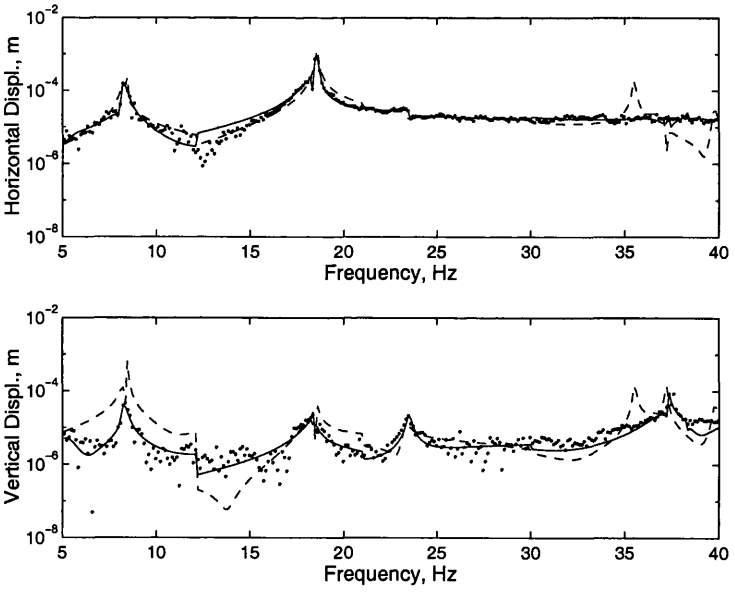

(b) Bearing B responses

Figure 6.9 Measured and estimated responses for run (3-1) with Regularization Method 2 for the experimental New small rig (• Measured, _ _ _ Linear, and ____ Non-linear estimation)

Unbalance run(2-1)

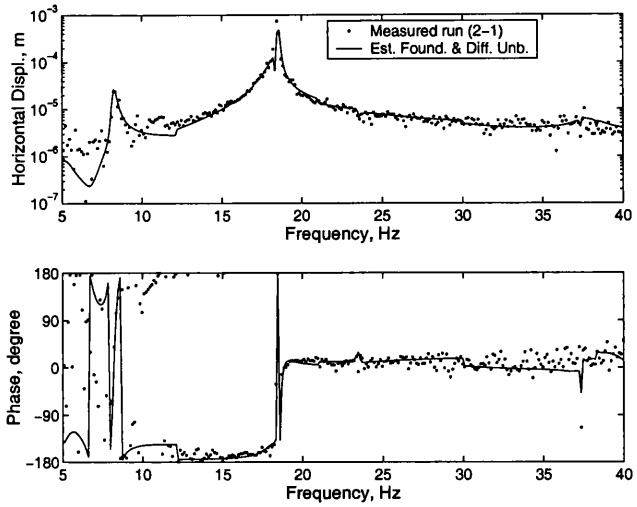

Unbalance run (2-4)

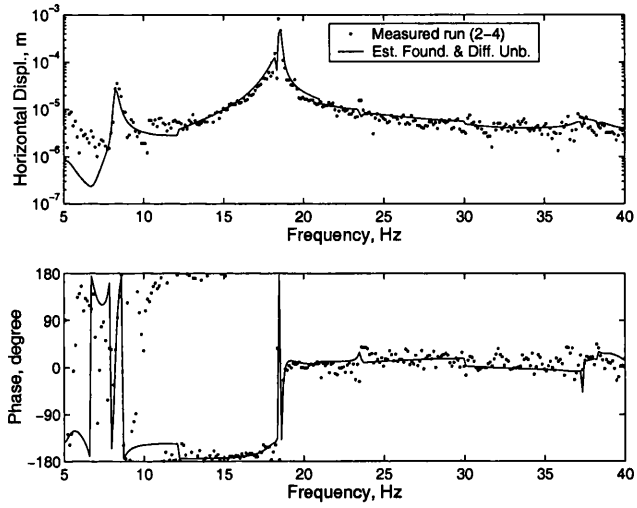

Unbalance run (5-1)

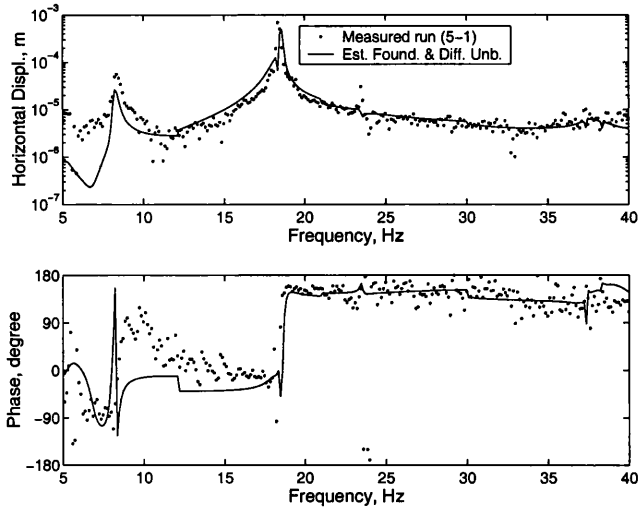

Figure 6.10 Prediction capacity of estimated foundation models using unbalance run (3-1) and Regularization 2, at bearing A, by different unbalances for the New small rig

6.4. EXPERIMENTAL EXAMPLE 2: THE ASTON RIG

Details of the *Aston rig* were given in Section 4.3 of Chapter 4 and the rotor FE model and the fluid bearings model is shown in Figure 6.1. The machine was run-down from 55 Hz to 5 Hz in 200 frequency steps at the frequency spacing of 0.25Hz. The first order responses for the horizontal and vertical acceleration at the bearing pedestals were extracted by the process of order tracking. The runs were performed, the first with the residual unbalance and the second and third cases with the addition of different unbalance weight distributions. Since the residual unbalance was unknown, run 1 was subtracted from run 2, and the foundation models were then identified from the resulting responses and added unbalance in run 2 based on assumption that the system dynamics are linear.

Table 6.4 The unbalance added for the experimental run-downs for the Aston rig

Run	Disk	Unbalance (Amplitude (g m) @ phase (degree.))
2-1	2	1.7 @ 105
	5	1.7 @ 180
3-1	1	1.7 @ 225
	5	1.7 @ 315

Table 6.4 shows the added unbalance when the difference between the runs is considered. The static load at the bearings were estimated by Smart (1998) to be 221 N, 486 N, 461 N and 400 N at bearings 1 to 4 respectively, and were used for the bearing modelling. The frequency range was again divided into four smaller bands, 5Hz to 17Hz, 17Hz to 28Hz, 28Hz to 40Hz and 40Hz to 55Hz. The estimation of the foundation model was carried out for each frequency band in turn by both the linear and the non-linear iterative process starting from the linearly estimated values for the foundation model. The following physical constraints for the foundation models for *Regularization Method 2* were considered one by one to compare the behaviour of the estimated foundation models.

(a) Symmetric stiffness matrix, and diagonal damping and mass matrices (assuming the same mass at a node for vertical and horizontal DoF).
(b) Symmetric stiffness and damping matrices, and diagonal mass matrix (assuming the same mass at a node for vertical and horizontal DoF).
(c) Symmetric stiffness and damping matrices, and diagonal mass matrix (assuming the different masses at a node for vertical and horizontal DoF).
(d) Symmetric stiffness, damping and mass matrices

Figure 6.11(a) compares typical measured and estimated responses using unbalance run (2-1) with *Regularization Method 2(a)*. Poor estimation at lower frequencies is expected as the measurement was contaminated with noise. Figure 6.11(b) gives the prediction capacity of the estimated foundation models for the unbalance configuration for run (3-1). The prediction is not as good as the simulated examples.

Using different *Regularization Methods -2(b), (c) and (d)*, the foundation models were also estimated for run (2-1) and the responses were predicted for run (3-1). Figures 6.12 to 6.14 give typical comparisons of the estimated and predicted responses with the measured responses. Table 6.5 summarizes the fit errors for the estimation and prediction using different regularizations.

6.4.1. Results and Discussion

As can be seen from Table 6.5 and Figures 6.11 to 6.14, the estimation (fit) errors are least for *Regularization Method-2(d)* but the prediction errors are very high. These exercises bring out the importance of the regularization used in solving such problems. Regularization based on some physical meaning is essential, for example *Regularization Method 2(a) and (b)*. Although the estimation (fit) errors for *Regularization 2(a) and (b)* are slightly higher than *Regularization 2(d)*, the prediction (output) errors are much less and the predictions and measurements also share many common features. However these predictions are not totally satisfactory and need rigorous investigation for further improvement.

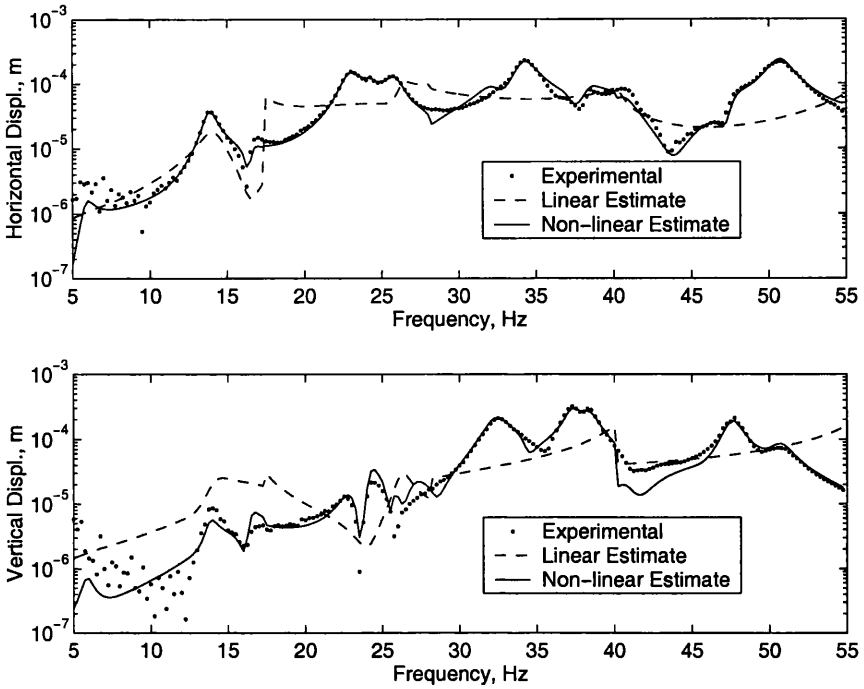

(a) Measured and estimated responses for unbalance run (2-1) at bearing 4

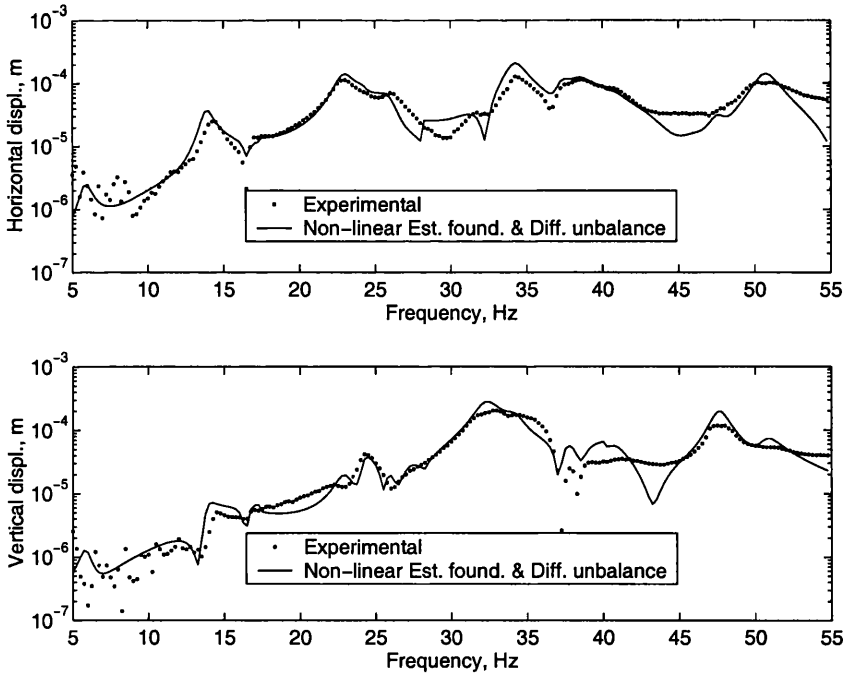

(b) Measured and predicted responses for unbalance run (3-1) at bearing 3

Figure 6.11 Dynamic behaviour of estimated foundation for run (2-1) with Regularization Method 2(a) for the experimental Aston rig

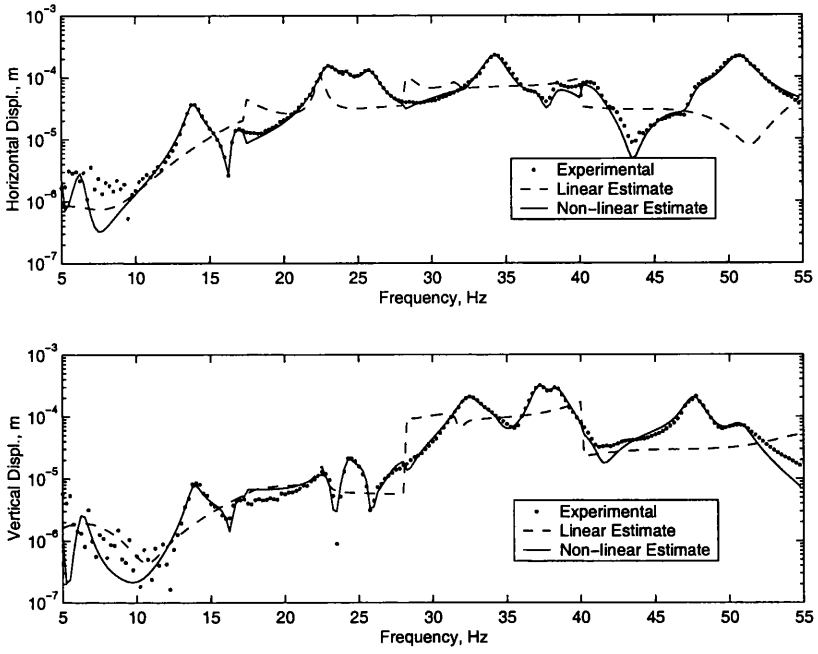

(a) Measured and estimated responses for unbalance run (2-1)

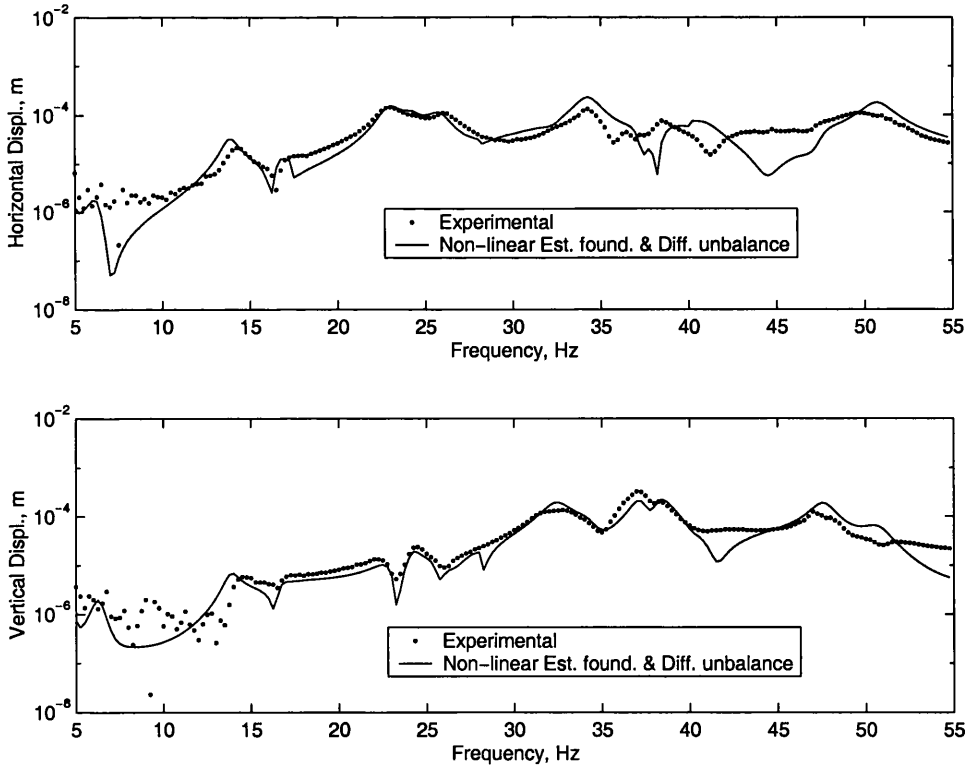

(b) Measured and predicted responses for unbalance run (3-1)

Figure 6.12 Dynamic behaviour of estimated foundation at bearing 4 for run (2-1) with Regularization Method 2(b) for the experimental Aston rig

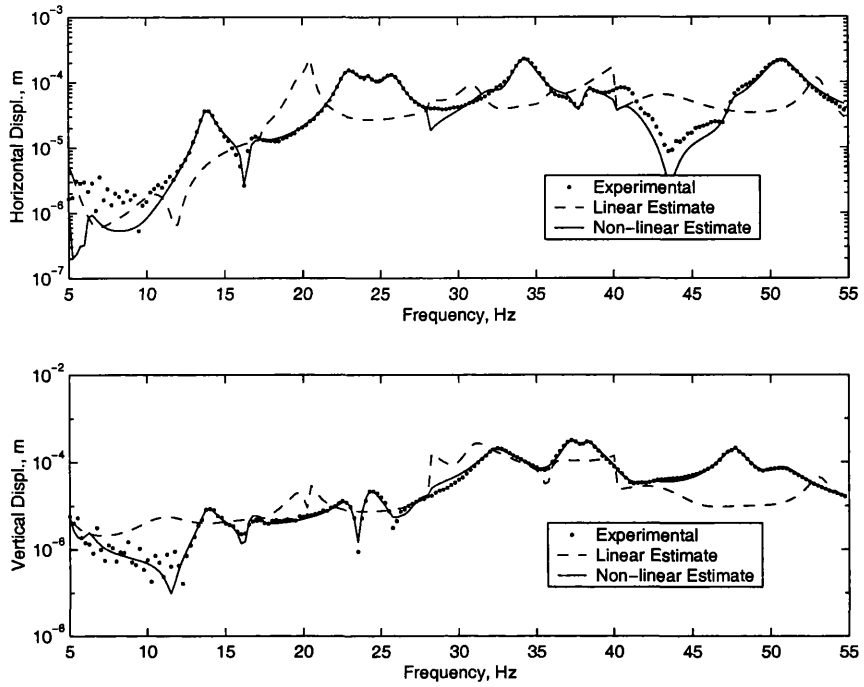

(a) Measured and estimated responses for unbalance run (2-1)

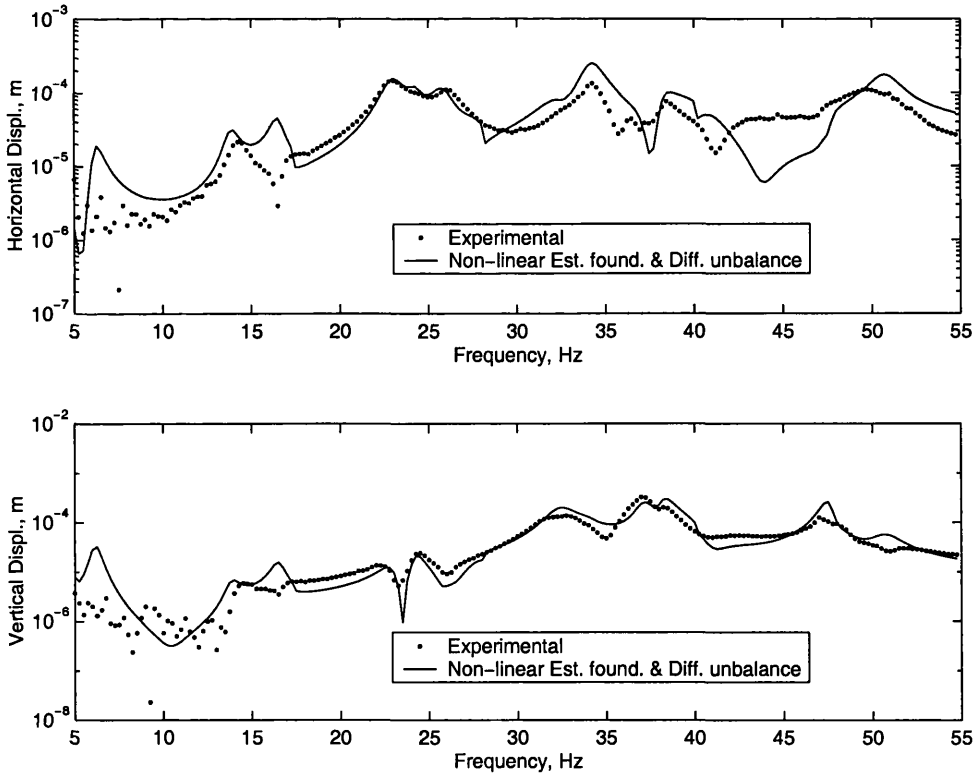

(b) Measured and predicted responses for unbalance run (3-1)

Figure 6.13 Dynamic behaviour of estimated foundation at bearing 4 for run (2-1) with Regularization Method 2(c) for the experimental Aston rig

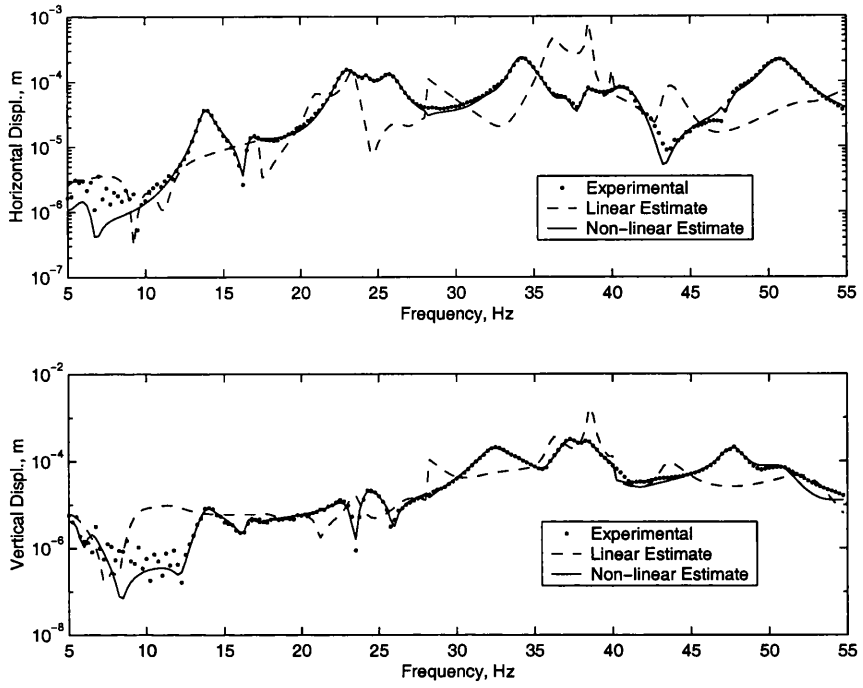

(a) Measured and estimated responses for unbalance run (2-1)

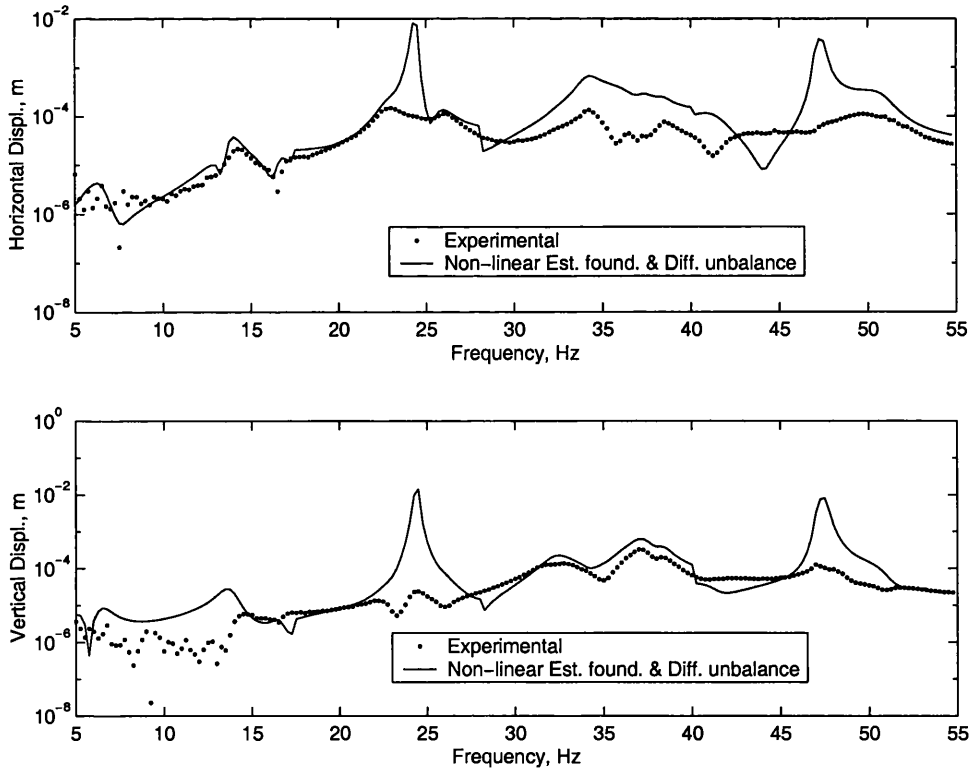

(b) Measured and predicted responses for unbalance run (3-1)

Figure 6.14 Dynamic behaviour of estimated foundation at bearing 4 for run (2-1) with Regularization 2(d) for the experimental Aston rig

Table 6.5 Fitting and relative output errors (%) for the experimental Aston rig data

$$\%Error = \frac{\varepsilon_o^T \varepsilon_o}{\mathbf{r}_m^T \mathbf{r}_m} 100$$

Method	Regularization 2(a)		Regularization 2(b)		Regularization 2(c)		Regularization 2(d)	
DOF	Est. run (2-1)	Pred. run (3-1)	Est. run (2-1)	Pred. run (3-1)	Est. run (2-1)	Pred. run (3-1)	Est. run (2-1)	Pred. run (3-1)
B1H	4.430	29.25	0.751	18.51	1.003	25.42	0.496	2.11e4
B1V	5.098	41.11	2.530	96.78	1.482	87.04	0.740	3.28e5
B2H	2.513	26.29	0.808	27.11	0.510	25.73	0.290	1.58e5
B2V	2.466	28.65	2.867	32.43	0.991	61.92	0.504	7.57e5
B3H	4.733	52.02	3.117	56.06	1.062	72.67	0.308	1.76e5
B3V	4.613	17.45	1.005	16.04	1.122	22.08	0.397	5.67e4
B4H	3.756	79.44	1.392	76.57	2.735	87.58	0.733	2.51e4
B4V	3.352	63.80	0.969	41.86	0.760	93.70	0.691	4.02e4
Average % Error	3.430	37.82	1.540	39.55	1.026	53.89	0.471	2.29e5

6.5. SUMMARY

The suggested method is simple and results are very encouraging. The simulated and experimental examples have brought out the importance of regularization. The quality of the estimated foundation models has been found to be excellent based on their prediction capabilities for the simulated examples with and without noise, and an experimental example of the New *small rig*. However the suggested method seems to struggle in the experimental *Aston rig* case which consists of fluid bearings in comparison to the *New small rig*. It was observed that the estimation was always close to the measured data, but the prediction was not as good though there is reasonable agreement between the measured and predicted responses using *Regularization methods 2(a) & (b)*. Frequency peaks are common in both responses but there is some difference in the amplitudes. Different regularization methods are used to improve the prediction capability with respect to a different unbalance, but none of them was found to be totally satisfactory. There could be many possible reasons for such differences and this is the subject of future research. But the following are the most likely reasons for this foundation behaviour.

(i) *Fluid Bearing Modelling:* Error in the bearing forces. This should be checked by using the measured dynamic force at the bearings in the bearing model or alternatively by including the shaft response measured by the proximity probes near the bearing pedestals to avoid using a bearing model in the estimation process.

(ii) *The Foundation Dynamic Behaviour:* It is also likely that the foundation behaviour may not be linear. When a small structural system (with many joints) is designed to have many modes in a small run-down frequency range, as for real life foundations of TG sets, the fabrication of such a small system may have some non-linear dynamic effects. In this case one should perform stepped-sine tests (Ewins, 2000) with different excitation amplitudes to check the linear behaviour of the structure before carrying out any run-down experiments. Of course a stepped sine test on the foundation of a TG set is not possible due to practical problems. Hence for the cases like this it would be better to perform three run-downs of a machine with increasing added mass at a constant phase angle at a number of unbalance planes to check the linearity in the responses, similar to run 1 to run 3 for the *New small rig*.

Unfortunately none of the above possibilities could be confirmed during the period of the present research study for the *Aston rig*. In spite of all these suspected problems, the predicted responses show a promising similarity to the measured responses. Some frequency dependent faults could still be identified using the estimated foundation models by the appearance of the same frequency peaks in the predicted and measured responses. However the prediction capacity of the estimated foundation models were found to be excellent for the simulated examples and the other experimental example of the *New small rig*. It has also been demonstrated that *Regularization Method 2* based on physical constraints for the foundation is important for the estimation. Hence the suggested method can be considered a robust method and needs no further improvement at present other than to check the linear behaviour of the foundation and the fluid bearing model for the experimental *Aston rig*.

CHAPTER 7

ROTOR UNBALANCE AND MISALIGNMENT ESTIMATION: NUMERICAL SIMULATIONS AND EXPERIMENTAL EXAMPLES

7.0. INTRODUCTION

Three methods for unbalance estimation were suggested in Chapter 5. These methods have been applied initially to the numerically simulated examples of the *Aston rig* and then to the experimental examples. The advantages and limitations of each method will be brought out through the following examples. The estimation of both the rotor misalignment (at the flexible coupling) and unbalance as suggested in Chapter 5 has also been carried out on the experimental data from the *New small rig*.

7.1. SIMULATED EXAMPLE 1: THE ASTON RIG

Details of the rotor and the fluid bearings of the *Aston rig* are given in Section 4.3 of Chapter 4. For simulation the assumed foundation model given in Section 6.1 of Chapter 6 is used. As discussed in Chapter 6, the measured responses at the bearing foundation associated with the translational DoF were computed using the assumed foundation model and a given unbalance on the rotor, using equation (5.1). Table 7.1 shows the different unbalance configurations used to excite the rotor for the different runs. The machine was run-down from 60 Hz to 1 Hz, with measurements taken at a spacing of 0.5 Hz. Using these measured responses, the identification of the foundation model and the unbalance state (at known balance planes) was then carried out by the proposed methods in turn. Initially the proposed methods were applied to the simulated responses without noise and then the responses were contaminated with noise.

7.1.1. The Simulated Response without Noise

Method 1: The estimated unbalance amplitude and phase for the different runs are listed in Table 7.1. The estimated unbalance was quite accurate. However the response estimation using the identified foundation models and unbalance state were poor for all of the cases, even for the simulated example. Figure 7.1 shows a typical comparison and demonstrates that the estimated responses are quite different from measured ones.

Method 2: As in Section 6.1.1 of Chapter 6, the frequency range was divided into four bands, 1 Hz to 15 Hz, 15 Hz to 28 Hz, 28 Hz to 40 Hz and 40 Hz to 60 Hz, and the

estimation was carried out for each frequency band in turn. Table 7.1 gives the estimated unbalance. The estimated responses using the identified foundation models and unbalance state were nearly an exact fit to the simulated responses for all cases. Figure 7.2 shows a typical comparison of the estimated and measured responses. However, the unbalance estimation for each band were not close to each other, nor close to the simulated unbalance, for any case, except maybe cases 1 and 3 for band 4.

Method 3: The last column in Table 7.1 lists the estimated unbalances for the combined approach. Figure 7.3 gives the comparison of estimated and measured responses for a typical case. The unbalance estimates are accurate in all cases, and the fit to the simulated responses is quite good. The results are encouraging.

7.1.1.1. Discussion of the Results

In summary, ***Method 1*** predicts the unbalance reasonably well but the foundation poorly, ***Method 2*** predicts the foundation well and the unbalance poorly and ***Method 3*** predicts both the unbalance and foundation well. To verify the estimated foundation model the responses obtained by using the estimated foundation model but with the simulated unbalance are compared to the simulated responses. Figure 7.4 shows one such comparison, for the responses at bearing 1 due to unbalance configuration 5 (Table 7.1). This confirms that the estimated foundation model and unbalance state identified by ***Method 3*** is the only one that is close to the simulated case.

Poor foundation by ***Method 1*** only indicates that the measured DoFs are less than the number of modes in the run-down frequency range, and that has also caused some error in the unbalance estimation. Significant deviations are observed for the model identified by ***Method 2***. Although the estimated models by ***Method 2*** in each frequency band was an excellent fit as the measured DoFs were more than the number of modes present in each frequency band but resulted in the poor unbalance estimation in each band due to presence of fewer number of modes. However the ***Method 3*** that has exploited the strength of both the earlier methods by estimating a global unbalance and frequency band dependent foundation models and hence resulted in an excellent estimation.

7.1.2. The Simulated Response with Noise

In practice, the measured response data will be contaminated by some noise and the rotor and bearing models will contain errors. To simulate such conditions, the eight simulated translational responses at the bearings for unbalance configuration 3 of Table 7.1 were corrupted with 1% noise. The effect of modelling errors was demonstrated by adding 20% noise to the bearing static loads at each frequency to introduce uncertainty into the bearing parameters for the simulated responses. The static loads in the model used for the estimation remain constant. The regularization used removes the noise from the measured data using the SVD of the autocorrelation matrix of the responses, as described in detail by Smart *et al.* (2000).

Table 7.2 shows the results for this example. Initially, the linear solution was obtained without regularization. The estimated values by ***Method 3*** are close to actual values, although the estimated responses were not a close fit to the measured responses. The regularized solution (Smart *et al.*, 2000) gives the reasonable good fit to the measured responses, as shown in Figure 7.5, and the estimated unbalances remain accurate. These results were also compared with the results using ***Method 1***, which gives reasonable unbalance estimates, but the estimated responses are very poor, as shown in Figure 7.5. Hence, ***Method 3*** is the best for the estimation of both the state of unbalance and the frequency dependent foundation models. Regularization improves the quality of the foundation model, but does not significantly improve the unbalance estimates.

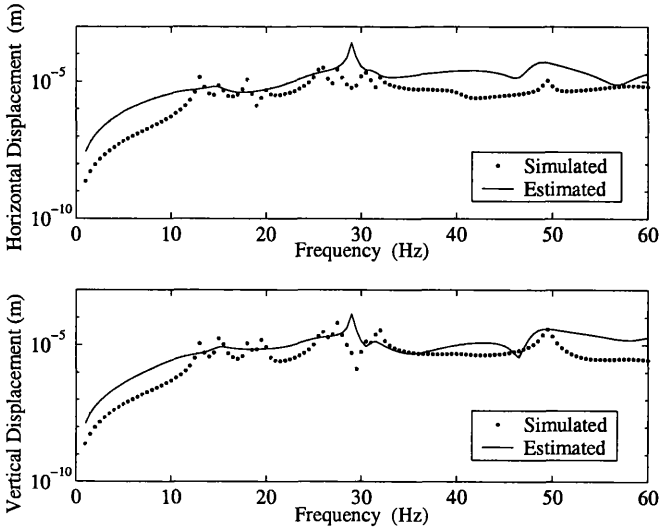

Figure 7.1 Simulated and estimated responses by Method 1, at bearing 1, for unbalance configuration 5 for the Aston rig simulation

Table 7.1 Estimated unbalance for the Aston rig simulation without noise

Unbal-ance Config	Bal-ance Disk	Actual Unbalance (amplitude in g m, phase in degrees)		Estimated Unbalance (amplitude in g m, phase in degrees)											
				Method 1		*Method 2*								*Method 3*	
						Band 1		Band 2		Band 3		Band 4			
		Unbalance	Phase	Unbalance	Phase	Unbalance	Phase	Unbalance	Phase	Unbalance	Phase	Unbalance	Phase	Unbalance	Phase
1	3	0.160	45	0.1678	44.4	7482.0	128.6	0.1910	42.0	0.1633	47.8	0.1669	52.43	0.1639	47.7
2	1	0.160	195	0.1797	188.2	16728.0	183.6	3102.0	356.6	632.0	163.6	1.0975	9.0	0.1630	191.0
	3	0.160	45	0.1606	37.5	19269.0	29.93	2734.0	178.6	914.0	344.8	2.2237	358.7	0.1560	40.3
3	3	0.160	45	0.1715	48.4	5979.9	62.0	493.5	14.8	2.0787	347.1	0.1694	52.9	0.1712	45.8
	4	0.160	150	0.2108	149.1	12022.7	358.9	3581.3	11.0	14.913	139.3	0.1484	148.5	0.1506	151.1
4	1	0.160	195	0.1737	195.9	11045.2	145.1	389.9	78.4	0.5310	105.3	0.1563	194.2	0.1599	196.9
	5	0.160	0	0.1811	-0.02	3108.5	310.9	2636.6	79.3	6.3760	273.0	0.1515	14.46	0.1514	17.93
5	1	0.160	195	0.1624	182.3	15005.0	183.8	3916.0	328.5	2009.0	24.4	81.2	254.5	0.1704	199.2
	3	0.160	45	0.1318	42.9	26038.0	40.2	3299.0	146.3	2956.0	205.7	187.0	244.8	0.1862	45.9
	4	0.160	150	0.1941	154.2	34550.0	54.6	2121.0	23.0	375.8	5.6	9.3	118.5	0.1843	134.3
6	1	0.160	195	0.1852	195.7	29032.0	14.9	1892.0	208.8	1216.0	145.8	23.8	178.2	0.1589	197.8
	3	0.160	45	0.1829	42.2	31430.0	198.9	1861.0	33.6	1789.0	327.1	53.9	167.6	0.1671	48.5
	5	0.160	0	0.1830	2.77	66080.0	166.7	1614.0	54.6	255.2	125.1	27.5	42.9	0.1500	17.7

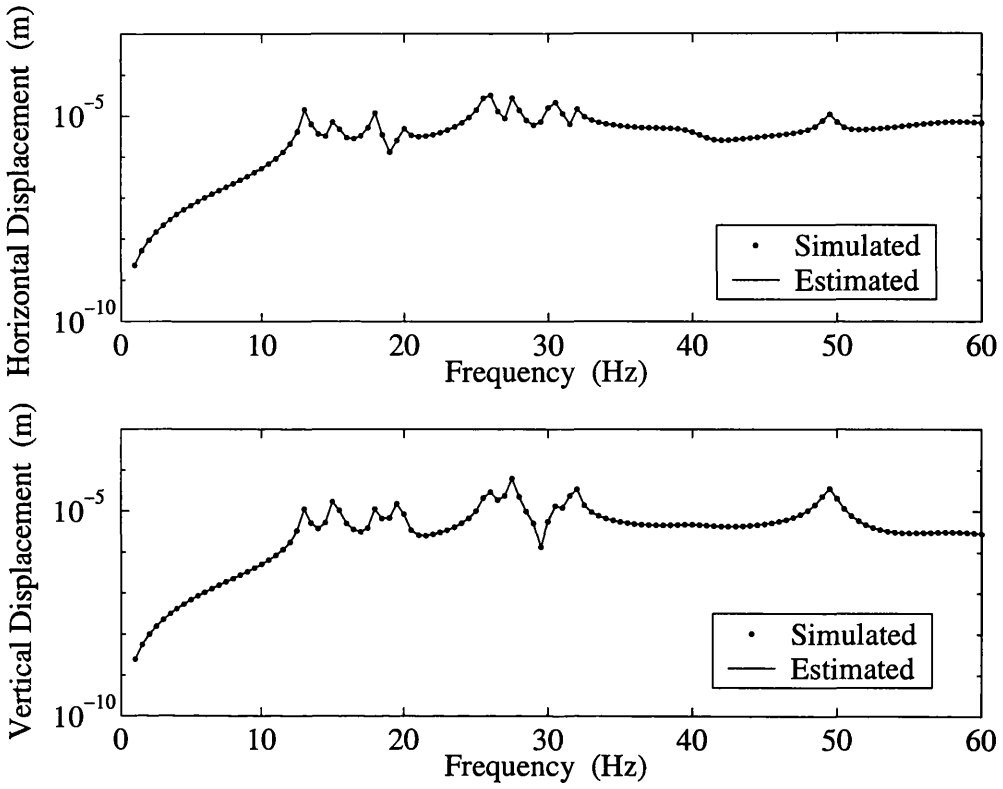

Figure 7.2 Simulated and estimated responses by Method 2, at bearing 1, for unbalance configuration 5 for the Aston rig simulation

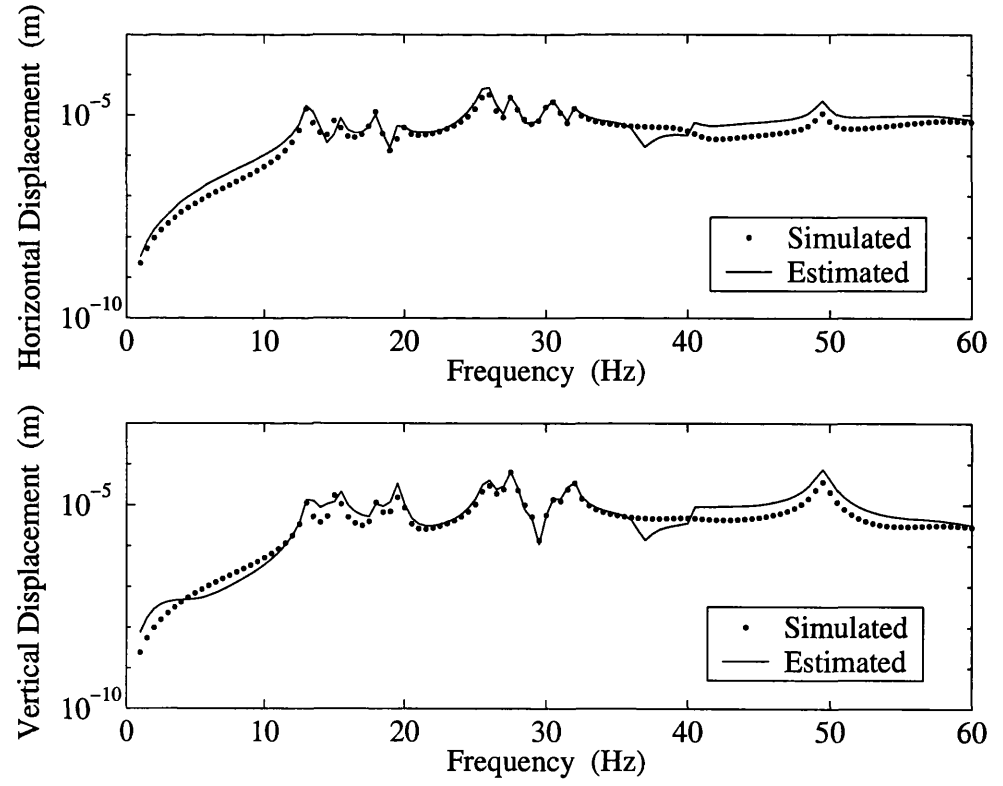

Figure 7.3 Simulated and estimated responses by Method 3, at bearing 1, for unbalance configuration 5 for the Aston rig simulation

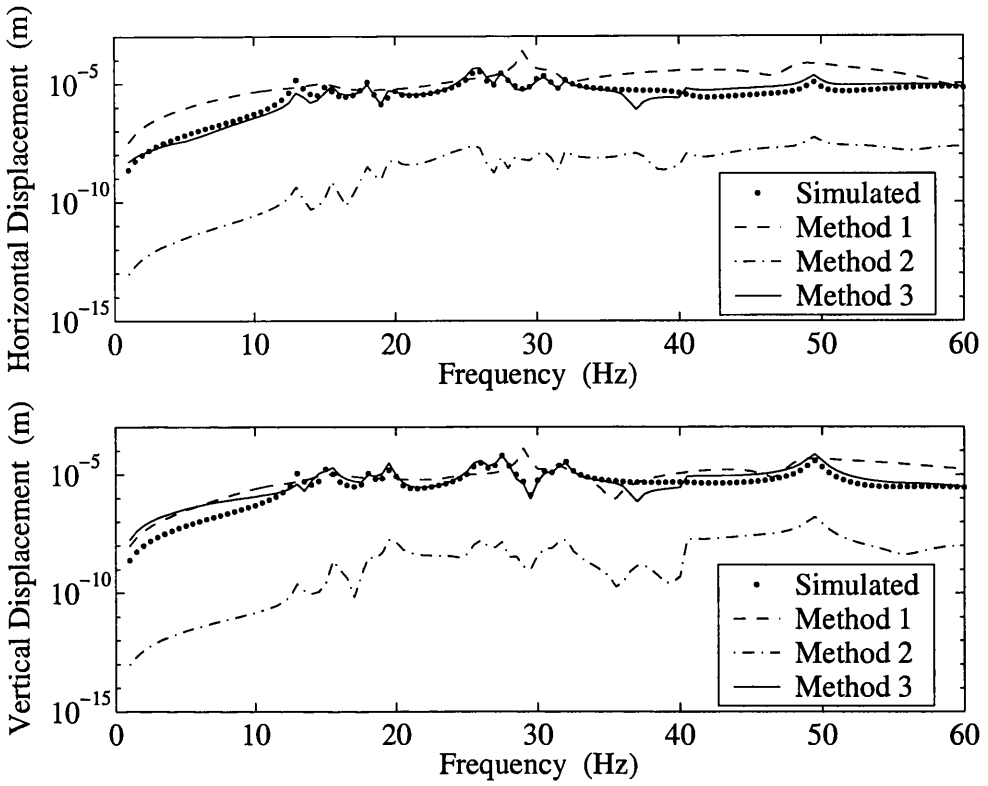

Figure 7.4 Simulated and estimated responses at bearing 1, using the estimated foundation models but the simulated unbalance, for unbalance configuration 5 for the Aston rig simulation

Table 7.2 Estimated unbalance for the Aston rig simulation with noise

	Balance Disk 3		Balance Disk 4	
	Amplitude (g m)	Phase (degrees)	Amplitude (g m)	Phase (degrees)
Actual	0.160	45	0.160	150
Method 3 Unregularized	0.1689	49.39	0.1735	138.73
Method 3 Regularized	0.1494	43.02	0.1735	138.63
Method 1	0.1739	48.45	0.2163	147.58

Having established the reliability of ***Method 3*** for the accurate estimation of the rotor state of unbalance both amplitude and phase at multi-balance planes and reasonably good foundation models on simulated examples, the method is now applied to the experimental examples. The unbalance estimation by ***Method 1*** is also shown for comparison.

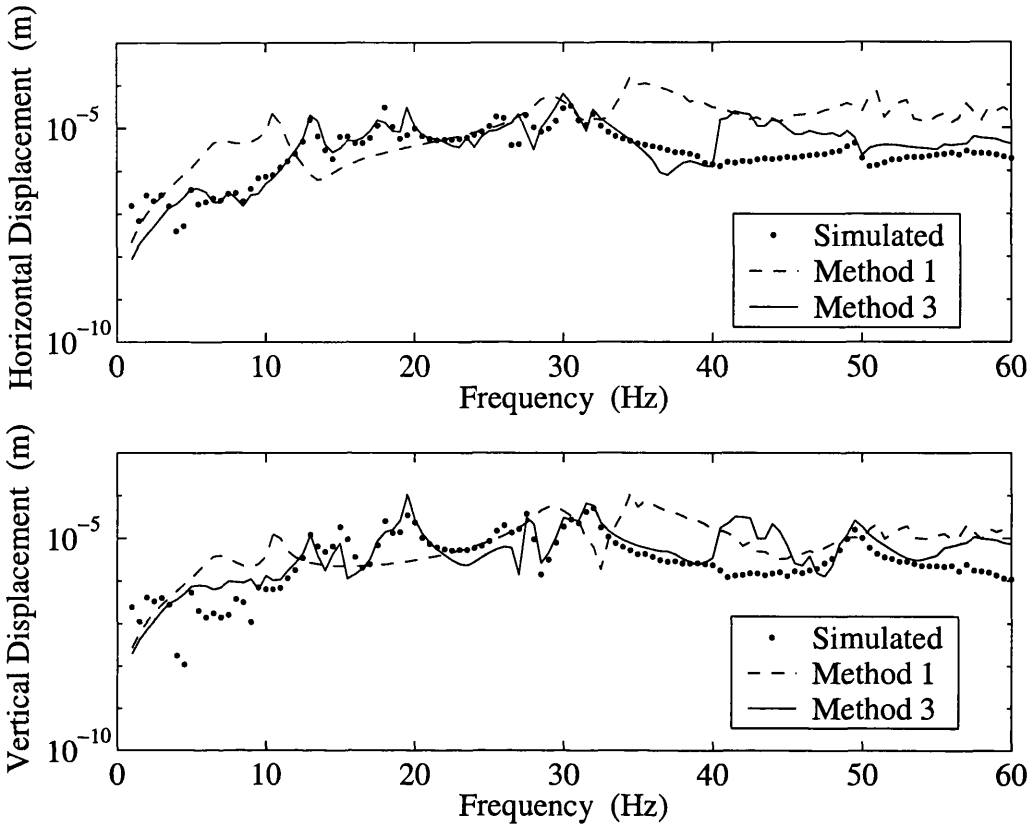

Figure 7.5 Simulated (with noise) and estimated responses at bearing 1, for unbalance configuration 3 for the Aston rig simulation

7.2. EXPERIMENTAL EXAMPLE 1: THE ASTON RIG

The identification methods were tested on experimental data from the *Aston rig*. The same run-down data that were used in Chapter 6 for the foundation model estimation were also used here. A total of three runs were performed, the first with the residual unbalance and the second and third cases with the addition of different unbalance weight distributions. Since the residual unbalance was unknown, two approaches were taken. The first approach subtracts the response for run 1 from that for run 2, and the unbalance state was then identified from the resulting responses. Assuming the system is linear then the identified unbalance will be the unbalance added. The alternative is to estimate the residual unbalance for run 1, estimate the unbalance for run 2, and difference these estimates to compare with the unbalance weights added. The process may be repeated for run 3.

7.2.1. Subtraction of Unbalance

Table 7.3 and Figure 7.6 show the equivalent results when the unbalance is estimated for each run, and the estimated unbalances are subtracted to compare with the actual unbalance. In ***Method 3*** the frequency range is split into four bands; 5-17 Hz, 17-28 Hz, 28-40 Hz and 40-55 Hz which are the same as Chapter 6. The results are close to the actual unbalances.

Table 7.3 Unbalance estimation from experimental run-down data by subtracting unbalance for the Aston rig

Method	Runs	Unbalance Planes	Estimated (Amplitude (g m) @ phase (deg.))			Actual Unbalance Added
			First Run	Second Run	Added Unbalance	
1	1 & 2	Disk 2	0.955 @ 208.51	0.877 @ 110.00	1.388 @ 67.21	1.70 @ 105
		Disk 5	0.516 @ 1.12	1.866 @ 161.50	2.360 @ 165.72	1.70 @ 180
3	1 & 2	Disk 2	0.958 @ 210.11	0.742 @ 85.60	1.508 @ 54.03	1.70 @ 105
		Disk 5	0.860 @ 6.90	1.067 @ 153.44	1.847 @ 168.31	1.70 @ 180
1	1 & 3	Disk 1	1.043 @ 207.61	2.050 @ 269.97	1.819 @ 300.50	1.70 @ 225
		Disk 5	0.605 @ 38.17	2.519 @ 36.29	2.035 @ 45.48	1.70 @ 315
3	1 & 3	Disk 1	1.053 @ 209.65	2.283 @ 266.36	1.919 @ 293.67	1.70 @ 225
		Disk 5	0.883 @ 11.71	2.498 @ 41.40	1.785 @ 56.43	1.70 @ 315

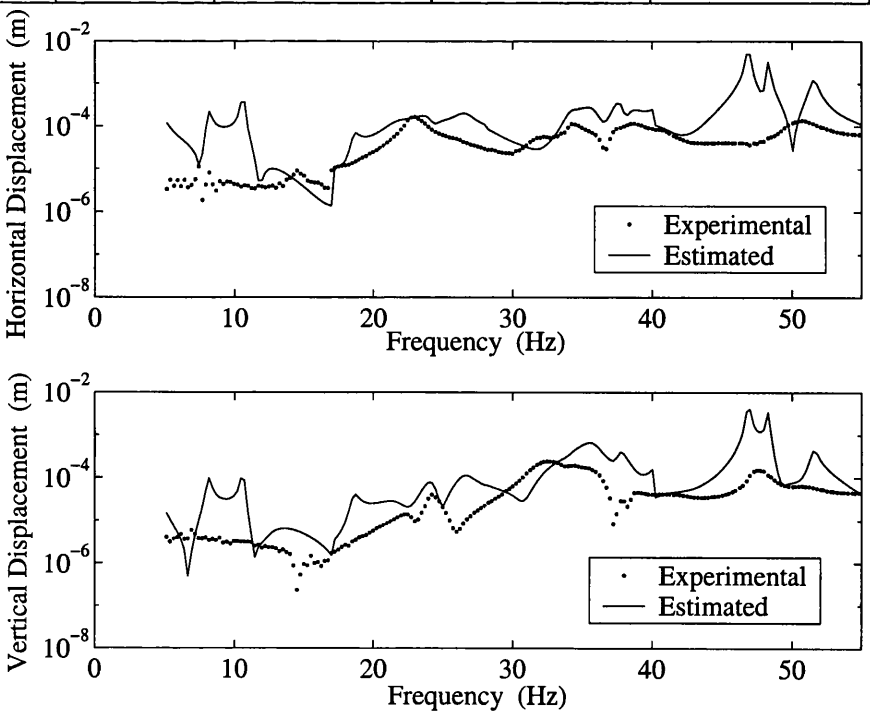

Figure 7.6 Measured and estimated responses at bearing 3 by Method 3, for run 3 for the experimental Aston rig

7.2.2. Subtraction of Run-down Data

Table 7.4 shows the results when the difference between the runs is considered, and Figure 7.7 compares typical measured and estimated responses, for ***Method 3***. The unbalance estimation by ***Method 3*** is once again better than ***Method 1***. The computed rotor natural frequency when pinned at the bearings was 38.41Hz and this may affect the unbalance estimation. Hence the unbalance estimation was carried out again using *Regularization 3* by removing a small frequency band of 1.25Hz on either side of 38.41Hz. The estimated unbalance is listed in Table 7.4 and the estimated amplitudes are now much closer to the actual values without much change in the estimated phase. The most important improvement is that now the fit of the estimated response is closer to the measured response. One such response is compared in Figure 7.7(b).

Table 7.4 Unbalance estimation from the experimental run-down data by subtracting runs for the Aston rig

Run	Disk	Actual Unbalance (Amplitude (g m) @ phase (deg.))	Estimated Unbalance (Amplitude (g m) @ phase (deg.))		
			Method 1	Method 3	
				Without *Regularization 3*	With *Regularization 3*
2-1	2	1.7 @ 105	1.380 @ 67.42	1.529 @ 51.42	1.70 @ 77
	5	1.7 @ 180	2.345 @ 164.78	1.759 @ 176.10	1.68 @ 152
3-1	1	1.7 @ 225	1.820 @ 300.97	1.943 @ 293.02	1.77 @ 304
	5	1.7 @ 315	2.067 @ 47.59	1.849 @ 51.40	1.65 @ 48

7.2.3. Discussion

As can be seen from Tables 7.3 and 7.4, the identified unbalances by both approaches for ***Method 1*** and ***3*** are almost same and close to the actual added unbalances. This confirms that the unbalance of the rotor can be estimated reliably even with the measured vibration data from a single run-down of machine.

Both approaches give good estimates of the unbalance, however ***Method 3*** consistently gives the better unbalance estimates. The amplitude of the unbalance is consistently estimated more accurately than the phase. There could be two possible reasons for the error in the estimated phase. One reason maybe the estimation phase may have same dynamic effect as the actual phase. Other maybe because of errors in the bearing model, or maybe small phase shifts in the measurement system, or

possibly a small non-linearity in the foundation as pointed out in Chapter 6. The *Regularization 3* has found to improve both the estimated unbalance and the fit of the estimated response to the measured response, thus indicates the significant reduction in the numerical ill-conditioning of the linear least squares solution.

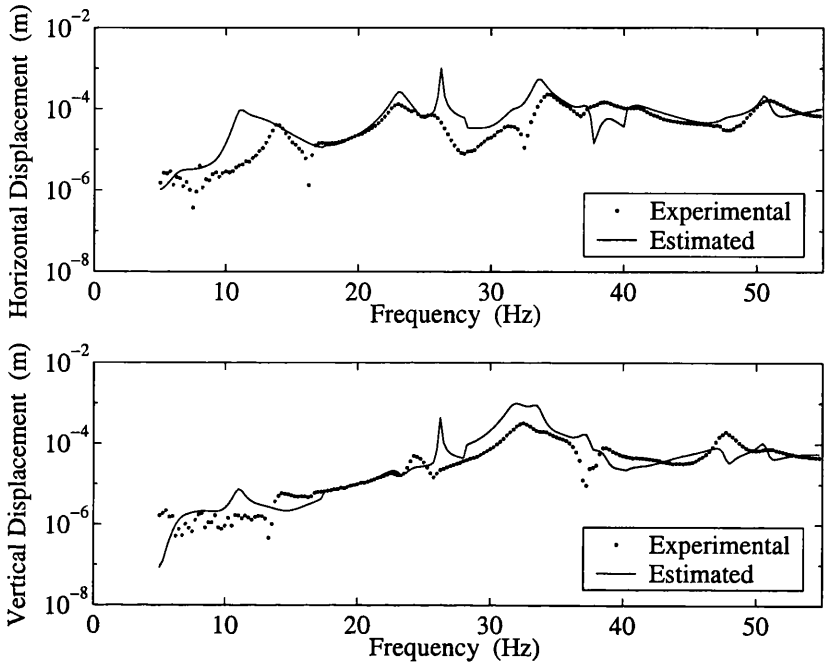

(a) Without *Regularization 3*

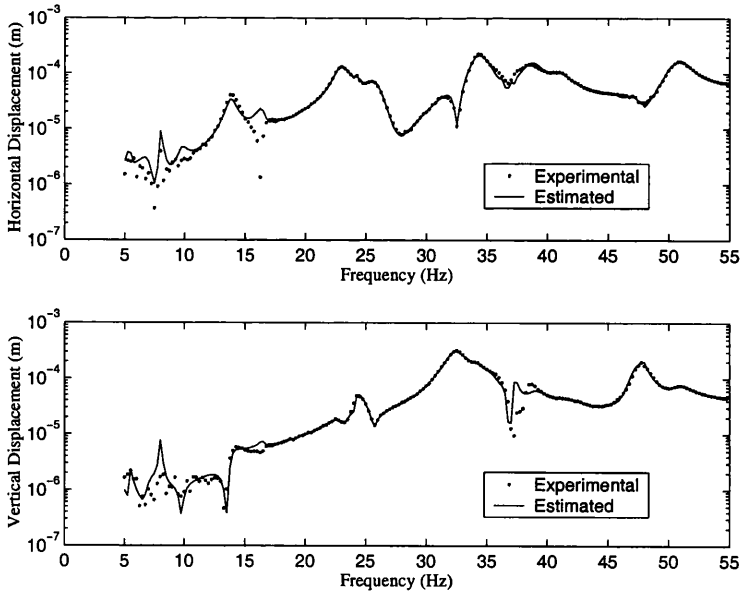

(b) With *Regularization 3*

Figure 7.7 Measured and estimated responses at bearing 3 by Method 3, using the difference of runs 1 and 2 for the experimental Aston rig

7.3. EXPERIMENTAL EXAMPLE 2: THE SMALL RIG

Once again the unbalance estimation has been qualified on the simulated case (without noise) of the *Small rig* (shown in Figure 4.2). The estimated unbalances were exactly the same as the assumed state of the rotor unbalances. The rotor unbalance estimation was then carried out on the measured run-down response for different combinations of added masses at the balance disks A and B.

7.3.1. Run-down Experiments

Different run-down experiments were performed with the rotor speed reducing from 3000 RPM to 60 RPM, for the different combinations of added masses to the balance disks A and B listed in Table 7.5. Run 1 was the residual run-down i.e., without any added unbalance mass to the disks and the subsequent runs had some added mass to the balance disks. The run down time was 10 minutes for each experiment. Four responses were measured, namely the horizontal and vertical accelerations at both bearings along with one tacho signal, as discussed in Chapter 3. The order tracking was performed such that the each set of the run-down data consisted of the 1X component of the displacement responses in the frequency range from 1.44 Hz to 48.44 Hz in steps of 0.25 Hz.

Table 7.5 Different sets of the experimental run-down for the Small rig

Run	Disk A (gm @ deg.)	Disk B (gm @ deg.)
1	Residual	Residual
2	7.280e-2 @ 22.5	5.445e-2 @ 157.5
3	5.445e-2 @ 247.5	5.445e-2 @ 67.5
4	5.445e-2 @ 247.5	2.280e-2 @ 90.0

7.3.2. Unbalance Estimation by *Methods 1* and *3*

The run-down frequency band of 5.94 Hz to 40.19Hz, that included all of the four critical speeds of the machine, was used for the unbalance estimation. Unbalance estimation was carried out using the complete run-down band as a single frequency band as well as dividing into a number of small bands for the foundation models. The number of small bands has been progressively increased so that the estimated response should be close to the measured response. It has been observed that the

estimation was most promising when the frequency band 5.95Hz to 40.19Hz was divided into 4 sub-bands – 5.94Hz to 11.19Hz, 11.19 to 18.19Hz, 18.19Hz to 28.69 Hz and 28.69 Hz to 40.19Hz. The estimated results for the subtracted runs are given in Table 7.6, and show that the results of ***Method 1*** are very poor. In fact, the estimated responses were not a close fit to the measured responses as they do not account for all of the modes in the run-down frequency range. Hence it seems for a lightly damped rotor system ***Method 1*** is not very good. However, the estimated unbalance amplitudes by ***Method 3*** are, once again, close to the actual values but the phases are not, which is similar to the observation made in the experimental Aston rig example of Section 7.2. The estimated responses were also a close fit to the experiments for all cases. Some typical responses for run (3-1) are shown in Figure 7.8 by both of the methods.

7.3.3. Unbalance Estimation using the Updated FE Model of Foundation

Recall from Chapter 5 that the proposed method for the rotor unbalance estimation assumes that a reliable FE model of the foundation could not be constructed. This is the reason why the proposed method estimates the foundation model as a by-product, along with the rotor unbalance. However for the experimental example of the *Small Rig*, an updated FE model fully representing the complete system is already available (Chapter 4). So the unbalance can be estimated directly using the FE model. For this estimation equation (5.30) can be modified as

$$\mathbf{R}(\omega_q)\mathbf{e} = \left[\mathbf{Q}(\omega_q) - \overline{\mathbf{Z}}_F(\omega_q)\right] \mathbf{r}_{F,b}(\omega_q) \tag{7.1}$$

Clearly there is an equation of the form of (7.1) at every frequency. The equations generated may be solved in a least squares sense directly as discussed earlier in Section 5.3.1 of Chapter 5. Hence the unbalance estimation was again carried out for the subtracted runs using the above equation. The estimated unbalances are also given in Table 7.6. The calculated responses for run (3-1) using the estimated unbalance are shown Figure 7.9 and compared to the measured responses. The calculated responses are not close to the measured ones. The estimated unbalances are not very close to the actual values, and are poor when compared to the estimated unbalances by the proposed ***Method 3***. Hence the dynamic behaviour of the foundation was further investigated to find out the reason for the error in the unbalance estimation.

Table 7.6 Unbalance estimation for subtraction of runs for the Small rig

	Proposed Methods assuming Foundation Model not known				Assuming known FE model for Foundation	
	Method 1		***Method 3***			
Run	Disk A (gm @ deg.)	Disk B (gm @ deg.)	Disk A (gm @ deg.)	Disk B (gm @ deg.)	Disk A (gm @ deg.)	Disk B (gm @ deg.)
2-1	2.04e-2 @ 348	1.58e-2 @ 170	7.53 e-2 @ 26	5.96e-2 @ 206	2.30e-2 @ 49	2.50e-2 @ 239
3-1	1.03e-2 @ 263	0.09e-2 @ 67	5.19e-2 @ 347	4.02e-2 @ 178	1.48e-2 @ 342	1.52e-2 @ 174
4-1	0.91e-2 @ 239	0.27e-2 @ 335	4.50e-2 @ 152	2.81e-2 @ 70	1.73e-2 @ 18	1.86e-2 @ 205

Method 1

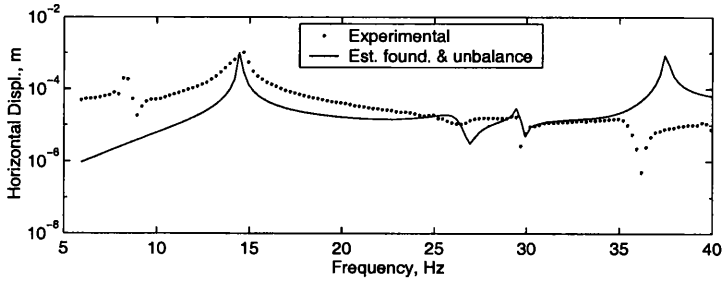

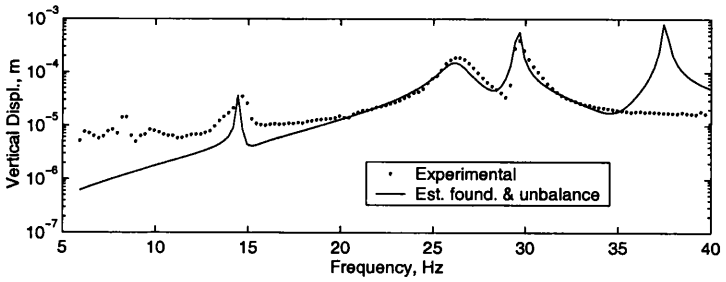

Method 3

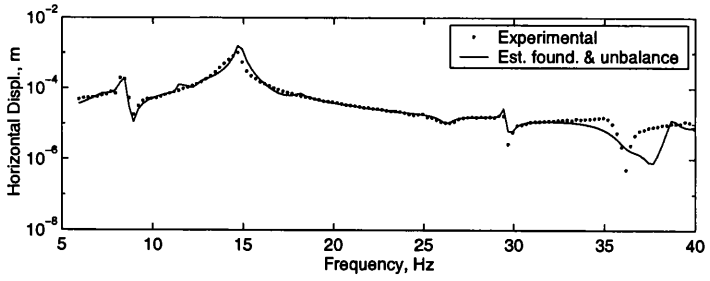

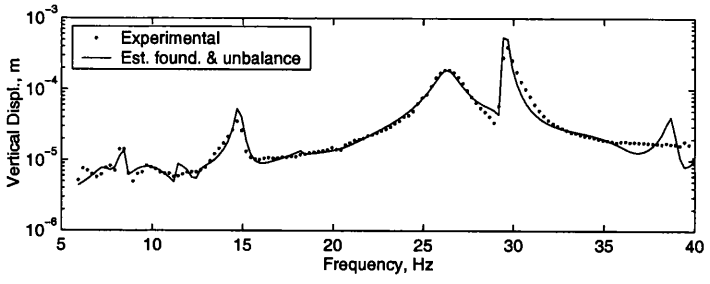

Figure 7.8 Measured and estimated responses at bearing A, for the difference of runs 1 and 3 for the experimental Small rig

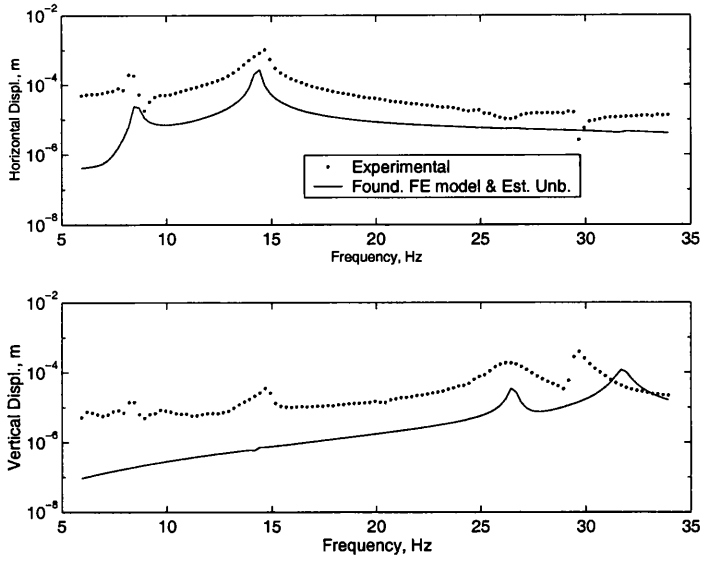

Figure 7.9 Measured and calculated responses at bearing A using the FE model of the foundation and estimated unbalances, for the difference of runs 1 and 3 for the experimental Small rig

7.3.4. The Foundation Dynamic Behaviour

The high amplitude of vibration seen during the machine run-down may be triggering some non-linear behaviour of the foundation and to some extent in the flexible coupling also. The suspicion of the non-linear behaviour has been confirmed by conducting a stepped-sine test.

The stepped-sine tests were carried out on the foundation alone (without the rotor). A portable LDS shaker was attached to the top plate of the foundation such that the shaker can excite the foundation in the lateral direction. The step-sine excitation was applied to the foundation through the LDS shaker. The level of the shaker excitation was varied from a very low to a high amplitude of the order of the expected run-down amplitude for different tests. A PCB force sensor and B&K accelerometer were used to measure the excitation force and the response respectively. The control of the stepped-sine signal to the shaker and the processing of the measured data were carried out through the MatLab based SigLab software (1998). Several typical measured frequency response functions (FRFs) inertance plots for three different shaker excitation levels for the foundation alone in the horizontal direction are shown in Figure 7.10. As can be seen from the inertance plots, when the amplitude of excitation was small only one peak at around 10.6Hz appeared. However, with increased excitation multiple peaks appeared varying from 10Hz to 11Hz and the amplification

at the natural frequency is also not linear. These observations indicate that the foundation behaviour is not linear, and this behaviour of the foundation may be a possible cause for the error in the unbalance estimation.

(a)

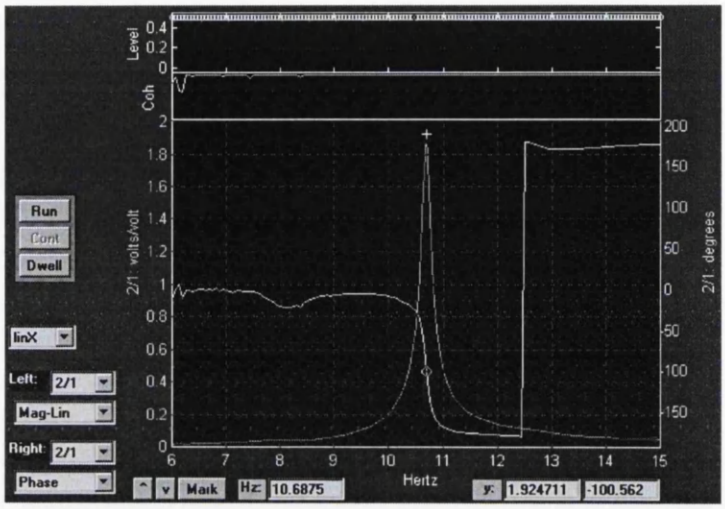

(b)

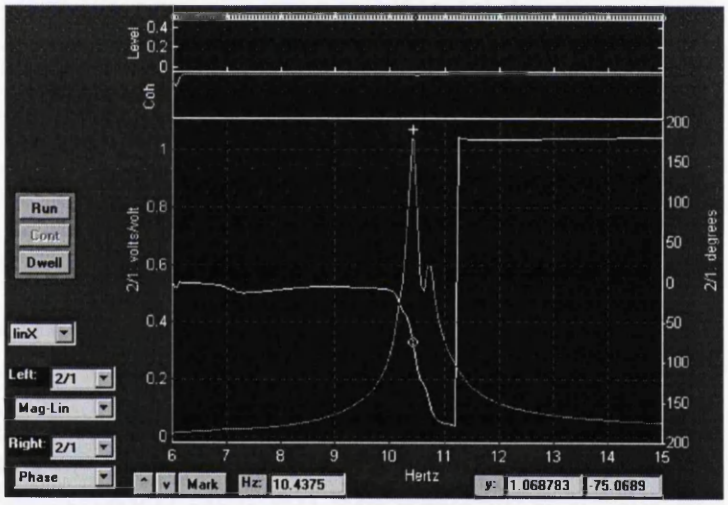

(c)

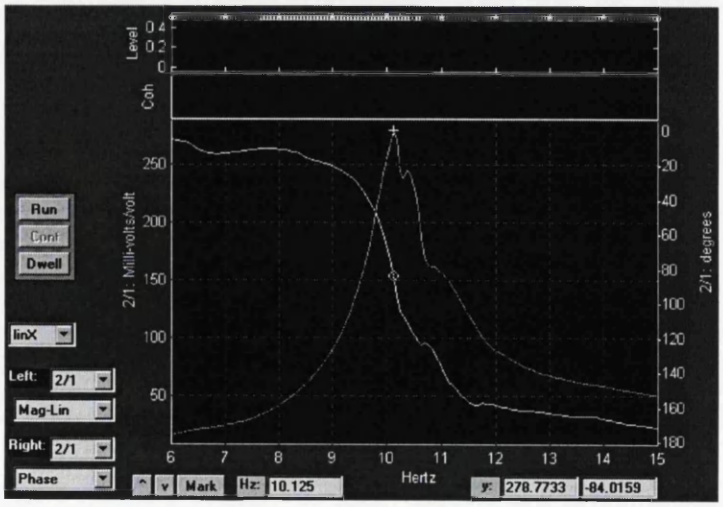

Figure 7.10 Experimental FRFs (inertance) with increasing excitation amplitude from (a) to (c)

7.3.5. Discussion

It was observed that even for a structurally simple foundation, with a good FE model confirmed by modal tests, the unbalance could not be reliably estimated. The example of the *Small rig* showed that some unknown dynamic behaviour of the foundation may lead to large errors in the estimation. The error in the estimation could be more for a complex real-life foundation of a rotating machine. However, the proposed ***Method 3*** (i.e., without using foundation models) gives much better results even for systems with some non-linear behaviour. Hence ***Method 3*** for the rotor unbalance and foundation estimation once again seems to be robust and the method accounts for all unknown dynamic behaviour of the foundation, although there is some error in the estimated phase.

7.4. EXPERIMENTAL EXAMPLE 3: THE NEW SMALL RIG

The same run-down data (Table 6.3) that were used in Chapter 6 for the foundation model estimation were also used here. A total of five runs were performed, run 1 and 4 with residual unbalance and other runs with added unbalance mass at the disks A and B. Since the residual unbalance was unknown, two approaches were taken. The first approach subtracts the response for run 1 (or run 4) from that for run 2, and the unbalance state was then identified from the resulting responses. Assuming the system is linear then the identified unbalance will be the unbalance added. The alternative is to estimate the residual unbalance for run 1 (or run 4), estimate the unbalance for run 2, and difference these estimates to compare with the unbalance weights added. The process may be repeated for other runs. The unbalance estimation was carried out using *Regularization 1-3* by assuming symmetric system matrices for the foundation parameters and a removal of small frequency band of 1.25Hz on either side of 38.37Hz (natural frequency of the rotor with pinned support at bearings) from the machine run-down range.

7.4.1. Subtraction of Run-down data

Four critical speeds (two in the horizontal and one each in the vertical and axial directions) of the machine were present in the run-down frequency range of 5.094Hz to 40.969Hz. The unbalance estimation was carried out by ***Methods 1*** and ***3*** for the resulting responses from the difference of the runs. In ***Method 3*** the frequency range is split into three bands; 5.094Hz to 12.094Hz, 12.094Hz to 27.469Hz, and 27.469Hz to 40.969Hz based on the observation that the estimated responses were close fit to the measured responses. The estimated results are listed in Table 7.7 and Figure 7.11 compares typical measured and estimated responses, for ***Methods 1*** and ***3***. The unbalance estimation by ***Method 3*** is once again better. ***Method 1*** has not accounted for the response of the first critical speed, as seen from Figure 7.11(a). The reason for the maximum error in phase of the order of 30 to 45 degrees and the high error seen in the estimated amplitude in some cases by ***Method 3*** could be the difference in the responses for runs are small and are highly contaminated by measurement noise.

7.4.2. Subtraction of Unbalance

Table 7.8 shows the results when the unbalance is estimated for each run by ***Method 3*** only, and the estimated unbalances are subtracted to compare with the actual unbalance added. The estimated unbalances are much higher than the actual unbalances. A typical comparison of the measured and the estimated responses is shown in Figure 7.12(a). Further investigation was made to understand the poor performance of the estimation.

7.4.3. Estimation of both Unbalance and Misalignment in the Rotor

There may be a small misalignment of the rotor at the coupling with the motor during the assembly of the complete rig. If this is the case it will generate a set of constant forces and moments at the coupling location. Perhaps a good unbalance estimation for the subtracted responses is possible because the influence of the misalignment is simply removed to first order. However the unbalance estimation for individual runs seems to accommodate the rotor misalignment in the rotor unbalance and results in higher amplitudes. Hence unbalance estimation, along with the rotor misalignment,

was carried out using the proposed method in Section 5.4 for individual runs. The results are listed in Table 7.9 and Figure 7.12(b) shows a typical comparison between the measured and the estimated responses. The fit of the estimated response is now much better when compared to the earlier estimation shown in Figure 7.12(a) by ***Method 3***. Table 7.9 also shows that the estimated unbalance by this method is excellent and close to the actual values and the estimated misalignment in the rotor at the coupling is quite consistent for each run. The order of the estimated misalignment (approximately 0.1 and 0.2 mm in the horizontal and vertical directions and their related angular misalignment is 0.4 and 0.2 degrees respectively) is very small and such a misalignment is quite possible during the rig assembly. The small deviation in the estimation may be because of noise in the measurements, however the estimation seems to be quite robust. Hence this experimental example confirms that an accurate estimation of both the rotor unbalance and misalignment is possible using measured responses from a single run-down of a machine.

7.4.4. Discussion

Unbalance estimation using ***Method 1*** again performed poorly, as it could not accommodate all the critical speeds in the run-down speed range. ***Method 3*** accurately estimated the unbalance using the responses from the subtracted runs. However high errors were seen in the estimated unbalance when the individual runs were used and the fit of the estimated responses to the measured responses were bad. This highlighted the need to account for misalignment in the rotor at the coupling during unbalance estimation for individual runs, whereas using the responses from the subtracted runs removes the effect of misalignment. Hence the unbalance estimation along with misalignment at the rotor coupling for the individual runs was found to be excellent and the response fit to the measured response was also found to be very good compared to the estimated response without including coupling effect.

Table 7.7 Unbalance estimation from the experimental run-down data by subtracting runs for the New small rig

Run	Disk	Actual Unbalance (Amplitude (g) @ phase (deg.))	Estimated Unbalance (Amplitude (g) @ phase (deg.))		Error in Estimated Unbalance (Amplitude (g) @ phase (deg.))	
			Method 1	***Method 3***	***Method 1***	***Method 3***
2-1	A	0.76 @ 180	1.01 @ 186	0.96 @ 180	+0.25 @ +6	+0.20 @ 0
	B	0.76 @ 0	0.89 @ 7	0.86 @ 0	+0.13 @ +7	+0.10 @ 0
2-4	A	0.76 @ 180	0.72 @ 168	0.81 @ 151	-0.04 @ -12	+0.05 @ -29
	B	0.76 @ 0	0.68 @ -4	0.71 @ -20	-0.08 @ -4	-0.05 @ -20
3-1	A	1.52 @ 180	1.64 @ 195	1.84 @ 188	+0.12 @ +15	+0.32 @ 8
	B	1.52 @ 0	1.46 @ 13	1.62 @ 7	-0.06 @ +13	0.10 @ 7
3-4	A	1.52 @ 180	0.75 @ 167	1.63 @ 157	-0.77 @ -13	+0.11 @ -23
	B	1.52 @ 0	0.76 @ -8	1.46 @ -19	-0.76 @ -8	-0.06 @ -19
5-1	A	0.76 @ 45	0.52 @ 76	0.87 @ 63	-0.24 @ +31	+0.11 @ +18
	B	0.76 @ 225	0.58 @ 248	0.87 @ 240	-0.18 @ +23	+0.11 @ +15
5-4	A	0.76 @ 45	0.67 @ 105	1.21 @ 83	-0.09 @ +60	+0.45 @ +38
	B	0.76 @ 225	0.61 @ 273	1.07 @ 257	-0.15 @ +48	+0.31 @ +32
3-2	A	0.76 @ 180	0.68 @ 216	0.73 @ 225	-0.08 @ +36	-0.03 @ +45
	B	0.76 @ 0	0.58 @ 28	0.61 @ 37	-0.18 @ +28	-0.15 @ +37

Table 7.8 Unbalance estimation by Method 3 from the experimental run-down data by subtracting unbalance for the New small rig

Runs	Disk	Actual Unbalance (Amplitude (g) @ phase (deg.))	Estimated Unbalance (Amplitude (g) @ phase (deg.))			
			First Run	Second Run	Added Unbalance	Error
1 & 2	A	0.76 @ 180	6.03 @ 108	6.91 @ 108	0.89 @ 104	+0.13 @-76
	B	0.76 @ 0	5.08 @ 286	5.78 @ 286	0.71 @ 293	-0.05 @ -67
4 & 2	A	0.76 @ 180	4.16 @ 107	6.91 @ 108	2.72 @ 108	+1.96 @ -72
	B	0.76 @ 0	3.68 @ 285	5.78 @ 286	2.12 @ 291	+1.36 @ -69
1 & 3	A	1.52 @ 180	6.03 @ 108	4.59 @ 132	2.64 @ 242	+1.12 @ +62
	B	1.52 @ 0	5.08 @ 286	3.98 @ 310	2.12 @ 58	+0.60 @ +58
4 & 3	A	1.52 @ 180	4.16 @ 107	4.59 @ 132	1.96 @ 198	+0.44 @ +18
	B	1.52 @ 0	3.68 @ 285	3.98 @ 310	1.71 @ 17	+0.19 @ +17
1 & 5	A	0.76 @ 45	6.03 @ 108	7.69 @ 102	1.81 @ 82	+1.05 @ +37
	B	0.76 @ 225	5.08 @ 286	6.52 @ 280	1.59 @ 258	+0.83 @ +33
4 & 5	A	0.76 @ 45	4.16 @ 107	7.69 @ 102	3.54 @ 96	+2.78 @ +51
	B	0.76 @ 225	3.68 @ 285	6.52 @ 280	2.88 @ 274	+2.12 @ +49
2 & 3	A	0.76 @ 180	6.91 @ 108	4.59 @ 132	3.29 @ 73	+2.53 @ -107
	B	0.76 @ 0	5.78 @ 286	3.98 @ 310	2.70 @ 249	+1.94 @ -111

Table 7.9 Estimation of both the rotor unbalance and misalignment from the experimental run-down data for the New small rig

Run	Disk	Actual Unbalance (g @ deg.)	Estimated Unbalance (g @ deg.)	Estimated Misalignment				Added Unbalance (g @ deg.)	
				Horizontal Δy (mm)	Vertical Δz (mm)	Hori. Angle $\Delta\theta_z$ (deg.)	Ver. Angle $\Delta\theta_y$ (deg.)	With respect to *Run 1*	With respect to *Run 4*
1	A	Residual	1.84 @ 130	0.10	0.21	0.40	0.69	-----	-----
	B	Residual	1.46 @ 350						
4	A	Residual	1.99 @ 127	0.09	0.18	0.32	0.20	-----	-----
	B	Residual	1.44 @ 341						
2	A	0.76 @ 180	2.48 @ 144	0.14	0.20	0.75	0.45	0.82 @ 181	0.82 @ 190
	B	0.76 @ 0	2.33 @ 354					0.88 @ -4	0.98 @ 14
3	A	1.52 @ 180	2.75 @ 158	0.14	0.18	0.42	0.16	1.41 @ 191	1.46 @ 202
	B	1.52 @ 0	2.96 @ 1					1.55 @ 11	1.67 @ 18
5	A	0.76 @ 45	2.54 @ 114	0.08	0.21	0.24	0.17	0.95 @ 79	0.76 @ 76
	B	0.76 @ 225	1.34 @ 323					0.66 @ 236	0.45 @ 228

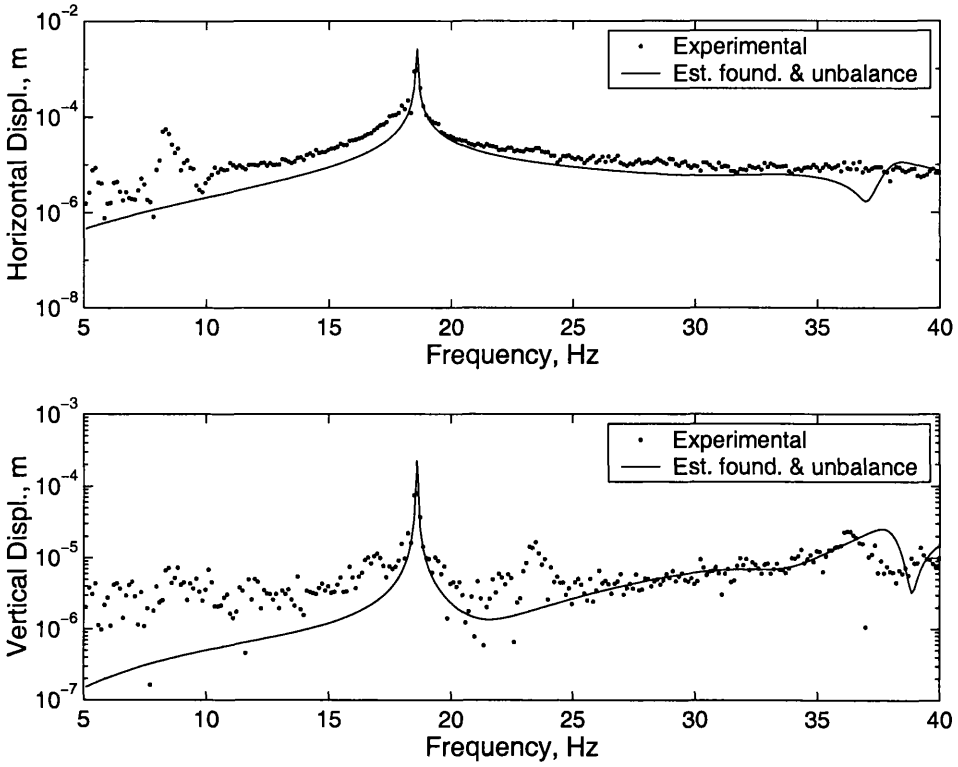

(a) Method 1

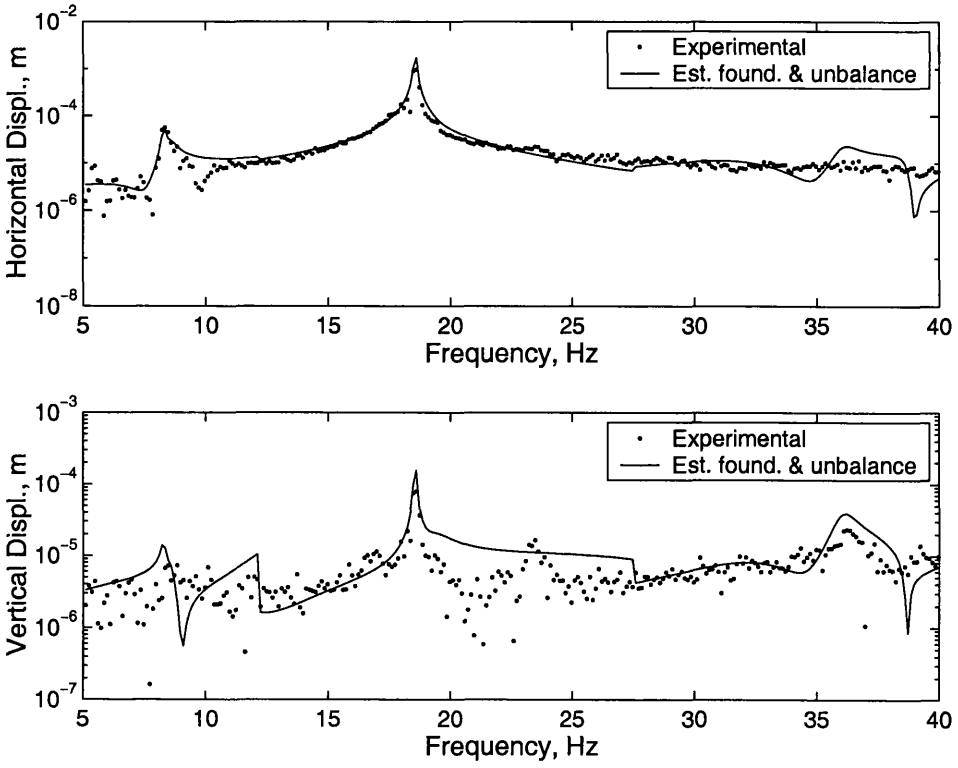

(b) Method 3

Figure 7.11 Measured and estimated responses at bearing A, for the difference of runs 3 and 4 for the experimental New small rig

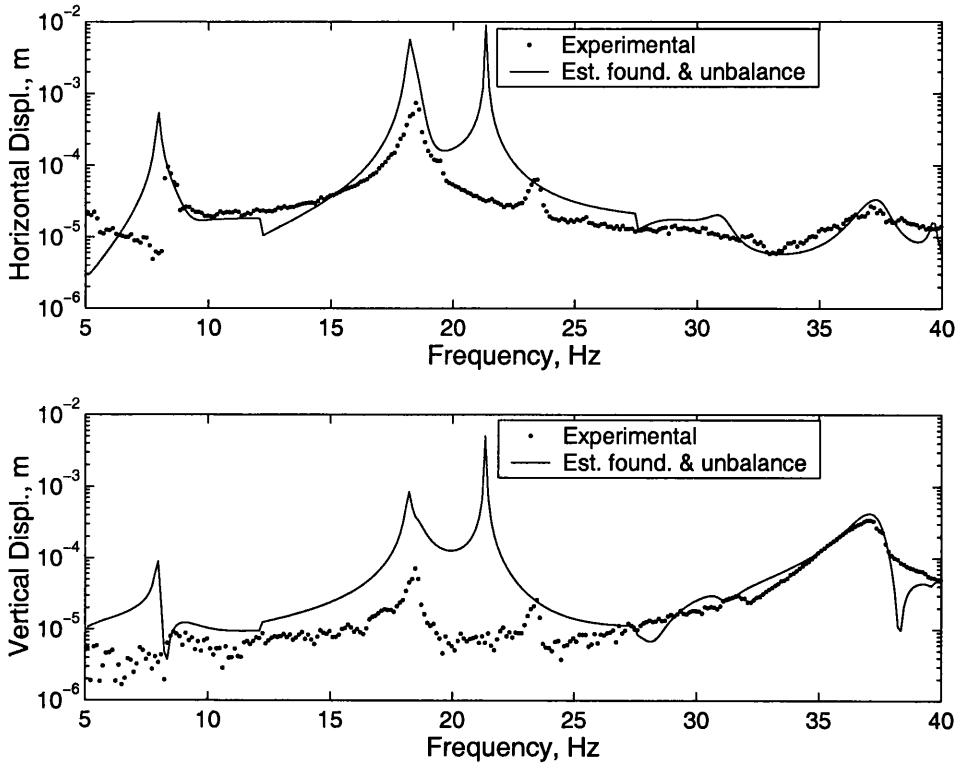

(a) Method 3 without Misalignment effect

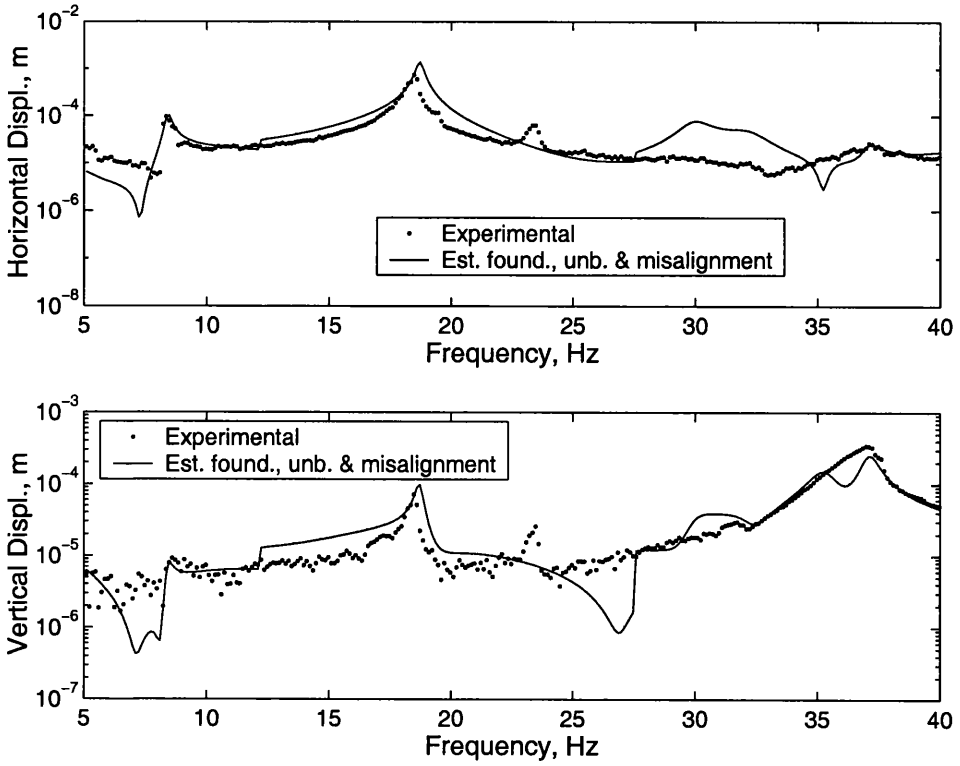

(b) Method 3 with Misalignment effect

Figure 7.12 Measured and estimated responses at bearing A, for run 2 for the experimental New small rig

7.5. SUMMARY

An identification method for the estimation of the state of rotor unbalance (amplitude and phase) and the misalignment in the multi-rotors of a rotor-bearing-foundation system has been presented. The estimation uses measured vibration data at the bearing pedestals from a single run-down or run-up of the machine, without prior knowledge of the state of unbalance and the misalignment. Initially three approaches were used for the unbalance estimation. The first method uses the whole frequency range at once. It has been observed that ***Method 1*** may gives a good estimate of the state of unbalance for sufficiently damped rotor system. However, the estimated foundation model is always not very good, since there are fewer degrees of freedom in the foundation model than system modes. This may be overcome by dividing the entire frequency range into smaller frequency bands and estimating the frequency dependent foundation models. The second method (***Method 2***) splits the frequency range, but identifies a different unbalance vector within each frequency band. This method provides multiple poor estimates of the unbalance, although the fit to the response is good. The final method (***Method 3***) combines these approaches by estimating a global unbalance vector, but a different foundation model in each frequency band. This combined method was found to be the most reliable for the estimation of both the frequency dependent foundation models and the state of unbalance. This method is also observed to be robust to noisy data, small modelling errors in the bearings and even when the measured responses are not linear. ***Method 3*** has been further modified to account for misalignment in the rotor. This has been successfully demonstrated through an experimental example of the *New small rig*. The importance of *Regularization 3* has also been demonstrated in the estimation process. The robustness check of the estimation method with respect to errors in the rotor and fluid bearing models has also been carried out and is presented in Chapter 8.

CHAPTER 8

SENSITIVITY STUDY OF THE METHOD FOR THE ROTOR UNBALANCE ESTIMATION OF FLEXIBLE MACHINES

8.0. INTRODUCTION

In Chapter 5, the theory of rotor unbalance and misalignment estimation for flexibly supported machines using measured vibration responses at bearing pedestals from a single run-down of a machine has been presented. The method has been validated in Chapter 7 through simulated and experimental examples. Fortunately it has been observed in the experimental examples (Chapter 7) that the linearly estimated unbalance by the suggested method seems to be quite robust, even when the measured responses were not found to be linear. For all the examples in Chapter 7, the physical and material properties of the rigs were exactly known, and the error in the modelling of the rotor, bearings, stiffnesses of flexible coupling between the rotor and driving motor, were expected to be negligible. However, in the case of real life systems like TG sets these parameters (especially bearing models and the coupling of the turbine shaft to the generator) may not be known exactly and it is often difficult to get the required information from the plant. So it is also important to confirm that the suggested method is robust with respect to errors in the rotor and fluid bearing modelling. Hence a sensitivity study on the unbalance estimation was carried out by introducing some perturbations in different parameters such as shaft diameter, density, elasticity, error in the bearing model, coupling stiffness, etc. to assess the robustness of the method. This sensitivity study was carried out initially on the simulated examples and then on the experimental examples. In the simulated examples it was assumed that the rotor was supported on rigid bearings as well as on fluid bearings and their sensitivity analysis results are compared and presented here.

8.1. PERTURBATION IN DIFFERENT MODELS

Perturbations in the different parameters required to model the rotor and the fluid bearings is introduced in the examples considered previously.

8.1.1. The Rotor Model

The shaft diameter (d) and the material properties, modulus of elasticity (E) and density (ρ), are the prominent parameters required for the rotor FE modelling. Other than these parameters, the mechanical coupling stiffnesses, translational stiffness (k_t) and rotational

stiffness (k_θ), are also the part of the rotor model and hence these are equally important. Errors in these parameters were introduced in turn before estimating the rotor unbalance at multi-balance planes. The errors introduced in different parameters were ±5% in shaft diameter (d) in steps of 0.5%, ±10% in the modulus of elasticity (E) and density (ρ), and ±20% in the coupling stiffnesses, k_t and k_θ, in steps of 1%. Simultaneous perturbation in all these parameters was also considered, although such a combination may be highly unlikely even for realistic problems like TG sets.

8.1.2. The Bearing Model

The ball bearing is generally considered to provide a rigid connection between the translational DoF of the rotor and the foundation at the location of the bearing. So no error is expected if the rotor is supported through ball bearings, and the *Small rig* and *New small rig* both have ball bearings. However when the rotor is supported on fluid bearings, the bearing model is then needed for the unbalance estimation. This is the case in the *Aston rig*. As justified earlier in Chapter 3, short bearing theory can be used for fluid bearing modelling. Such bearing modelling (Section 3.1.2 of Chapter 3) depends on the bearing static load, bearing clearance and oil viscosity. Hence perturbations in these parameters were also considered during the unbalance estimation.

With the above perturbations in the modelling of the rotor and fluid bearings, the effect on the rotor unbalance and the rotor misalignment estimation has been evaluated and are discussed below.

8.2. SENSITIVITY TO THE ROTOR MODEL

A total of four examples (two simulated and two experimental) have been considered. Of the two simulated examples, one has rigid bearings and the other has fluid bearings, are used to examine the difference between them in terms of the rotor unbalance estimation. On the other hand, of the two experimental examples, one has rigid bearings and other has fluid bearings, and these are used to confirm the observations made on the simulated examples.

8.2.1. Simulated Example 1: The *Small Rig*

This example simulates the existing experimental *Small rig* in the Dynamics Laboratory of University of Wales Swansea (UK) as discussed in Chapter 4. For the purpose of the simulation the calculated responses were obtained from an updated FE model of the complete rig for the unbalance configurations of added mass unbalance on both disks as listed in Table 6.2. Recall that the rig was run-down from 40Hz to 6Hz, with measurements taken at a spacing of 0.25Hz and the calculated responses associated with the translational DoF at bearing A (near coupling) and B (at free end) were assumed to be the measured responses.

These measured responses were now used for unbalance estimation with some perturbation in the rotor model (including the coupling stiffnesses). One by one, errors in the material and physical properties of the rotor and coupling stiffnesses were introduced during estimation of the rotor unbalance at disk A and B, as proposed in Section 8.1.1. The maximum deviation in the estimated unbalance amplitudes and phases with errors in different parameters is summarized in Table 8.1. The deviation in the unbalance in the table is calculated with respect to the estimated unbalance when there was no modelling error either in the rotor or the bearings i.e., with initial values of the estimated rotor unbalance. The variation in the unbalance estimates is shown graphically in Figure 8.1. Table 8.1 and Figure 8.1 show that the deviations in the unbalance estimation are small for the perturbation errors in individual parameters. The change in the estimated unbalance amplitudes seems to follow a pattern, either decreasing or increasing with error in different parameters, but the variation is not smooth. However the phase estimation seems to be more robust and remain almost unchanged with the rotor model error. Furthermore there may be a possibility that the values of all the parameters required for the modelling of the rotor and coupling may not be known exactly. These parameters may have small errors simultaneously and such a possibility was also examined. A 5% of the normally distributed random perturbations in all the parameters (Table 8.1) were introduced and then the unbalance was estimated. It is observed that the deviations in the estimated unbalance amplitudes are well within 38% and phases are within an error of 4 degrees. These estimated unbalance amplitudes and phases are shown in Figure 8.2.

Next the same rig is considered, but with fluid bearings in place of the rigid bearings to examine the effect of fluid bearings on the results.

8.2.2. Simulated Example 2: The *Small Rig* with Fluid Bearings

For the purpose of comparison between the two rigs, one with rigid bearings and the other with fluid bearings, the fluid bearings were assumed to replace the rigid bearings A and B in the rig. The properties of both of the fluid bearings were assumed to be 12mm diameter, 0.3 diameter to length ratio, 150μm clearance, and 0.0009 Ns/m^2 oil viscosity. The bearing forces at bearings A and B were calculated as F_A =13.7N and F_B=7N respectively. Short bearing theory was used to obtain values for bearing stiffness and damping coefficients (Hamrock, 1994). The measured responses at the bearings were again calculated for the unbalance configurations listed in Table 6.5. Once again a similar study to that in Section 8.2.1 was carried out, i.e., the unbalance was estimated with perturbations in different parameters of the rotor model. The summary of the results are listed in Table 8.2 and shown graphically in Figures 8.3 to 8.4.

8.2.2.1. Results and Discussion

Table 8.2 and the figures show that the deviations in the estimated unbalance are generally less for the fluid bearing machine when compared to the results of the rig with rigid bearings. Variation in the unbalance estimation with the perturbation errors in the rotor parameters is either smoothly increasing or decreasing when compared to the rig with rigid bearings (Figures 8.1 & 8.2). This observation clearly indicates that the fluid bearings have more capability to accommodate perturbations in the parameters (both physical and material) of the rotor, i.e., more error in the rotor model. Perhaps the damping provided by the fluid bearings to the rotor is making this difference between the two bearings.

(i) Fluid Bearings with Zero Damping Coefficient

To confirm that the presence of damping is beneficial, the unbalance was again estimated assuming zero damping in the fluid bearings. A typical variation in the unbalance estimation due to perturbations in the modulus of elasticity of the rotor is shown in Figure 8.5. The observations are now similar to those observed for the rig with rigid bearings, and confirm the above suspicion about the bearing damping.

(ii) Balance Run

It is also important to know whether the estimated unbalance, which is found to have errors due to perturbations in modelling, are useful or not. To confirm this a few simulated balancing runs were carried out. Figure 8.6 compares the response of machine before and after balancing for one such typical example for the unbalance configuration 1. Balancing responses are calculated using one of the estimated corrective unbalance – Disk A: 1.25x5.5e-2 g m @ (180+1.25x 75) degree and Disk B: 0.80x5.5e-2 g m @ (180+1.20x135) degree. Figure 8.6 shows that the rotor balancing is very effective even for high errors in the estimated unbalance.

Table 8.1 Unbalance estimation for the Small rig simulation, with perturbations in the rotor model

Rotor Model		Balance Disk A – Unbalance		Balance Disk B- Unbalance	
Perturbation in Parameters	Error	Max. % Error in Amplitude	Max. Phase Error (deg.)	Max. % Error in Amplitude	Max. Phase Error (deg.)
Shaft diameter (d)	±5 %	35 %	2	20 %	3
Elasticity (E)	±10 %	21 %	2	12 %	1
Density (ρ)	±10 %	10 %	2	6 %	1
Coupl. Stiff., k_t & k_θ	±20 %	6 %	1	8 %	1
5% Random error to all		20 %	2	38 %	4

Table 8.2 Unbalance estimation for the Small rig simulation with two fluid bearings, with perturbations in the rotor model

Rotor Model		Balance Disk A – Unbalance		Balance Disk B- Unbalance	
Perturbation in Parameters	Error	Max. % Error in Amplitude	Max. Phase Error (deg.)	Max. % Error in Amplitude	Max. Phase Error (deg.)
Shaft diameter (d)	±5 %	14 %	3	18 %	3
Elasticity (E)	±10 %	10 %	1	11 %	1
Density (ρ)	±10 %	7 %	1	2 %	5
Coupl. Stiff., k_t & k_θ	±20 %	4 %	0.5	4 %	0.5
5% Random error to all		20 %	4	25 %	4

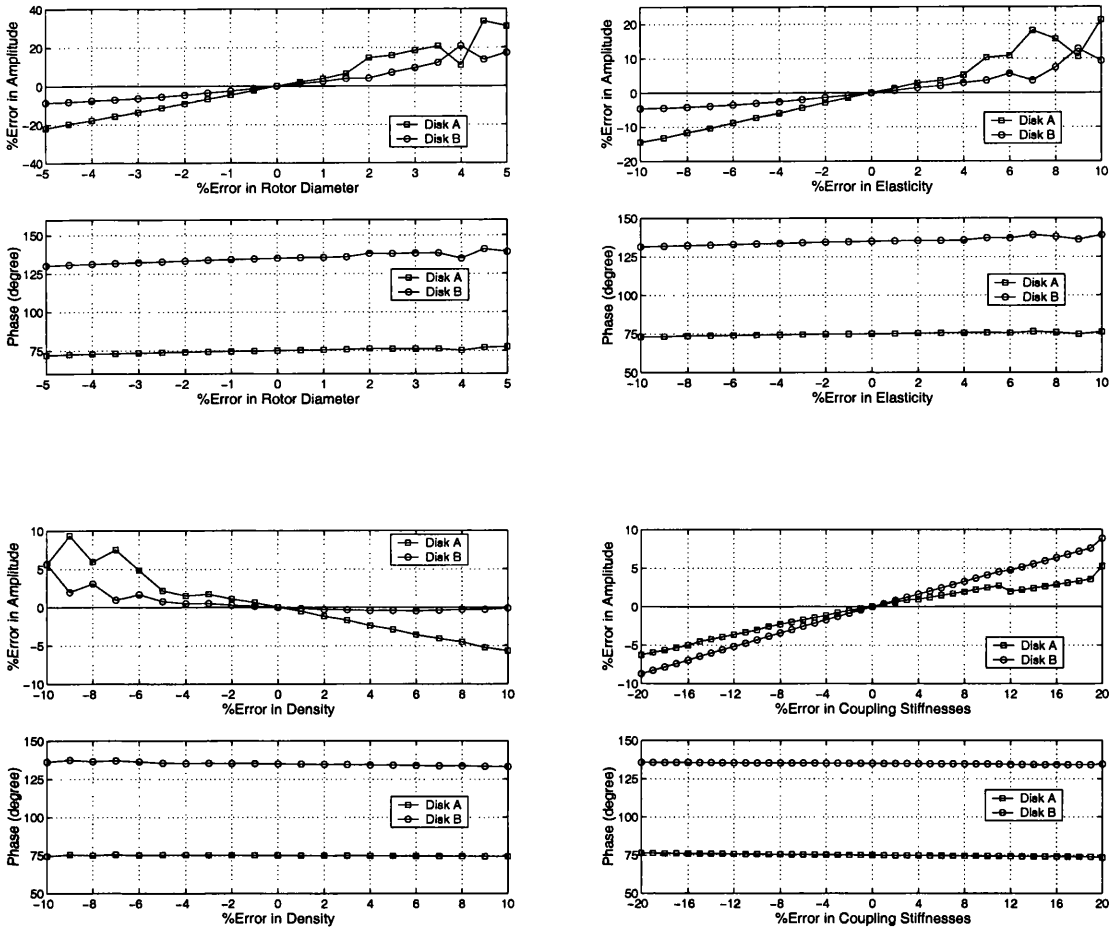

Figure 8.1 Deviation in the rotor unbalance estimation with the error in the rotor model of the Small rig simulation for unbalance configuration 1

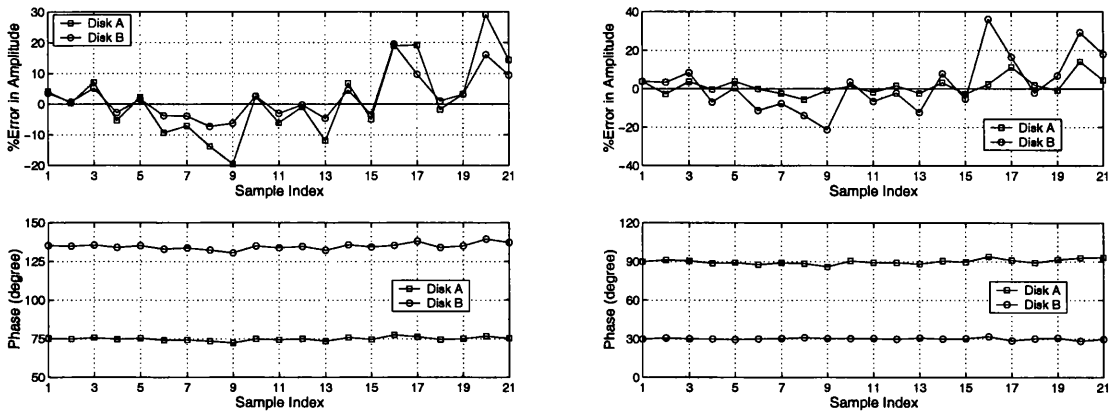

(a) Unbalance Configuration 1 **(b) Unbalance Configuration 2**

Figure 8.2 Deviation in the rotor unbalance estimation with 5% random perturbations in all rotor modelling parameters of the Small rig simulation

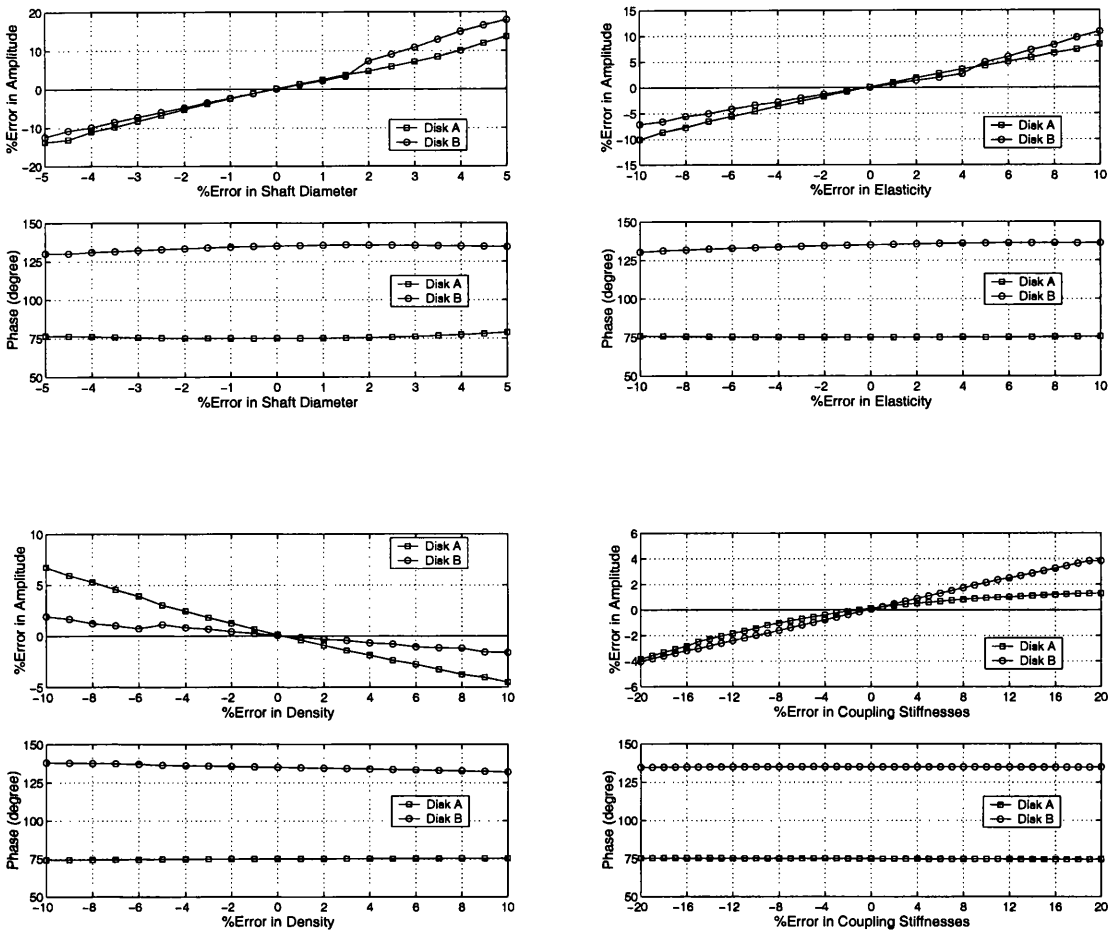

Figure 8.3 Deviation in the rotor unbalance estimation with the error in the rotor model of the Small rig simulation (with fluid bearings) for unbalance configuration 1

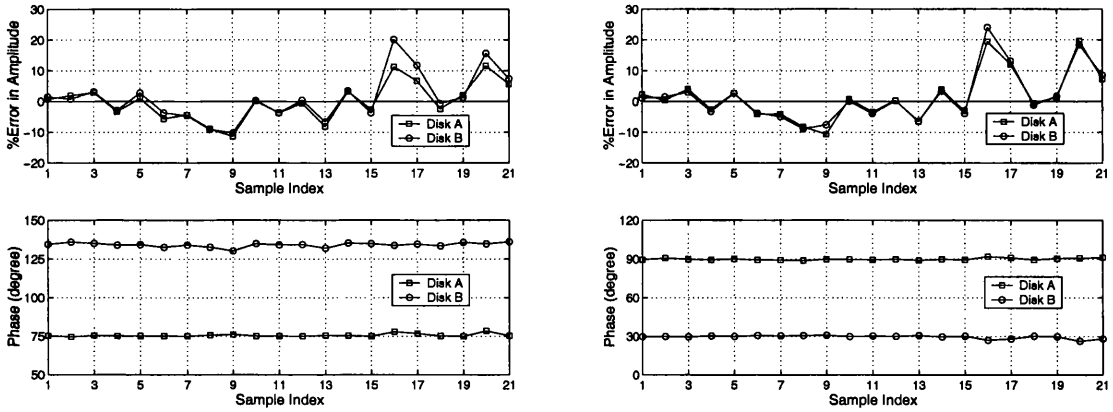

(a) Unbalance Configuration 1 **(b) Unbalance Configuration 2**

Figure 8.4 Deviation in the rotor unbalance estimation with 5% random perturbations in all rotor modelling parameters of the Small rig simulation with fluid bearings

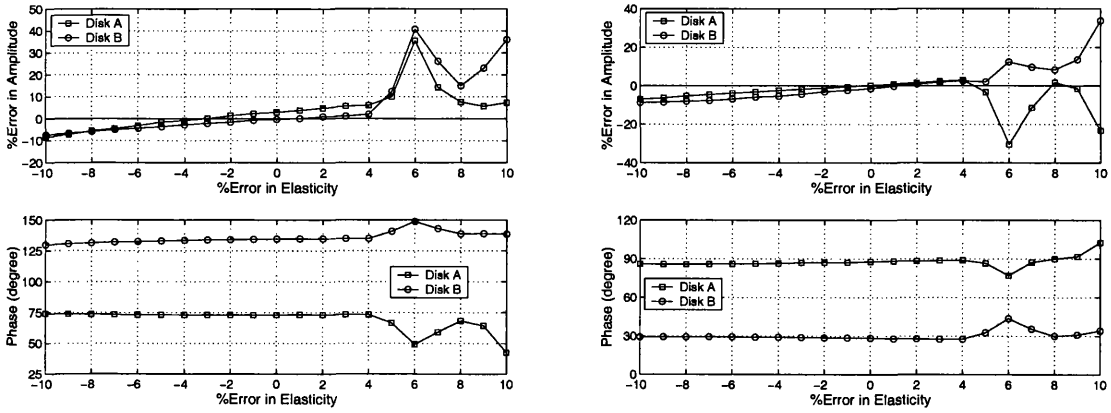

(a) Unbalance Configuration 1 **(b) Unbalance Configuration 2**

Figure 8.5 Effect of zero damping in the fluid bearings on the unbalance estimates for the Small Rig with fluid bearings

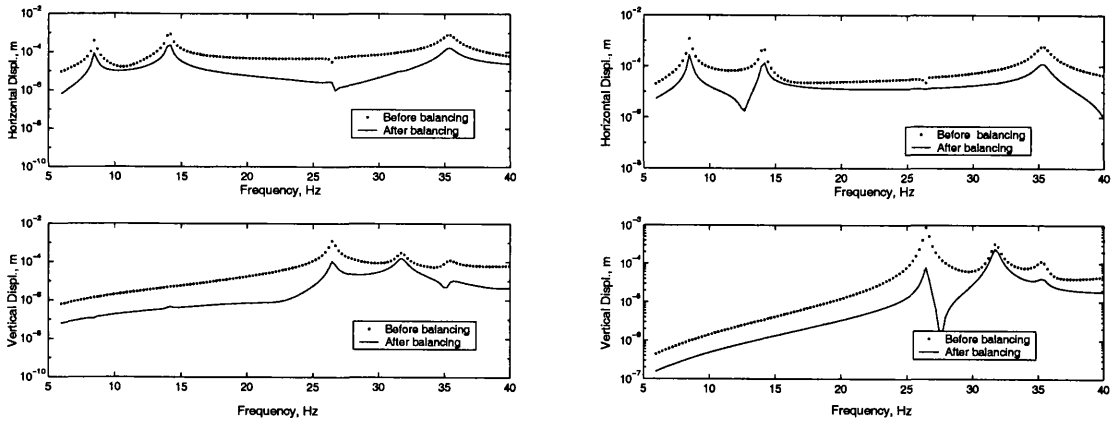

(a) Bearing A responses **(b) Bearing B responses**

Figure 8.6 Responses before and after balancing runs with errors in corrective unbalance masses and phases for unbalance configuration 1

8.2.3. Experimental Example 1: The *New Small Rig*

The sensitivity analysis for the unbalance estimation due to perturbations in the rotor modelling parameters was carried out for the individual experimental runs shown in Table 6.3 of Chapter 6. Figure 8.7 gives a typical graphical representation of the variation in the rotor unbalance estimation for the subtracted unbalance for runs 1 and 2 with the perturbation errors in the individual rotor modelling parameters. For a 5% normally distributed random perturbation error in all modelling parameters simultaneously, the variation in the estimation is shown in Figure 8.8. Figures 8.7 and 8.8 show that the phase estimation is more robust than the unbalance amplitude. Usually the estimated unbalance is less than 40-50% except in some cases where it is of the order of 70-75%. Table 8.3 summarizes the maximum deviation in the estimated unbalance amplitudes and phases. A typical variation in the linear and angular misalignment estimation with the rotor modelling error is also shown in Figure 8.9 for run 3. The maximum effect on the misalignment estimation is seen when the rotor stiffness decreases by 6-10%, otherwise the variation in the estimation is small.

The above sensitivity has been carried out by using all the regularization methods discussed in Chapter 5. The effect on the estimation with or without *Regularizations 1 & 2* is usually not very adverse or dominating, however the use of *Regularization 3* is essential particularly when the rotor model has some error. Figure 8.10 shows a typical example for the subtracted unbalance for runs 1 and 2 with the error in the rotor modelling when *Regularization 3* has not been used. The deviation in the unbalance estimation was found to be very high compared to the earlier estimation using *Regularization 3*, as shown in Figure 8.7. Hence the use of *Regularization 3* is essential for reliable unbalance estimation.

Table 8.3 Unbalance estimation for the experimental New small rig, with perturbations in the rotor model

Rotor Model		Balance Disk A – Unbalance		Balance Disk B- Unbalance	
Perturbation in Parameters	Error	Max. % Error in Amplitude	Max. Phase Error (deg.)	Max. % Error in Amplitude	Max. Phase Error (deg.)
Shaft diameter (d)	±5 %	70 %	45	60 %	30
Elasticity (E)	±10 %	55 %	35	38 %	25
Density (ρ)	±10 %	60 %	30	30 %	25
Coupl. Stiff., k_t & k_θ	±20 %	40 %	20	25 %	25
5% Random error to all		75 %	20	70 %	20

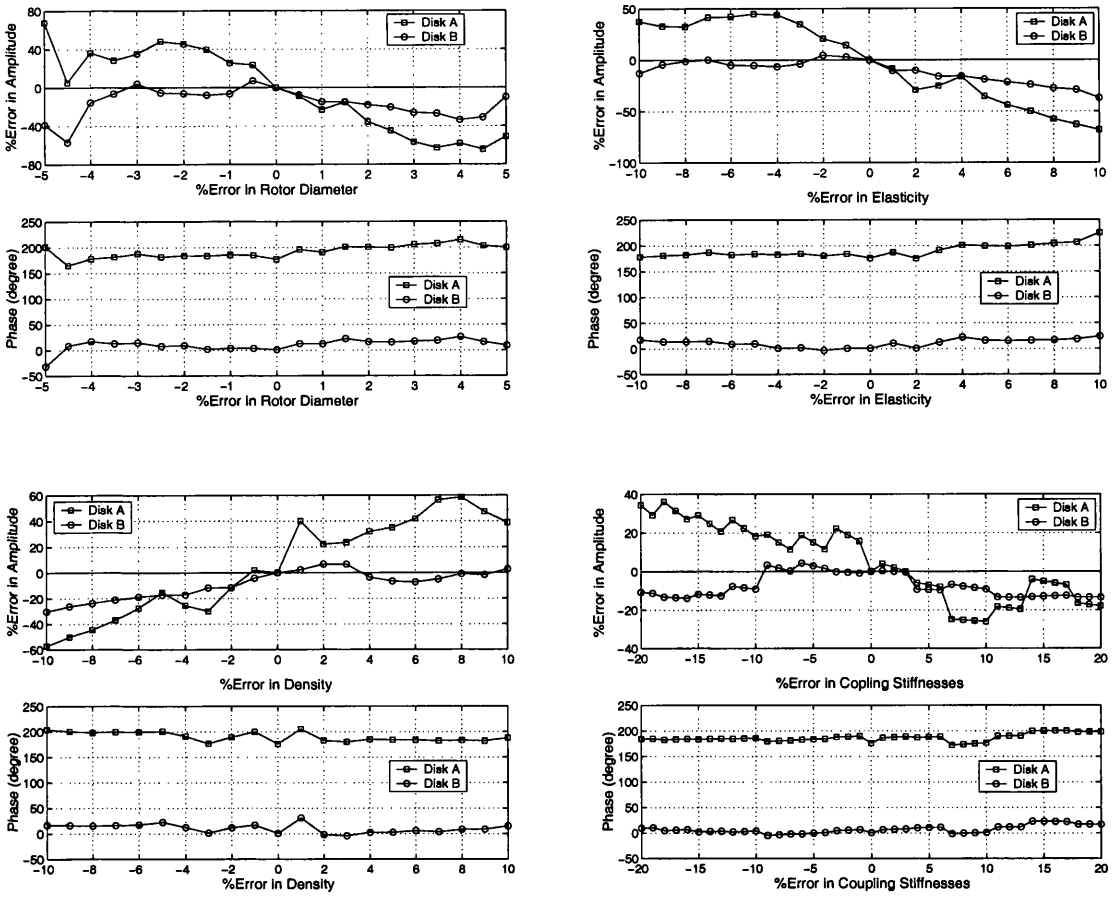

Figure 8.7 Typical deviation in the rotor unbalance estimation with the error in the rotor model of the experimental New small rig for the subtracted unbalance for runs 1 and 2

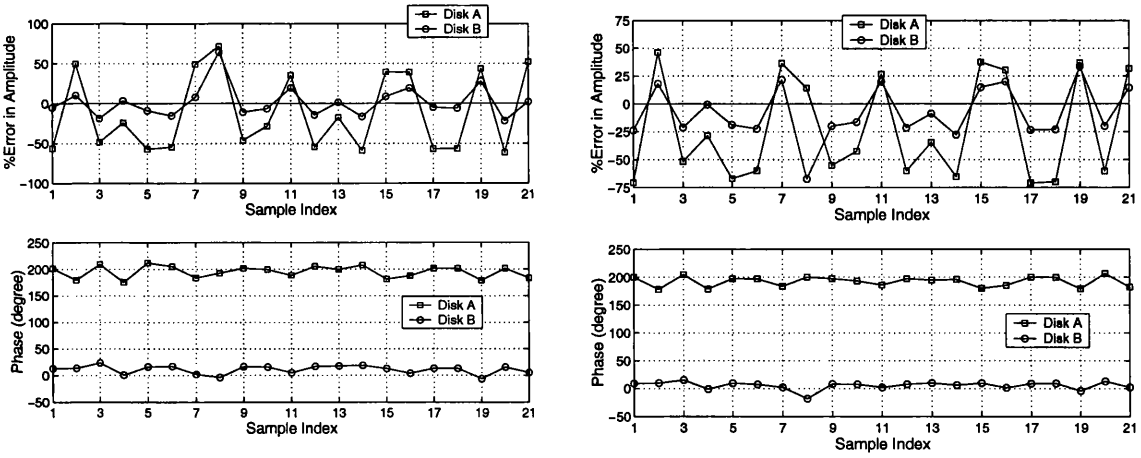

(a) Subtracted unbalance for runs 1 & 2 **(b) Subtracted unbalance for runs 1 & 3**

Figure 8.8 Typical deviation in the rotor unbalance estimation with 5% random error in all rotor modelling parameters of the experimental New small rig

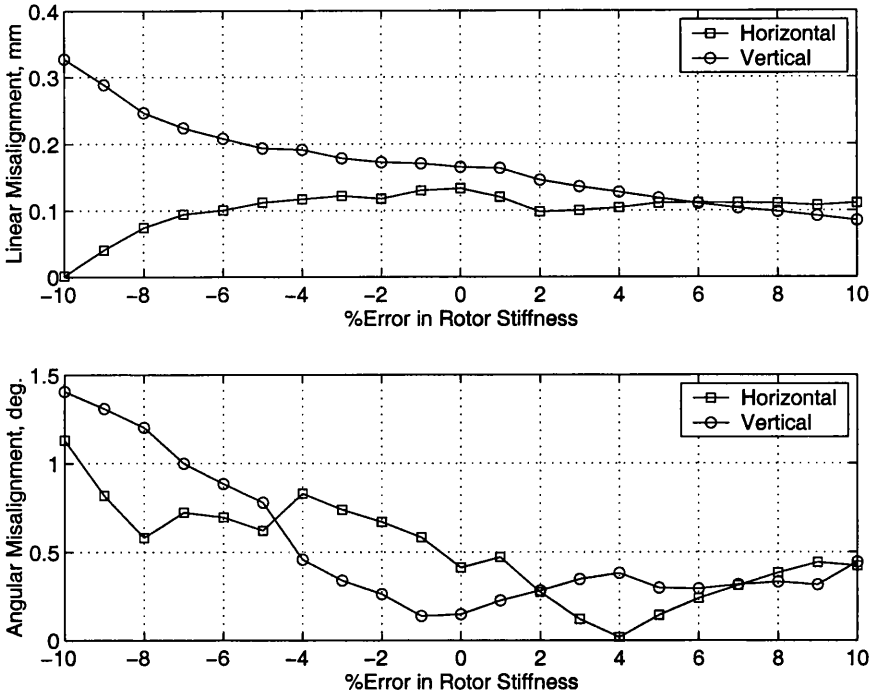

Figure 8.9 A typical deviation in the rotor misalignment estimation with the error in the rotor model of the experimental New small rig for run 3

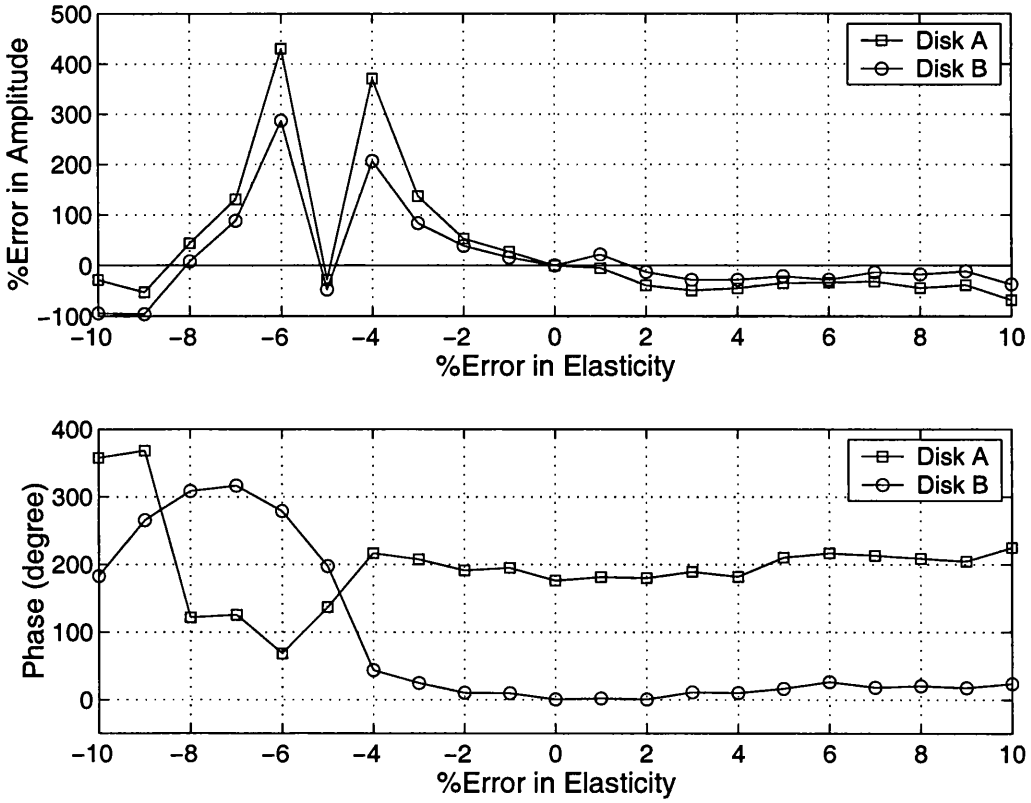

Figure 8.10 A typical deviation in the rotor unbalance estimation with the error in the rotor model of the experimental New small rig for the subtracted unbalance for runs 1 and 2, without Regularization 3

8.2.4. Experimental Example 2: The *Aston Rig*

The sensitivity analysis for the unbalance estimation due to perturbations in the rotor modelling parameters was carried out for the subtracted experimental runs (2-1) and (3-1) listed in Table 6.4 of Chapter 6. Figure 8.11 gives a typical graphical representation of the variation in the rotor unbalance estimation with the perturbation in the rotor modelling parameters for run (2-1). Table 8.4 summarizes the maximum deviation in the estimated unbalance amplitudes and phases.

Table 8.4 Unbalance estimation for the experimental Aston Rig, with perturbations in the rotor model

Rotor Model		*Balance Disk 2 – Unbalance		Balance Disk 5- Unbalance	
Perturbation in Parameters	Error	Max. % Error in Amplitude	Max. Phase Error (deg.)	Max. % Error in Amplitude	Max. Phase Error (deg.)
Run (2-1)					
Shaft diameter (d)	±5 %	15 %	15	37 %	10
Elasticity (E)	±10 %	40 %	50	35 %	20
Density (ρ)	±10 %	38 %	25	25 %	20
5% Random errors in all		60 %	45	80 %	20
Run (3-1)					
Shaft diameter (d)	±5 %	15 %	7	9 %	5
Elasticity (E)	±10 %	22 %	7	12 %	5
Density (ρ)	±10 %	45 %	15	12 %	7
±5% Random errors in all		45 %	35	20 %	8

* Disk 1 for *run (3-1)*.

Figure 8.11 shows a smoother variation in the estimated unbalance amplitudes and phases with the error in the rotor parameters. The deviation in the estimated unbalance is also small for most of the cases compared to the experimental *New small rig* with rigid bearings. The observation is once again quite similar to the *Small rig* simulation with and without fluid bearings although the experimental *Aston rig* is much bigger than the experimental *New small rig*. In general the phase estimation is robust and usually invariant with the modelling error,

and in some cases the estimated phase at disk 2 for run (2-1) is found to be closer to the actual phase.

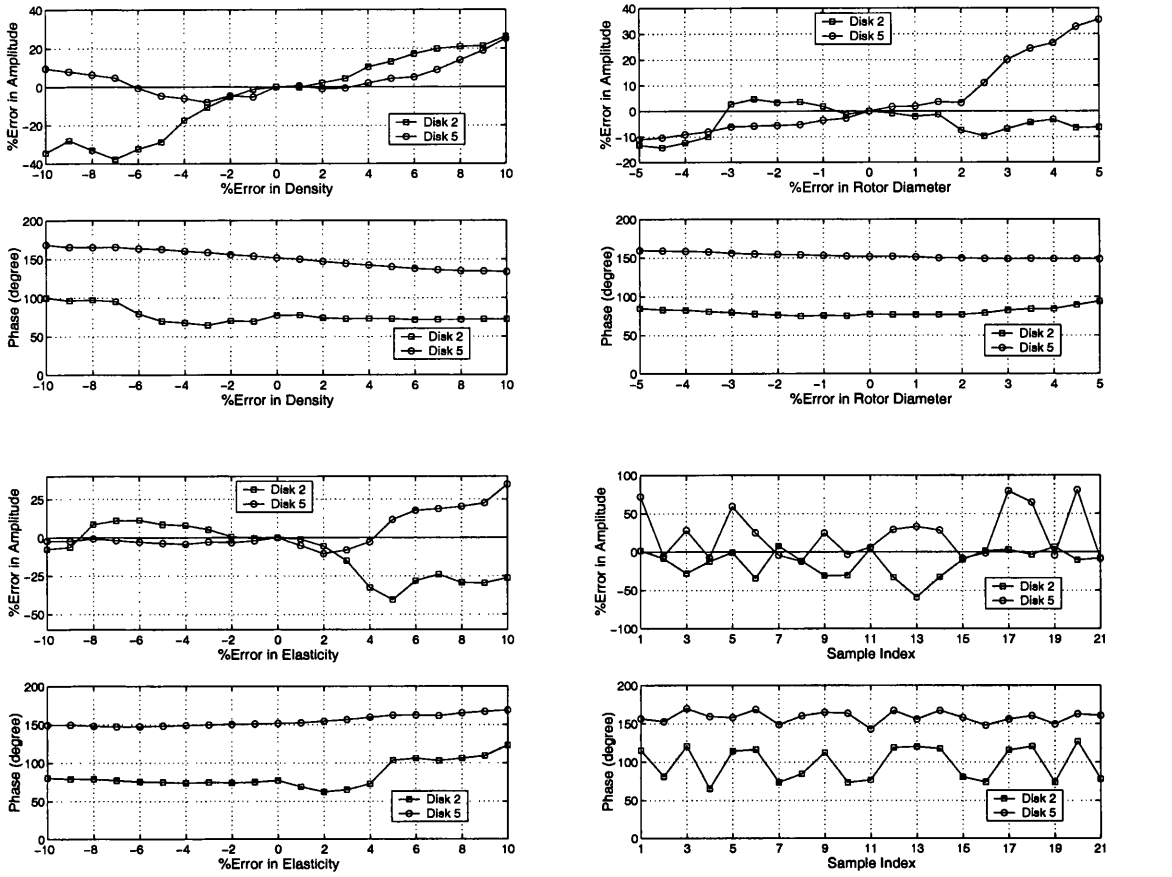

5% random errors in all rotor parameters

Figure 8.11 Typical deviation in the rotor unbalance estimation with the error in the rotor model of the experimental Aston Rig for subtracted run (2-1)

8.3. SENSITIVITY TO THE FLUID BEARING MODEL

The effect of modelling errors in the fluid bearings on the unbalance estimates was also examined. All of the above examples with fluid bearings were considered again. One by one errors in the bearing parameters – bearing forces, clearance and oil viscosity - were introduced and the unbalance were estimated. A linear and identical variation in the individual bearing parameters was assumed for all of the bearings in the rotor system. A case of random perturbations in all of the bearing modelling parameters was also studied. The summary of the results are listed in Tables 8.5 –8.6 and typical graphical representations in Figures 8.12 to 8.13.

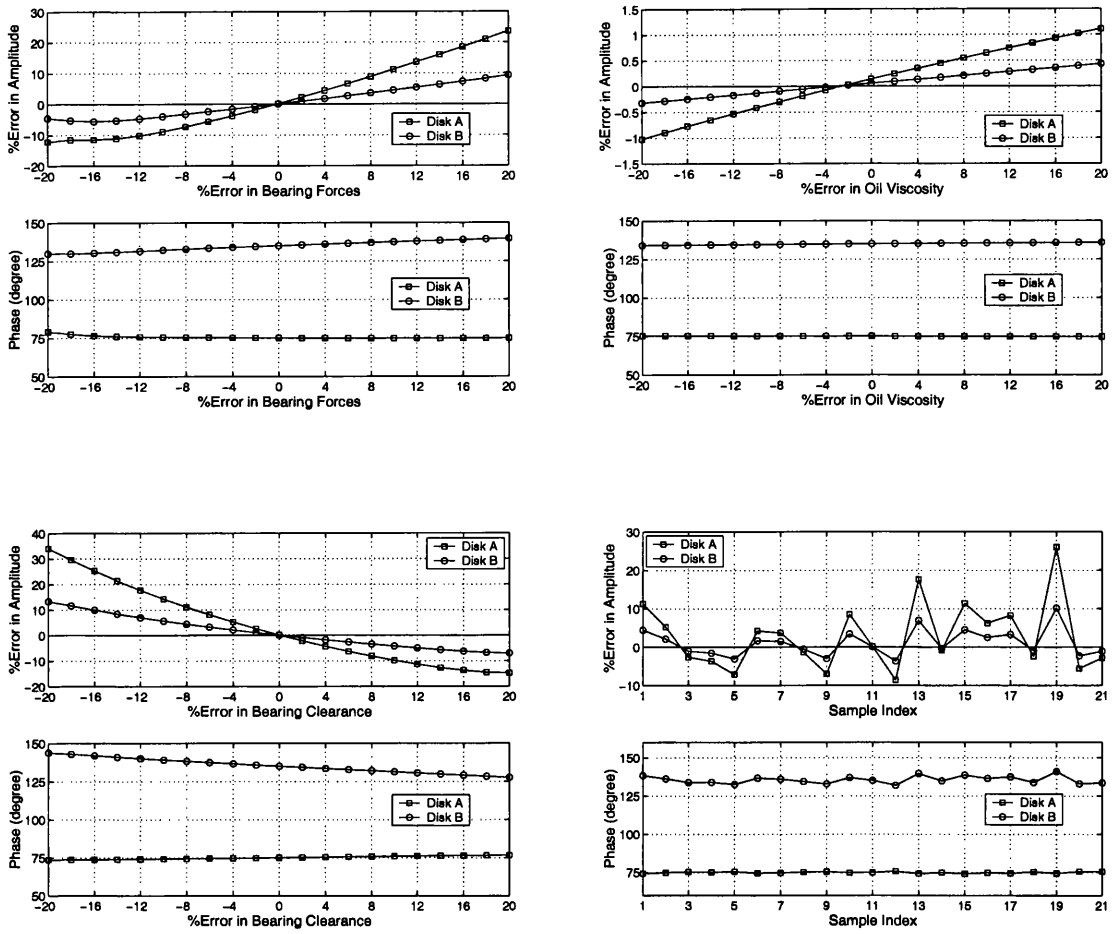

10% random error in all parameters

Figure 8.12 Typical deviation in the rotor unbalance estimation with perturbations in the fluid bearing model for the unbalance configuration 1 of the Small rig simulation with fluid bearings

Table 8.5 Unbalance estimation for the Small rig simulation with fluid bearings, with perturbations in the fluid bearing model

Fluid Bearing Model		Balance Disk A – Unbalance		Balance Disk B- Unbalance	
Perturbation in Parameters	Error	Max. % Error in Amplitude	Max. Phase Error (deg.)	Max. % Error in Amplitude	Max. Phase Error (deg.)
Bearing Forces	±20 %	24 %	5	10 %	5
Oil Viscosity (μ)	±20 %	1.2 %	0.3	0.4 %	0.3
Bearing Clearance (ε)	±20 %	45 %	2	14 %	7
10 % random errors in all		28 %	2	12 %	5

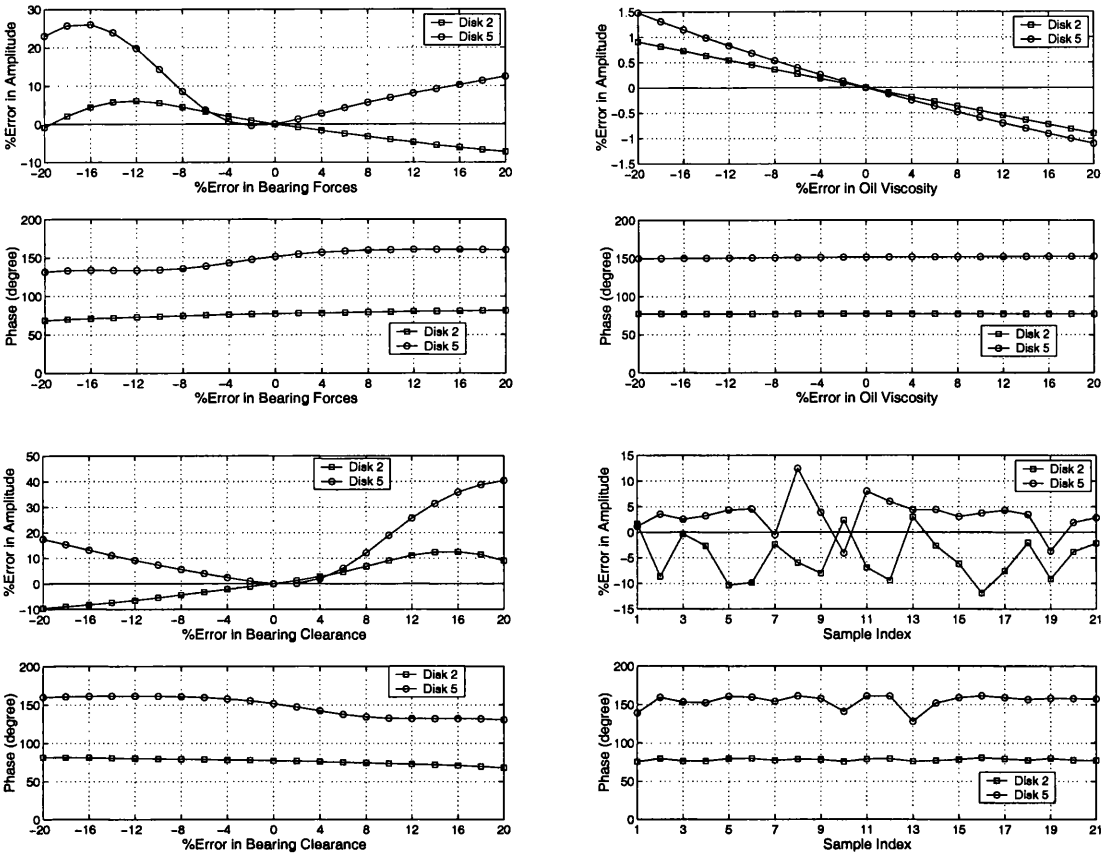

10% random error in all parameters

Figure 8.13 Typical deviation in the rotor unbalance estimation with perturbations in the fluid bearing model for the run (2–1) for the experimental Aston rig

Table 8.6 Unbalance estimation for the experimental Aston Rig, with perturbations in the fluid bearings model

Fluid Bearing Model		*Balance Disk 2 – Unbalance		Balance Disk 5- Unbalance	
Perturbation in Parameters	Error	Max. % Error in Amplitude	Max. Phase Error (deg.)	Max. % Error in Amplitude	Max. Phase Error (deg.)
Run (2-1)					
Bearing Forces	±20%	6 %	5	27 %	20
Oil Viscosity (μ)	±20 %	0.8 %	2	1.5 %	2
Clearance (ε)	±20 %	12 %	7	40 %	20
10 % Random errors in all		12 %	3	12 %	20
Run (3-1)					
Bearing Forces	±20%	12 %	7	17 %	5
Oil Viscosity (μ)	±20 %	1.8 %	10	1.8 %	5
Clearance (ε)	±20 %	26 %	25	22 %	10
10 % Random errors in all		8 %	20	13 %	20

* Disk 1 for *run (3-1)*.

8.3.1. Discussion

The following observations (Figures 8.12 - 8.13, Tables 8.5 - 8.6) may be made based on the sensitivity analysis of the rotor unbalance estimation due to the error in the fluid bearing modelling through the simulated and the experimental examples.

(1) The unbalance estimation is not found to be sensitive to the value of the bearing oil viscosity.

(2) Bearing forces and the bearing clearance are found to have some effect on the unbalance amplitude estimation, however the phase estimation is once again quite robust and the error is less than 20 degrees.

(3) In general it has been observed that the error in the unbalance estimates due to the fluid bearing modelling errors is less than that due to the rotor modelling errors.

Hence this study indicates that the rotor unbalance estimation method can accommodate more error in the fluid bearing models compared to the rotor model error. However a reasonably good model for the fluid bearings is required for reliable estimation of foundation model suggested in Chapter 5.

8.4. SENSITIVITY TO BOTH THE ROTOR AND FLUID BEARING MODELS

Perturbations in both the rotor and bearing models were also introduced simultaneously. A 10% of the normally distributed random variation in all the modelling parameters for the fluid bearings and a 5% of the normally distributed random variation in all rotor parameters were considered. The sensitivity analysis was then carried out for the combination of the random errors in the rotor and the fluid bearing models to further check the robustness of the suggested rotor unbalance estimation method, although it would be a rare combination of errors even for a real-life rotor system. Figure 8.14 shows the results and the following may be observed.

(1) The error in the estimated amplitudes at disks A and B is generally small and less than 30 % and the phase estimation is robust within an error of 12 degrees for the *Small rig* simulation with fluid bearings.

(2) For the experimental *Aston rig*, the error in the estimated amplitudes is normally less than 45 % except for some combinations of random errors in the rotor and bearing models for run (2-1) when the error is up to 70 %. However the estimated phases seem to be robust, and the maximum phase error is found to be 40 degrees.

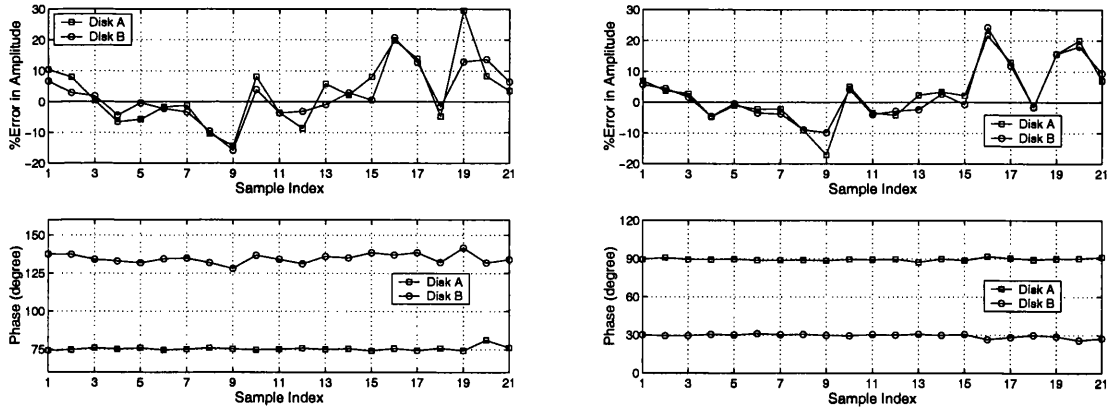

Unbalance Configuration 1 Unbalance Configuration 2

(a) Small rig simulation

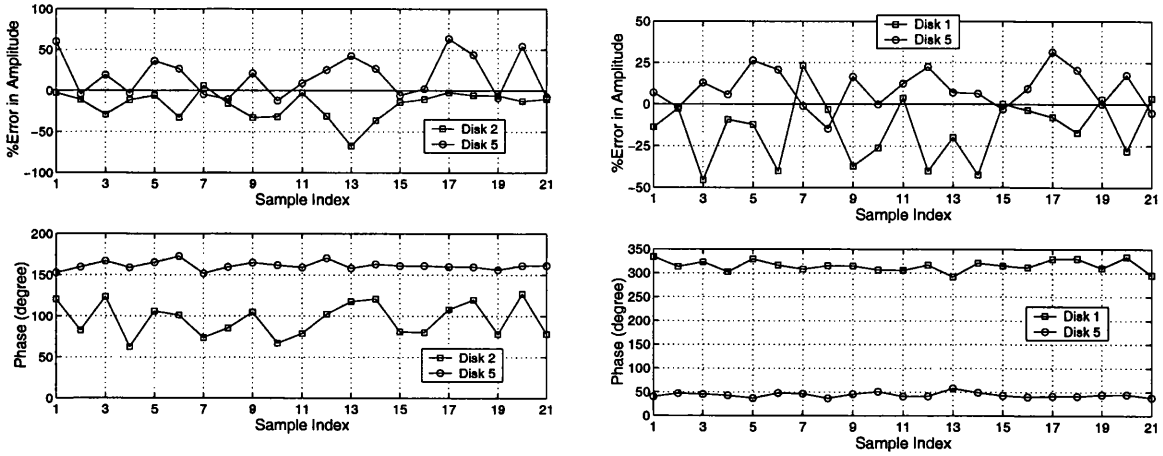

Run (2-1) Run (3-1)

(b) Aston rig

Figure 8.14 Deviation in the rotor unbalance estimation with random perturbations in both the rotor and the fluid bearing models

8.5. SUMMARY

The methods for the estimation of rotor unbalance (both amplitude and phase at multi-planes) and misalignment for flexibly supported rotating machines have been proposed in Chapter 5. The methods use the rotor FE model and the model of the fluid bearings along with the measured vibration response at the bearing housings during a machine run-down. The validation of the proposed methods has been demonstrated in Chapter 7. However it may be that the physical and material properties are not known exactly, producing errors in the models of the rotor and the fluid bearings. These modelling errors may affect the estimation. Hence a sensitivity analysis for the proposed methods was carried out by introducing perturbations in the modelling parameters of the rotor and bearings to check the effect on the multi-plane rotor unbalance and misalignment estimation. Such a sensitivity analysis was applied to the *Small rig* simulation and the experimental examples of the *New small rig* and the *Aston rig*. The comparison between the two types of rigs – one rig supported by ball bearings (i.e. rigid bearings) and the other rig with fluid bearings - has also been highlighted. In general the rotor unbalance estimation method is robust for both type of bearings. However, it has been observed that the rotor system with fluid bearings is generally less sensitive to the modelling error in the rotor due to the presence of the bearing damping. Furthermore the deviation in the unbalance estimates due to errors in the fluid bearing models is smaller compared to the rotor model error. In general, the deviation in the estimated phase is quite robust and almost invariant to the errors in the rotor and bearing models compared to the estimated unbalance amplitudes. The small variation in the misalignment estimation for the experimental *New small rig* with the errors in the rotor model also indicates the robustness of the proposed method, however it would be good to confirm the same on a larger rig with multi-coupled rotors. Hence, the proposed method for the rotor unbalance and misalignment estimation can be considered to be robust. The level of the error seen in the unbalance estimation during the sensitivity analysis should be acceptable for the real-life rotor systems like TG sets considering the following facts.

(1) The proposed method for the rotor unbalance estimation is straightforward to apply to the field balancing problem and the method does not require any existing balancing skills and experiences.

(2) Generally speaking, none of the existing balancing methods have found to reduce the amplitude of machine vibration by 90 - 100% and they require considerable balancing experience. Often the reduction in machine vibration by 30% to 40% is considered to a successful balancing exercise for large scale machines.

(3) The observation of the robust phase estimation even with modelling errors is a very good indication for field balancing problems. So with a good balancing phase, and even with the some error in the estimated amplitude, a significant reduction in machine vibration can be achieved without any trial runs.

CHAPTER 9

CONCLUSIONS AND RECOMMENDATIONS

9.0. SUMMARY AND CONCLUSIONS

In this thesis, the topic of health monitoring of rotating machinery in particular the TG set of power generation industry has been addressed. An overall simplified summary of the vibration based diagnosis for rotating machinery has also been discussed. As discussed in the thesis the identification procedure for the presence of faults is well known for different kind of faults, however their quantification is still an ongoing research topic, and it usually requires a reliable mathematical model of the complete machine along with the measured vibration response of the system. The rotating machine consists of three major parts - a rotor, fluid journal bearings and a foundation which is often flexible. It is also known that a reliable model for the rotor and an adequate model for the fluid bearings are possible to construct, but a reliable modelling for the foundation is difficult due to a number of practical difficulties. In addition to these limitations, it was also assumed that only the vibration response at the bearing pedestals using accelerometers in both the horizontal and vertical directions along with the shaft keyphasor/ tacho signal are measured. No proximity probes signals for the shaft relative vibration are used, since many older power plants may not be equipped with this facility. Hence *a priori* models for the rotor and fluid bearings, and the bearing pedestal vibration data were utilized for the present study. Broadly the study has been concentrated on following two objectives.

(a) Foundation model estimation so that a reliable mathematical model of the complete system can be developed.
(b) Reliable fault estimation (Rotor unbalance and misalignment) even if the foundation model is not known.

For both of the objectives the proposed methods have been qualified initially on the simulated examples and then applied to the experimental examples. A total of three experimental rigs were used. Two rigs are in Swansea (UK), which are small and their rotors are supported on flexible foundations through self lubricated ball bearings, and the third one is at Aston University, Birmingham (UK), which is much bigger with four fluid journal bearings.

For the foundation model estimation, two run-down responses (one with residual unbalance and the other with added unbalance at a number of balance disks) of machine have been considered. Assuming the machine dynamics are linear the responses of two runs were subtracted to produce a response of the machine for a known unbalance in the rotor. Hence a method has been proposed for the foundation model estimation directly from the subtracted responses for a known state of rotor unbalance and using *a priori* rotor and fluid bearings models. The proposed approach restricts the size of the estimated foundation model to be equal to the measued DoFs at the bearing pedestals. Hence the run-down frequency range has been split into smaller bands to accommodate more modes than measured DoFs. Two *Regularization Methods* were proposed to solve the resulting equation. *Regularization 1* just involved numerical conditioning whereas *Regularization 2* was based on the physical behaviour of the foundation along with *Regularization 1*. The importance of these regularization techniques has been highlighted through the prediction capacity of the estimated foundation models. It has been observed that *Regularization 2* is essential for an accurate prediction capability of the estimated foundation model. The excellent predication capacity of the estimated foundation model has been demonstrated through several simulations with and without noise and an experimental example of the *New small rig* by the proposed method. The small differences in the prediction of the estimated foundation models for the experimental *Aston rig* requires some more investigation which may be a future research topic. This is discussed in the next section. Apart from this example the proposed method is seems to be a simple and robust method for the reliable estimation for the foundation model, and hence a reliable mathematical model of a complete system may now be possible.

For the state of rotor unbalance and misalignment estimation, a different approach has been suggested. The proposed methods just assume that the foundation models are not known and they use *a priori* models for the rotor and fluid bearings along with the measured vibration response at the bearing pedestals from a single run-down. Hence the proposed method is quick, as it does not require several run-downs of a machine. The proposed method estimates a global estimate of unbalance (both amplitude and phase) at multi-balance planes and the misalignment at the couplings for multi-

coupled rotor as a least squares estimation. The band dependent foundation parameters are obtained by splitting the machine run-down range into small bands as a by-product to account the foundation dynamics. The importance of different regularization methods required during the estimation process has also been brought out. The method has been tested on both simulations and on the experimental examples. The estimated unbalance and misalignment were found to be excellent for all examples. The error in the unbalance phase estimation for the experimental *Small rig* has been confirmed to be due to the non-linear dynamic behaviour of its foundation. However the reason for the error in the phase estimation for the experimental *Aston rig* could not be identified during the course of the study and this can be considered as scope for future work.

The sensitivity analysis of the proposed method for the rotor unbalance and misalignment estimation was also carried out by introducing perturbation errors in the different modelling parameters for the rotor and fluid bearings, to check the extent of robustness of the proposed method. It has been observed that the maximum error in estimated unbalance amplitude at multi-planes is usually less than 50% for the 5% simultaneous random errors in rotor modelling parameters and 10% in fluid bearing modelling parameters. However the most gratifying observation is that the phase estimation is quite robust which a very good indication for rotor balancing. The variation in the estimated linear and angular misalignment was also found to be small with the change in rotor modelling error for the *New small rig*. In general it has been observed that the estimation method is far less sensitive to errors in the fluid bearing modelling compared to the rotor modelling error, and rotor systems having fluid bearings are also less sensitive to modelling errors, compared to systems having rigid bearings. Hence the proposed method seems to be quite robust.

9.1. RECOMMENDATIONS FOR FUTURE WORK

As far as future work in this field is concerned, the following recommendations may be made:

9.1.1. Foundation Model Estimation

(i) The linear dynamic behaviour of the machine should be confirmed first by performing three run-down experiments as suggested in Section 6.5 of Chapter 6.

(ii) The error in the fluid bearing modelling should be checked by using measured dynamic forces at the bearings during a machine run-down. Alternatively, shaft responses measured by proximity probes near bearing pedestals may be included to avoid using the bearing model in the estimation process. In fact the use of proximity probe data, along with the bearing pedestal vibration, allows the foundation model, the rotor unbalance and the bearing forces to be estimated from a single run-down of machine.

(iii) The identification of a modal model for the foundation should be developed and the usefulness of the identified modal model should be compared with the present proposed method.

(iv) The proposed method should be tested on the data obtained from a power station.

(v) It would be good to develop a method that can identify the models for the foundation which are known to have non-linear dynamic behaviour.

9.1.2. Rotor Unbalance and Misalignment Estimation

The proposed method was found to be reliable and robust, and no further improvement is needed at present. However the method should be tested on a large, more complex machine like the TG set of a power plant to increase the confidence level in the proposed method.

9.2. CONCLUDING REMARKS

It is hoped that the work discussed above, which has a practical relevance to the power industry, will play a significant role in the overall improvement in health condition monitoring techniques for rotating machinery in power plants.

REFERENCES

BACHSCHMID, N., and PENNACCHI, P., 2000 *Proceedings of the Institution of Mechanical Engineers – Vibrations in Rotating Machinery,* C576/043/2000, 571-580, *University of Nottingham, UK,* September 12-14. Model-based Malfunction Identification from Bearing Measurements.

BACHSCHMID, N., PENNACCHI, P., and VANIA, A., 2002 *Journal of Sound and Vibration* **254**(2), 327-366. Identification of Multiple Faults in Rotor Systems.

BAKER, J. G., and EVANSVILLE, W., 1939 *Transaction of the ASME – Journal of Applied Mechanics* **6**, A1-A6. Methods of Rotor-Unbalance Determination.

BALMES, E., 2000. *MatLab based software Structural Dynamics Toolbox*, Ver 4.

BENDAT, J. S. and PIERSOL, A. G., 1980 *Engineering Applications of Correlation and Spectral Analysis.* NY: Wiley.

BENTLY, D. E., 1982 *Orbit,* 2, 10-11, *Bently Nevada Corporation, USA*, July. Detecting Cracked Shafts at Earlier Levels.

BENTLY, D. E., 1983a *Orbit,* 3-5, *Bently Nevada Corporation, USA*, October. Studies Reveal Physical Phenomena of Rotor Rubs.

BENTLY, D. E., 1983b *Orbit,* 2-3, *Bently Nevada Corporation, USA*, March. Meaningful Machinery Information.

BENTLY, D. E., 1986 *Orbit,* 18-23, *Bently Nevada Corporation, USA*, January. Vibration Analysis Techniques for Detecting and Diagnosing Shaft Cracks.

BENTLY, D. E., and WERNER, M., 1990 *Orbit,* 5-9, *Bently Nevada Corporation, USA*, September. Extending Machinery Life.

BENTLY, D. E., 1994 *Orbit,* 11-15, *Bently Nevada Corporation, USA*, June. Using Full Spectrum Plots, Part-2.

BISHOP, R. E. D., and GLADWELL, G. M. L., 1959 *Journal of Mechanical Engineering Science* **1**(1), 66-71. The Vibration and Balancing of an Unbalanced Flexible Rotor.

BISHOP, R. E. D., and PARKINSON, A. G., 1972 *Transaction of the ASME – Journal of Engineering for Industry* **94**, 561-576. On the use of Balancing Machines for Flexible Rotors.

BOSSLEY, K.M., MCKENDRICK, R.J., HARRIS, C.J. and MERCER, C., 1999 *Mechanical Systems and Signal Processing* **13**(4), 627-641. Hybrid Computed Order Tracking.

CAMPBELL, A. J., 1993 *Orbit,* 24-29, *Bently Nevada Corporation, USA*, June. Static and Dynamic Alignment of Turbomachinery.

CHILDS, D., 1993 *Turbomachinery Rotordynamics: Phenomena, Modelling and Analysis*. Chichester: Wiley.

COOK, R. D., MALKUS, D. S. and PLESHA, M. E., 1989 *Concept and Applications of Finite Element Analysis*. NY: Wiley.

COWPER, G. R., 1966 *Journal of Applied Mechanics* **33**, 335-340. The Shear Coefficient in Timoshenko's Beam Theory.

DARLOW, M. S. 1987 *Mechanical Systems and Signal Processing* **1**(1), 105-134. Balancing of High Speed Machinery: Theory, Methods & Experimental Results.

DEWELL, D. L., and MITCHELL, L. D., 1984 *Transactions of the ASME - Journal of Vibration Acoustics Stress and Reliability in Design* **106**(1), 9-16. Detection of a Misaligned Disk Coupling using Spectrum Analysis.

DOEBLING, S. W., FARRAR, C. R., PRIME, M. B., and SHEVITZ, D. W., 1996 *Los Alamos National Laboratory Report*, No. LA-13070-MS. Identification and

Health Monitoring of Structural Systems from Changes in their Vibration Characteristics.

DOEBLING, S. W., FARRAR, C. R. and PRIME, M. B., 1998 *Shock and Vibration Digest* **30**(2), 91-105. A Summary Review of Vibration-based Damage Identification Methods.

EDWARDS, S., LEES, A. W. and FRISWELL, M. I., 1998 *Shock and Vibration Digest* **30**(1), 4-13. Fault Diagnosis of Rotating Machinery.

EDWARDS, S., 1999 *PhD Thesis, Department of Mechanical Engineering., University of Wales Swansea, UK.* Fault Diagnosis of Rotating Machinery.

EDWARDS, S., LEES, A. W. and FRISWELL, M. I., 1999 *Journal of Sound and Vibration* **225**(4), 767-778. The Influence of Torsion on Rotor-Stator Contact in Rotating Machinery.

EDWARDS, S., LEES, A. W. and FRISWELL, M. I., 2000 *Journal of Sound and Vibration* **232**(5), 963-992. Experimental Identification of Excitation and Support Parameters of a Flexible Rotor-Bearing-Foundation System from a Single Run-Down.

EHRICH, F. F., 1988 *Transactions of the ASME - Journal of Vibration Acoustics Stress and Reliability in Design* **110**(1), 9-16. High-Order Subharmonic Response of High-Speed Rotors in Bearing Clearance.

EHRICH, F. F., 1992a *Transactions of the ASME - Journal of Vibration and Acoustics* **114**(1), 93-100. Observations of Subcritical Superharmonic and Chaotic Response in Rotordynamics.

EHRICH, F. F. (Editor), 1992b *Handbook of Rotordynamics*. NY: McGraw-Hill.

EISENMANN, R. C., 1997 *Orbit,* 12-17, *Bently Nevada Corporation, USA*, June. Some Realities of Field Balancing.

El-SHAFEI, A. 1995 *Journal of Vibration and Acoustics* **117**(4), 462-469. Modelling Fluid Inertia Forces on Short Journal Bearings for Rotordynamic Applications.

EWINS, D. J. 1998 *IFToMM Proceedings of 5th International Conference on Rotor Dynamics, Darmstadt*, September 2002. Modal Analysis for Rotating Machinery.

EWINS, D. J., 2000 *Modal Testing: Theory, Practice and Application.* 2nd edition, Hertfordshire, England: Research Studies Press Ltd.

FENG, N. S. and HAHN, E. J., 1995 *Mechanical Systems and Signal Processing* **9**, 243-256. Including Foundation Effects on the Vibration Behaviour of Rotating Machinery.

FLACK, R. D., ROOKE, J. H., BIELK, J. R., and GUNTER, E. J., 1982 *Transactions of the ASME - Journal of Mechanical Design* **104**(2), 318-328. Comparison of the Unbalance Responses of Jeffcott Rotors with Shaft Bow and Shaft Runout.

FOILES, W. C., ALLAIRE, P. E., and GUNTER, E. J., 1998 *Shock and Vibration* **5**(5-6), 325-336. Review: Rotor Balancing.

FORLAND, C., 1999 *Orbit,* 29-31, *Bently Nevada Corporation, USA*, 2nd/3rd Quarter. Why phase information is important for diagnosing machinery problems.

FRISWELL, M. I., PENNY, J. E. T., GARVEY, S. D. and LEES, A. W., 2002 *Fundamentals of Rotor Dynamics: Modelling and Computation.* In preparation.

FRISWELL, M. I. and MOTTERSHEAD, J. E., 1995 *Finite Element Model Updating in Structural Dynamics*. Kluwer Academic Publishers.

FYFE, K.R. and MUNCK, E.D.S., 1997 *Mechanical Systems and Signal Processing* **11**(2), 187-205. Analysis of Computed Order Tracking.

GASCH, R., 1993 *Journal of Sound and Vibration* **160**(2), 313-332. A Survey of the Dynamics Behaviour of a Simple Rotating Shaft with a Transverse Crack.

GENTA G., 1993 *Vibration of Structures and Machines: Practical Aspects.* NY: Springer-Verlag.

GENTA, G., 1997 *DYNROT 8.2: A Finite Element Code for Rotordynamic Analysis.* Dipartimento di Meccanica, Politecnicodi Torino, Torino, Italy.

GIBBONS, C. B., 1976 *Proceedings of the 15th Turbomachinery Symposium, Gas Turbine Laboratory,* 111-116, *Texas A & M University, College Station, Texas.* Coupling Misalignment Forces.

GILL, P. E., MURRAY, W. and WRIGHT, M. H., 1981. *Practical Optimization.* Academic Press.

GOLDMAN, P. and MUSZYNSKA, A., 1994a *Transactions of the ASME - Journal of Engineering for Gas Turbine and Power* **116**(3), 692-701. Chaotic Behaviour of Rotor/Stator Systems with Rubs.

GOLDMAN, P. and MUSZYNSKA, A., 1994b *Transactions of the ASME - Journal of Vibration and Acoustics* **116**(4), 541-547. Dynamic Effects in Mechanical Structures with Gap and Impacting: Order and Chaos.

GOLDMAN, P. and MUSZYNSKA, A., 1999 *Orbit,* 17-21, *Bently Nevada Corporation, USA*, 1st Quarter. Application of Full Spectrum to Rotating Machinery Diagnostics.

GOLUB, G. H. and LOAN, C. F. VAN, 1996. *Matrix Computations.* 3rd edition, John Hopkins, Baltimore, Maryland.

GOODMAN, T. P., 1964 *Transaction of the ASME – Journal of Engineering for Industry* **86**(3), 273-279. A Least-Squares Method for Computing Balance Corrections.

GROBEL, L. P., 1953 *General Electric Review* **56**(4), 22-25. Balancing Turbine-Generator Rotors.

HAMROCK, B.J. 1994. *Fundamentals of Fluid Film Lubrication.* McGraw-Hill.

HANSEN, P. C., 1994 *Numerical Algorithms* **6**, 1-35. Regularisation Tools: A MATLAB Package for Analysis and Solution of Discrete Ill-posed Problems.

HARRIS, C. M. (Editor), 1988 *Shock and Vibration Handbook.* 3rd edition, NY: McGraw-Hill.

HOPKIRK, K. R., 1940 *The Engineer* **170**, 38-39. Notes on Methods of Balancing.

HUTCHINSON, J.R., 2001 *ASME Journal of Applied Mechanics* **68**, 87-92. Shear Coefficients for Timoshenko Beam Theory.

ISO 2372, 1974. *Mechanical Vibration of Machines with Operating Speeds from 10 to 200rps – Basis for Specifying Evaluation Standards.*

ISO 3945, 1980. *The Measurements and Evaluation of Vibration Severity of Large Rotating Machines, in Situ, Operating at Speeds 10 to 200rps.*

ISO 7919/1, 1986. *Mechanical Vibration of Non-Reciprocating Machines – Measurements on Rotating Shafts and Evaluation, Part 1: General Guidelines.*

ISO 7919/2, 1986. *Mechanical Vibration of Non-Reciprocating Machines – Measurements on Rotating Shafts and Evaluation, Part 2: Measurement and Evaluation of Shaft Vibration of Large Turbine-Generator Sets.*

JORDAN, M. A., 1993 *Orbit,* 8-15, *Bently Nevada Corporation, USA*, December. What are Orbit plots, anyway?

JUN, O. S., EUN, H. J., EARMME, Y. Y., and LEE, C. W., 1992 *Journal of Sound and Vibration* **155**(2), 273-290. Modelling and Vibration Analysis of a Simple Rotor with a Breathing Crack.

LALANNE, M., and FERRARIS, G., 1998. *Rotordynamics Prediction in Engineering*. 2nd edition, Chichester, Wiley.

LAWS, B., 1998 *Orbit,* **18**(4), 20-25, *Bently Nevada Corporation, USA*, December. Turbine Generator Vibration Transducer Selection Criteria for Machinery Protection and management.

LEES, A. W. and SIMPSON, I. C., 1983 *Proceedings of the Institution of Mechanical Engineers – Conference on Steam and Gas Turbine Foundations and Shaft Alignment*, Bury St. Edmunds, Paper C6/83, 37-44. The Dynamics of Turbo-Alternator Foundations.

LEES, A. W., 1988 *Proceedings of the Institute of Mechanical Engineers – Vibrations in Rotating Machinery,* Paper C306/88, 209-216. The Least Squares Method Applied to Identified Rotor/Foundation Parameters.

LEES, A. W. and FRISWELL, M. I., 1997 *Journal of Sound and Vibration* **208**, 671-683. The Evaluation of Rotor Unbalance in Flexibly Mounted Machines.

LEES, A.W., EDWARDS, S., and FRISWELL, M. I., 2000 *Proceedings of the Institute of Mechanical Engineers – Vibrations in Rotating Machinery*, C576/010/2000, 21-40, *University of Nottingham, UK*, September 12-14. The Estimation of Foundation Parameters and Unbalance.

LEES, A. W., SINHA, J. K., and FRISWELL, M. I., 2002 *Proceedings of ASME Turbo Expo Conference,* ASME paper GT-2002-30420, *Amsterdam, Holland,* 3-6 June. The Identification of the Unbalance of a Flexible Rotating Machine from a Single Run-Down.

MatLab: 1999 A User's Guide, The Mathworks Inc., Version 5.3.1.

MAYES, I. W., and DAVIES, W. G. R., 1984 *Transaction of the ASME – Journal of Vibration Acoustics Stress and Reliability in Design* **106**, 139-145. Analysis of the Response of a Multi-Rotor-Bearing System Containing a Transverse Crack in a Rotor.

MEACHAM, W. L., TALBERT, P. B., NELSON, H. D., and COOPERRIDER, N. K., 1988 *Journal of Propulsion and Power* **4**(3), 245-251. Complex Modal Balancing of Flexible Rotors including Residual Bow.

MITCHELL, J. S., 1978 *Presented at the winter meeting of the ASME* pp. 15-24. Bearing Diagnostics: An Overview.

MORTON, P. G., 1985 *Proceedings of the Institution of Mechanical Engineers Part C – Journal of Mechanical Engineering Science* **199**(C1), 71-78. Modal Balancing of Flexible Shafts without Trail Weights.

MUSZYNSKA, A., 1986a *Journal of Sound and Vibration* **110**(3), 443-462. Whirl and Whip – Rotor/Bearing Stability Problems.

MUSZYNSKA, A., 1986b *The International Journal of Analytical and Experimental Modal Analysis* **1**(3), 15-34. Modal Testing of Rotor/Bearing Systems.

MUSZYNSKA, A., 1988 *Journal of Sound and Vibration* **127**(1), 49-64. Stability of Whirl and Whip in Rotor/Bearing Systems.

MUSZYNSKA, A., 1989 *Shock and Vibration Digest* **21**(3), 3-11. Rotor to Stationary Element Rub-Related Vibration Phenomena in Rotating Machinery – Literature Survey.

MUSZYNSKA, A., and BENTLY, D. E., 1989 *Orbit,* **10**, 6-14, *Bently Nevada Corporation, USA*, April. Fluid-Generated Instabilities of Rotors.

MUSZYNSKA, A., 1993 *Orbit,* 8-13, *Bently Nevada Corporation, USA*, March. Thermal Rub Effect in Rotating Machines.

MUSZYNSKA, A., and BENTLY, D. E., 1996 *Orbit,* 7-15, *Bently Nevada Corporation, USA*, March. Fluid-Induced Instabilities of Rotors: Whirl and Whip – Summary of Results.

NICHOLAS, J. C., GUNTER, E. J., and ALLAIRE, P. J., 1976a *Journal of Engineering for Power* **98**(2), 171-181. Effect of Residual Shaft Bow on Unbalance Response and Balancing of a Single Mass Flexible Rotor Part 1 – Unbalance Response.

NICHOLAS, J. C., GUNTER, E. J., and ALLAIRE, P. J., 1976b *Journal of Engineering for Power* **98**(2), 182-189. Effect of Residual Shaft Bow on Unbalance Response and Balancing of a Single Mass Flexible Rotor Part 2 – Unbalancing.

Orbit 1981-2001. The Magazine of M/s. Bently Nevada Corporation, USA.

PARKINSON, A. G., DARLOW, M. S., and SMALLEY, A. J., 1984 *AIAA Journal* **22**(5), 683-689. Balancing Flexible Rotating Shafts with an Initial Bend.

PARKINSON, A. G., 1991 *Proceedings. of the Institute of Mechanical Engineers Part C – Journal of Mechanical Engineering Science* **205**(C1), 53-66. Balancing of Rotating Machinery.

PARKINSON, A. G., and McGUIRE, P. M., 1995 *Proceedings. of the Institute of Mechanical Engineers Part C – Journal of Mechanical Engineering Science* **209**(C5), 315-322. Rotordynamics Standards: New Developments and the Need for Involvement.

PENNY, J.E.T., and FRISWELL, M. I., 2002 *Proceedings of 3rd International Conference – Identification in Engineering Systems,* 221-231, *Swansea, UK,* April 15-17. Crack Modelling for Structural Health Monitoring.

PILKEY, W. D., and BAILEY, J. T., 1979 *Transactions of the ASME – Journal of Mechanical Design* **101**(2), 304-308. Constrained Balancing Techniques for Flexible Rotors.

PILKEY, W. D., BAILEY, J. T., and SMITH, P. D., 1983 *Transactions of the ASME – Journal of Vibration Acoustics Stress and Reliability in Design* **105**(1), 90-93. A Computational Technique for Optimizing Correction Weights and Axial Location of Balance Planes of Rotor Shafts.

PLATZ, R., MARKERT, R., and SEIDLER, M., 2000 *Proceedings of the Institution of Mechanical Engineers – Vibrations in Rotating Machinery,* C576/025/2000, 581-590, *University of Nottingham, UK,* September 12-14. Validation of online Diagnostics of Malfunctions in Rotor Systems.

PROVASI, R., ZANETTA, G. A., and VANIA, A., 2000 *Mechanical Systems and Signal Processing* **14**(3), 327-341. The Extended Kalman Filter in the Frequency Domain for the Identification of Mechanical Structures excited by Sinusoidal Multiple Inputs.

RAO, J. S., 1996 *Rotor Dynamics.* 3rd edition, India: New Age International Publishers.

RAO, J. S., 2000 *Vibratory Condition Monitoring of Machines.* India: CRC Press.

RAO, J. S., and SHARMA, M., 2000 *Proceedings of VETOMAC-I,* Paper - CP022 *Bangalore (India),* October. Dynamic Analysis of Bowed Rotors.

RAO, A. R. and SINHA, R. K., 2000 *Proceedings of VETOMAC-1*, Paper – CP061, *Bangalore (India),* October. Insitu Measurement on Turbo-Generators for Detection of Blade Vibrations.

RAO, J. S., PATHAK, A. and CHAWLA, A., 2001 *Transactions of the ASME - Journal of Engineering Gas Turbine and Power* **123**, 886-892. Blade Life: A Comparison by Cumulative Damage Theories.

RUSSEL, P. 1997 *Orbit, Bently Nevada Corporation, USA*, June, pp. 34-35. Why install a Keyphasor Transducer?

SABIN, S., 1997 *Orbit,* 8-14, *Bently Nevada Corporation, USA*, March. The Limitations of Protecting and Managing Machinery using Vibration "Transmitters".

SAITO, S., and AZUMA, T., 1983 *Transactions of the ASME – Journal of Vibration Acoustics Stress and Reliability in Design* **105**(1), 94-100. Balancing of Flexible Rotors by the Complex Modal Method.

SCHOUKENS, J. and PINTELON, R., 1991. *Identification of Linear Systems : A Practical Guideline to Accurate Modeling.* Pergamon Press.

SEKHAR, A. S., and PRABHU, B. S., 1995 *Journal of Sound and Vibration* **185**(4), 655-671. Effects of Coupling Misalignment on Vibrations of Rotating Machinery.

SigLab 1998 User Guide Version 3.0. DSP Technoligy Inc., USA.

SIMON, G., 1992 *Proceedings of the Institution of Mechanical Engineers, Part C – Journal of Mechanical Engineering Science* **206**(C1), 29-39. Prediction of Vibration Behaviour of large Turbo-machinery on Elastic Foundations due to Unbalance and Coupling Misalignment.

SINHA, J. K., LEES, A. W., and FRISWELL, M. I., 2001 *Proceedings of 19th International Modal Analysis Conference, Florida, USA,* pp. 109-115. Estimating the Unbalance of a Rotating Machine from a Single Run Down.

SINHA, J. K., LEES, A. W., FRISWELL, M. I., and SINHA, R. K., 2002a *Proceedings of 3rd International Conference – Identification in Engineering Systems,* 300-309, *Swansea, UK,* April 15-17. The Estimation of Foundation Models of Flexible Machines.

SINHA, J. K., FRISWELL, M. I., and LEES, A. W., 2002b *Mechanical Systems and Signal Processing* **16** (2-3), 255-271. The Identification of the Unbalance and the Foundation Model of a Flexible Rotating Machine from a Single Run Down.

SINHA, J. K., FRISWELL, M. I., and EDWARDS, S. 2002c *Journal of Sound and Vibration* **251**(1), 13-38. Simplified Models for the Location of Cracks in Beam Structures using Measured Vibration Data.

SMART, M. G., 1998 *PhD Thesis, Department of Mechanical Engineering, University of Wales Swansea, UK.* Identification of Flexible Turbogenerator Foundations.

SMART, M. G., FRISWELL, M. I. and LEES, A. W., 2000 *Proceedings. of Royal Society of London, Series A: Mathematical, Physical and Engineearing Sciences* **456**, 1583-1607. Estimating Turbogenerator Foundation Parameters – Model Selection and Regularisation.

SMITH, D. M., 1969. *Journal of Bearing in Turbomachinery.* Champman and Hall.

SOUTHWICK, D., 1993 *Orbit,* 19-21, *Bently Nevada Corporation, USA*, December. Using Full Spectrum Plots.

SOUTHWICK, D., 1994 *Orbit,* **15**(2), 11-15, *Bently Nevada Corporation, USA*, June. Using Full Spectrum Plots, Part 2.

TESSARZIK, J. M., BODGLEY, R. H., and ANDERSON, W. J., 1972 *Transactions of the ASME – Journal of Engineering for Industry* **94**(1), 148-157. Flexible Rotor Balancing by the Exact Point-Speed Influence Coefficient Method.

THEASLE, E. L., and SCHENECTADY, N. Y., 1934 *Transaction of the ASME* **56**, 745-753, Paper No. APM-56-19. Dynamic Balancing of Rotating Machinery in the Field.

THOMAS, R., 1995 *Orbit,* 16-22, *Bently Nevada Corporation, USA*, September. The Importance of Transient Data Analysis.

VANCE, J. M., 1988 *Rotordynamics of Turbomachinery*. Chichester: Wiley.

VANIA, A., 1996 *Politecnico di Milano, Dipartimento di Meccanica,* Internal Report 9-96. Estimating Turbo-Generator Foundation Parameters.

VSI Rotate 2.0, 2000. Vold Solusions, USA.

WAUER, J., 1990 *Applied Mechanics Reviews* **43**(1), 13-17. On the Dynamics of Cracked Rotors: A Literature Survey.

WOWK, V., 1991 *Machinery Vibration*. New York: McGraw-Hill.

WU, M-C, and HUANG, S-C, 1998 *International Journal of Mechanical Science* **40**(6), 545-555. Vibration and Crack Detection of a Rotor with Speed-dependent Bearings.

XU, M., and MARANGONI, R. D., 1994a *Journal of Sound and Vibration* **176**(5), 663-679. Vibration Analysis of a Motor-Flexible Coupling-Rotor System subjected to Misalignment and Unbalance, Part I: Theoretical Model and Analysis.

XU, M., and MARANGONI, R. D., 1994b *Journal of Sound and Vibration* **176**(5), 681-691. Vibration Analysis of a Motor-Flexible Coupling-Rotor System subjected to Misalignment and Unbalance, Part II: Experimental Validation.

YANG, B., SUH, C. S., and CHAN, A. K., 2002 *Transactions of the ASME – Journal of Vibration and Acoustics* **124**, 40-48. Characterization and Detection of Crack-induced Rotary Instability.

ZANETTA, G. A., 1992 *Proceedings. of the Institution for Mechanical Engineers - Vibrations in Rotating Machinery, Bath* Paper C432/092, 173-181. Identification Methods in the Dynamics of Turbogenerator Rotors.

ZANG, C., LEES, A. W., and FRISWELL, M. I., 2002 *IFToMM Proceedings of 6th International Conference on Rotor Dynamics, Australia*, September 2002. Multi-Plane Balancing of a Rotating Machine Using a Single Transducer.

ZHENGJIA, H., SHENG, Y., and QU, L.., 1990 *Mechanical Systems and Signal Processing*, **4**(5), 417-424. Rub Failure Signature Analysis for Large Rotating Machinery.

ZHOU, S. and SHI, J., 2001 *Shock and Vibration Digest* **33**(5), 361-371. Active Balancing and Vibration Control of Rotating Machinery: A Survey.

ZIENKIEWICZ, O. C. and TAYLOR, R. L., 1994 *The Finite Element Method: Volume 1, Basic Formulations and Linear Problems*. Fourth Edition, McGraw-Hill Book Company Europe.